AN INVESTIGATION OF TECTONIC DEFORMATION ON WATER LEVELS IN
DEVILS HOLE, DEATH VALLEY NATIONAL PARK, NEVADA

by

GREGORY DOUGLAS ROBERTSON

B.A., University of Colorado at Boulder, 2003

A thesis submitted to the

Faculty of the Graduate School of the

University of Colorado in partial fulfillment

of the requirement for the degree of

Master of Science

Department of Geological Sciences

2006

This thesis entitled:

An investigation of tectonic deformation on water levels in Devils Hole,

Death Valley National Park, Nevada

written by Gregory D. Robertson

has been approved for the Department of Geological Sciences

_____

Shemin Ge, Chair of Committee

_____

Paula Cutillo, Committee Member

_____

Matt Pranter, Committee Member

Date _____

The final copy of this thesis has been examined by the signatories, and we find that both the content and the form meet acceptable presentation standards of scholarly work in the above mentioned discipline.

Robertson, Gregory Douglas (M.S., Geology)

An investigation of tectonic deformation on water levels in Devils Hole, Death Valley National Park, Nevada

Thesis directed by Associate Professor Shemin Ge

ABSTRACT

The purpose of this study was to examine the effects of tectonic deformation on the water level in Devils Hole, southwest Nevada. Devils Hole is a fluid-filled fault-dissolution cavern located along a 15 kilometer spring-discharge line in a carbonate rock aquifer 130 kilometers west of Las Vegas, Nevada. It is an area of high attention as it provides the habitat to an endangered species of fish, *Cyprinodon diabolis*. The survival of the fish is dependent upon a bounded water level in Devils Hole.

Tectonic deformation was examined using the volumetric strain field present throughout the Great Basin. Extension in the Devils Hole area is aligned at N 65 W with an extension rate of 8 nanostrain/yr. The carbonate rock aquifer that provides ground-water to Devils Hole is heterogeneous and anisotropic containing fractures and faults of multiple scales. Rates of hydraulic head fluctuation are on the order of millimeters per year due to strain. Strain was incorporated into a numerical ground-water flow model through specific storage and initial hydraulic head values.

Implications of ground-water pumping have previously been investigated and show that the long term trend in water-level declines in Devils Hole may be strongly influenced by distant ground-water pumping. The impacts of strain, precipitation, and ground-water pumping were examined in this study. Ground-water pumping and

precipitation were found to be the dominating factors controlling the observed water levels in Devils Hole. Results of strain simulations showed that tectonic deformation can cause the water level in Devils Hole to decline at a rate of 0.00018 m/yr for a maximum strain case. When results of strain cases, which include yearly precipitation, were added to previously determined ground-water pumping results, the trend of the observed water level in Devils Hole was satisfactorily matched. To further account for differences in modeled to observed water levels, more accurate measurements of strain, precipitation, and other atmospheric and environmental parameters need to be assessed in the Devils Hole area.

ACKNOWLEDGEMENTS

CONTENTS

TABLES

FIGURES

CHAPTER I

INTRODUCTION

1.1 PURPOSE

Devils Hole is a water-filled fault-dissolution cavern located among the Amargosa Ridges in Ash Meadows National Wildlife Refuge. A large interest is taken at Devils Hole because of its inhabitants. An endemic species of fish, *Cyprinodon diabolis* or pupfish, live in Devils Hole. The pupfish are dependent upon a water covered shelf in Devils Hole for survival. It is at that location where the pupfish can feed and reproduce (Dudley and Larson, 1976).

Past water levels in Devils Hole have fluctuated greatly due to various factors, which causes a concern for the existence of the pupfish. As a result, a Desert Pupfish Task Force (DPTF) was established in the U.S. Department of the Interior in 1969 (Dudley and Larson, 1976). The purpose of the DPTF was to study the cause or causes of water-level declines in Devils Hole. They concluded that ground-water pumping in the Devils Hole area had caused declines in the water-level within Devils Hole (Dudley and Larson, 1976). Based on the findings of the DPTF, the pupfish were one of the first species added to the Endangered Species Act of 1973 (Dudley and Larson, 1976) and ground-water pumping in the Devils Hole area was reduced.

Water levels in Devils Hole began recovering after ground-water pumping was reduced in the 1970's. Currently, water levels are declining in Devils Hole. The purpose of this study is to examine the effects of long term tectonic deformation in relation to water-level fluctuations in Devils Hole. The carbonate rock aquifer that encompasses Devils Hole contains multiple fractures and faults where ground-water

movement is dominated by compartmentalized flow. Larger well defined faults in proximity to Devils Hole could impact the stress field in the Devils Hole area by annual slippage. This could influence compartmentalized flow, aquifer porosity, and hydraulic head values resulting in long term effects on ground-water levels.

1.2 STUDY AREA

Devils Hole is located in Ash Meadows National Wildlife Refuge (NWR) , which is a detached unit of Death Valley National Park in Nevada. NWR is situated near the California-Nevada border in Nye County, Nevada (Fig. 1-1). NWR was established in 1984 and contains more than 89 km^2 of wetlands. It was officially included into Death Valley National Monument in 1952 by Presidential Proclamation (Dudley and Larson, 1976). It is approximately 120 km west-northwest of Las Vegas, Nevada.

Locally, Devils Hole resides at the contact of a rock outcrop and a desert basin that borders the eastern flank of the Amargosa Desert. The outcrop of rock is part of the lower carbonate rock aquifer (Denny and Drewes, 1965), which is discussed in Chapter II. The ridge formed by the outcrop trends in the same direction as the Amargosa Desert, to the north-northwest. Devils Hole is located on the southern most tip of this ridge.

The study area is characterized by low lying desert basins, outcropping rock units, and large mountain ranges. Multiple lithologies and fault zones exist in the study area that lead to the complexity of ground-water flow. Adding to the complexity of the ground-water system are the climatic controls of the study area and
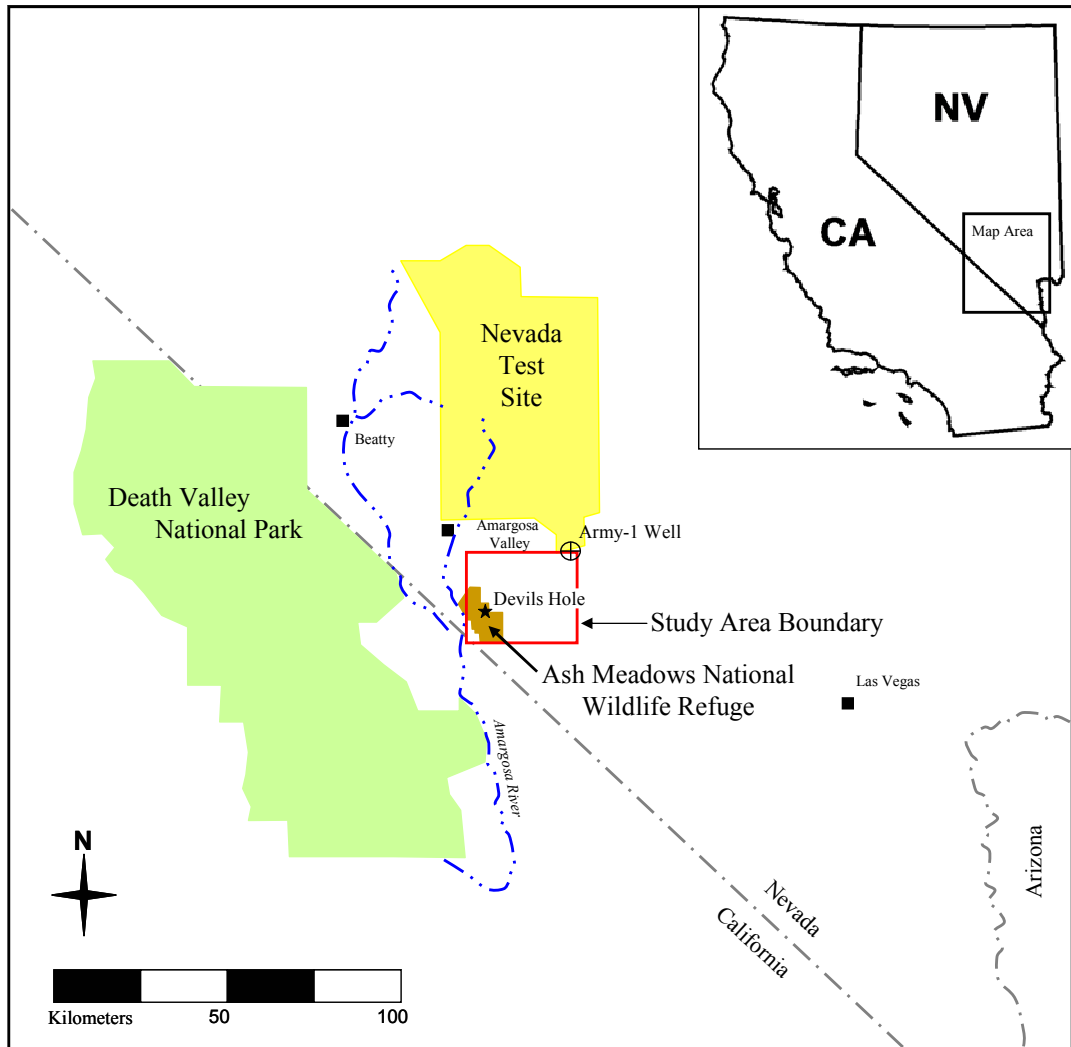
Figure 1-1. Location map.

the presence of a natural spring line. Since the study area encompasses both desert basin areas and mountainous regions, large fluctuations in evapotranspiration and precipitation occur.

1.3 HYDROLOGIC ENVIRONMENTS

1.3.1 Physiography

The study area is defined by desert basins and mountain ranges generally trending from north to south. Elevations in desert basins range from 640 m to 700 m above sea level. The mountain ranges that outline the study area include the Amargosa Ridges, Specter Mountains, and Spring Mountains (Fig. 1-2). These mountain ranges extend above the basin floor about 100 m, 800 m, and 1200 m, respectively. The principal desert basin in the study area extends some 21 km north-south between the Specter Mountains and Amargosa Ridges to cover an area of approximately 340 km^2.

Extending beyond the study area to the northeast where ground-waters originate that feed into the study area, mountain ranges trend to the northeast and parallel each other (Fig. 1-2). Mountain ranges cover lengths up to 128 km along their trendlines; basins between these ranges are 8 to 24 km across (Harrill and Prudic, 1998). Elevations of these mountain ranges are 1524 m to 2700 m, which are noticeably higher than those present in the study area (Waddell et al., 1984).

1.3.2 Drainage

The drainage basin that feeds ground-water to Ash Meadows is roughly 10,000 km^2 (Laczniak et al., 1996). The outline of the drainage basin is referenced on
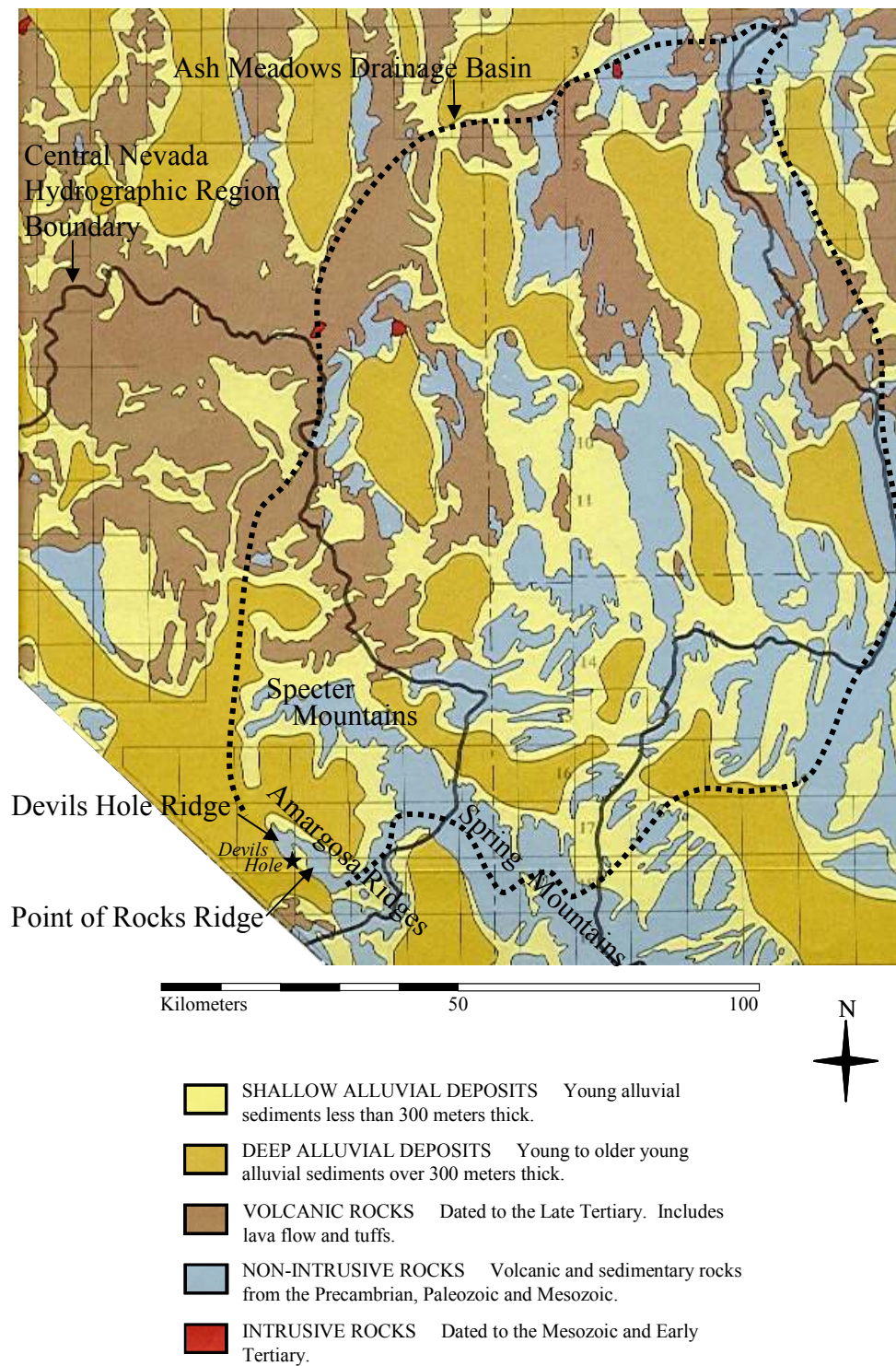
Figure 1-2. Regional geology of southern Nevada. Figure modified from Archbold (1972).

Figure 1-3. The boundaries to the drainage area were defined by Dudley and Larson (1976) based on the locations of mountainous ground-water divides and faults. Ground-water travels through the drainage basin through a carbonate rock aquifer, which is present throughout the drainage basin. Ground-water discharges through evapotranspiration and through the occurrence of a natural spring line.

1.3.3 Climate

The climate of the study area is arid in the desert basins to semiarid in the mountain ranges. Temperatures in the desert basins average 60˚F annually with daily fluctuations from minimum to maximum temperatures of about 50˚F (Eakin et al., 1976). Mean annual humidity values of desert basins are less than 10 percent (Prudic et al., 1995). The low humidity is representative of limited overcast days with light to moderate winds, which cause increased evaporation (Eakin et al., 1976). The changes in topography cause large temperature differences between basins and mountain areas in the study area. Because of this, it is estimated that temperatures in mountain ranges average 50˚F annually. Annual mean humidity in the mountain ranges is greater than the desert basins and is about 20 percent (Eakin et al., 1976).

1.4 WATER-LEVEL MONITORING AND FLUCTUATIONS

The water level in Devils Hole has been monitored by the National Park Service (NPS) since 1989. Water levels are measured every 15 minutes in Devils Hole by instrumentation installed near the water surface (Fig. 1-4). The water level is measured as the distance from the water level to a general datum bolt that was installed in 1962 on the north wall in Devils Hole (Dudley and Larson, 1976). The
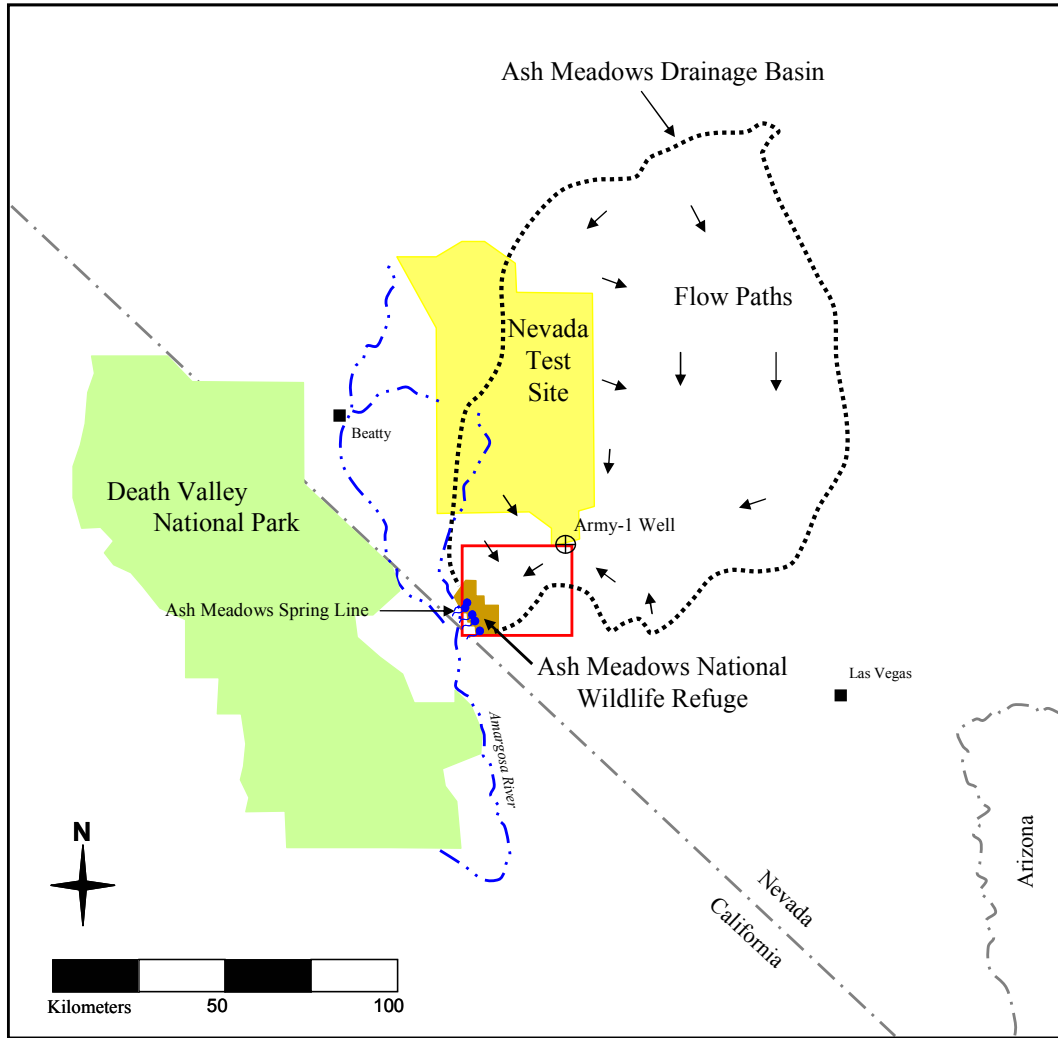
Figure 1-3. Drainage boundary and flow paths of ground-water for Ash Meadows National Wildlife Refuge. The boundary is based off interpretations of Winograd and Thordarson (1975) and Dudley and Larson (1976).
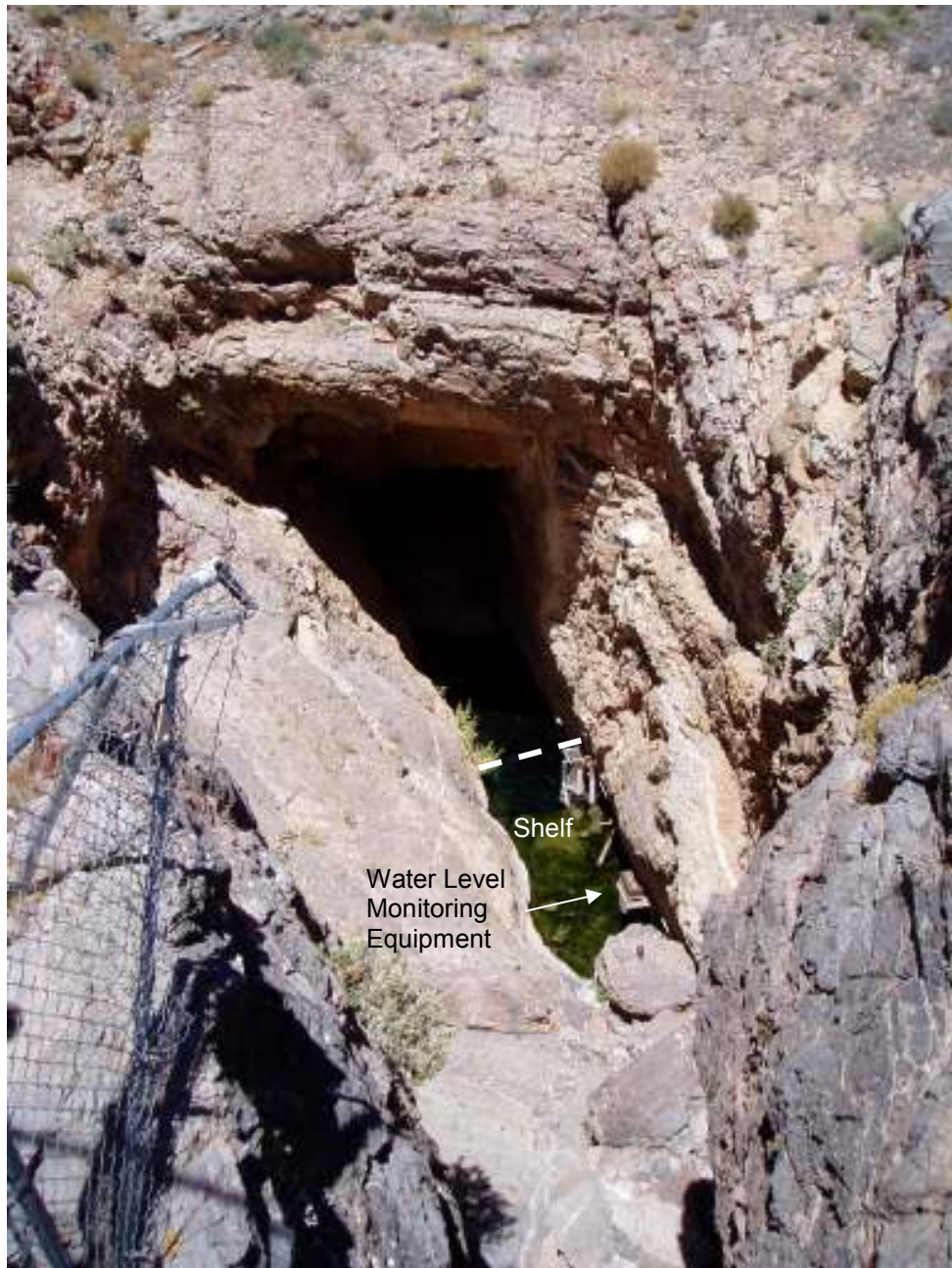
Figure 1-4. Photograph of Devils Hole taken from the south in May, 2005. Water-level monitoring equipment is located in the south end of the pool over the shelf.

NPS records document that from the period of 1989 to 2000, the water level in Devils Hole declined at a rate of 0.71 cm/yr (Fig. 1-5). Causes of water-level fluctuation in Devils Hole have been studied and eluded to by Dudley and Larson (1976), Winograd and Szabo (1986), and Winograd and Thordarson (1975) where ground-water pumping was primarily addressed. NPS implements and supports studies investigating short-term water-level fluctuations and long-term declines. These studies have included earth tides, climatic effects, ground-water pumping, and earthquake related water-level changes.

Earth tides are the tidal forces caused by the Moon on the structure of the lithosphere. The pull of the moon can change the storage volume within the carbonate aquifer through elastic deformation. Contraction will lessen the storage volume; expansion will increase the storage volume and reduce the water level. This is a well documented phenomenon. Earth tide magnitude is not continuous though time; peak water-level fluctuation due to tidal forces is on a biweekly cycle (Dudley and Larson, 1976).

Similar to tidal loading are the effects of barometric pressure. Dudley and Larson (1976) note that a large barometric event can cause up to 3 cm of change in the water level from its mean value. In addition to barometric pressure, localized atmospheric pressure differences can also have an effect on the water level. Wind gusts and high winds can lead to increased or decreased pressure on the pool water and thus water-level fluctuations. These fluctuations do not extend for large periods of time and are recorded as noise on a hydrograph (Dudley and Larson, 1976).
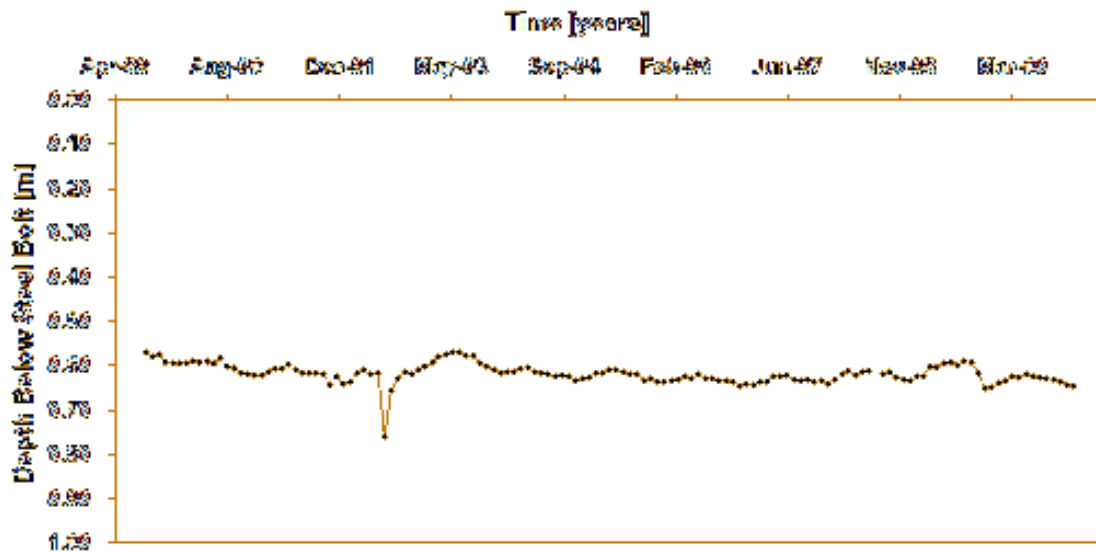
Figure 1-5. Observed monthly mean water level in Devils Hole measured as a distance below a reference datum. The large spike in 1992 is from the Landers and Little Skull Mountain earthquakes. A constant decline of 0.7 cm/yr is apparent from 1989 to 2001.

Ground-water pumping is the primary reason for large scale fluctuations in the water level in Devils Hole. For the period of 1969 to 1971, an extensive study was performed by Dudley and Larson (1976) to examine the effects of local ground-water pumping on the water level in Devils Hole. In their study, they were able to attribute water-level declines and recoveries in Devils Hole to individual production rates of pumping wells in the Ash Meadows area. Water-level declines on the order of 0.3 to 21.0 cm were observed due to ground-water pumping. Although pumping in the Ash Meadows area ceased in the mid-1970's, distant pumping can be correlated to ongoing declines in the water level in Devils Hole (Bedinger and Harrill, in press). The Army-1 pumping well, located on the southern boundary of the Nevada Test Site, is just northeast of the study area approximately 29 km from Devils Hole (Fig. 1-1). The pumping record for this well is depicted in Figure 1-6. Using a Theis curve approximation, Bedinger and Harrill (in press) matched the long term decline of the water level in Devils Hole to the pumping rate occurring at the Army-1 well. Ground-water pumping may explain the overall long term trend in water levels, but ignores daily to yearly fluctuations presumably due to tidal loading, precipitation, and seismic events. Ground-water pumping is considered the dominating factor in determining the overall long term trend in water levels in Devils Hole.

Seismic waves caused from earthquakes are documented to cause large scale, short term water-level fluctuations in Devils Hole (Cutillo and Ge, in press). In general, factors that influence earthquake related water-level fluctuations are earthquake magnitudes, depths and locations in proximity to observed water-level changes. In addition, rock and sediment types, aquifers and aquitards, and geometries
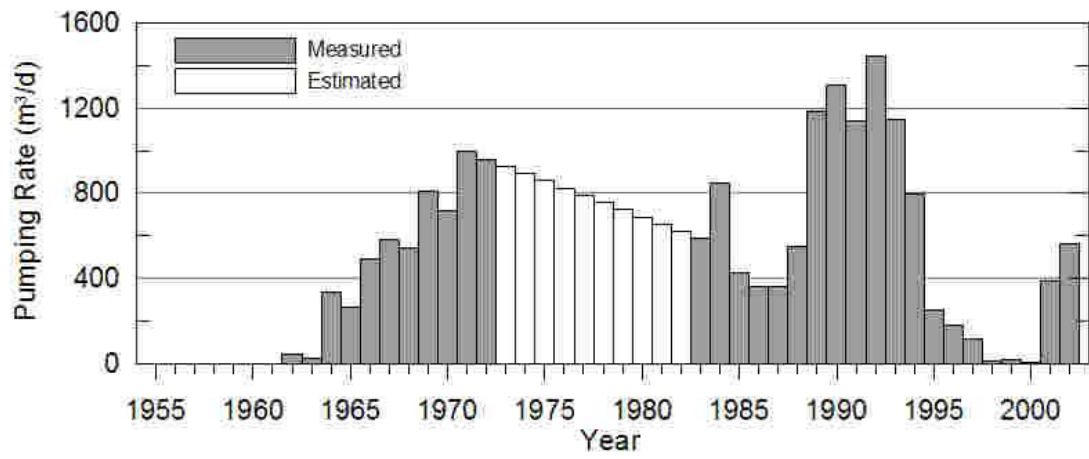
Figure 1-6. Pumping record of the Army-1 Well (Bedinger and Harrill, in press).

of locations where water-level fluctuations are observed need to be considered (Sneed et al., 2003). It has been well documented that earthquakes, even at far distances, have caused water-level fluctuations in wells, streams, and springs (Vorhis, 1966; Fleeger et al., 1999; Quilty et al., 1995; Rojstaczer and Wolf, 1992; Muir-Wood and King, 1993). Devils Hole is located in a region where small seismic events occur frequently. Seismic waves generated by large earthquakes occurring in the Devils Hole area and even as far away as Chile induce water-level changes in Devils Hole (Dudley and Larson, 1976). Earthquakes open and close crustal fractures and faults to alter water levels (Muir-Wood and King, 1993). Large earthquakes have also caused instrument failure in Devils Hole. Earthquakes occurring on July 30, 1972, and January 30, 1973, in Alaska and Mexico, respectively, caused fluctuations so great that the float used to measure water level was disabled (Dudley and Larson, 1976).

Work done by Montgomery and Manga (2003) and Muir-Wood and King (1993), indicates that stress and strain fields due to faulting and earthquakes can have effects on water levels in one or multiple wells. This is especially true for locations where active stress and strain fields are imposed on aquifers. Ground-water levels in aquifers can reflect the stress and strain imposed on the aquifer by increasing or decreasing through time. Typically, ground-water levels will recover to pre-earthquake levels with time; however, continuous changes in ground-water levels can be observed (Montgomery and Manga, 2003).

Muir-Wood and King (1993) document that wells and springs located adjacent to active faults and fractures can produce ground-water levels atypical of regional

ground-water levels monitored in wells and springs at greater distances from the faults and fractures. The geometry of faulting also has been shown to influence different ground-water responses. Normal faulting in stress and strain fields are more likely to yield ground-water level fluctuations; strike-slip faulting creates complex ground-water flows and may not have as large an influence on ground-water levels (Muir-Wood and King, 1993). It should be stated that the stress or strain field in an area is not always constant and can vary in space. In a strain field where a fault is present, the strain directly adjacent to the fault is typically greater in magnitude than the strain present in the surrounding field. Indication of variance in strain magnitude would be greater spring discharges in close proximity to a fault than spring discharges farther away from the fault (Muir-Wood and King, 1993). These concepts are applicable to Devils Hole because of its proximity to faulting and the occurrence of the Ash Meadows spring line.

1.5 ORIGINS OF DEVILS HOLE

The formation of Devils Hole is currently debated. Two competing theories exist for the formation of Devils Hole. The first is that Devils Hole was opened by faulting and continues to develop due to faulting (Riggs et al., 1994). The second theory incorporates the concept of dissolution of carbonate rock with faulting (Winograd and Thordarson, 1975; Dudley and Larson, 1976). In the latter, faulting opens pathways for ground-water to pass through and the continuous flow of ground-water erodes the carbonate rock away.

It is documented that there is a large network of faults in and around Devils Hole (Carr, 1988). These passageways allow for surface water to percolate through and enter the ground-water system. It is also well documented that Devils Hole is located within a regional carbonate rock aquifer (Carr, 1988). Given these factors, a large cavern will typically form due to dissolution of the carbonate rock by the water flowing through faults and fractures (Riggs et al., 1994). An instrumental factor in forming this type of open cavern in a rock is that the water needs to be able to flow through the system. Fresh waters that are not in equilibrium with the carbonate rock need to continue to enter the system to dissolve the carbonate rock while calcite-rich waters are discharged or calcite is deposited elsewhere.

The deposition of calcite on the walls in Devils Hole is common (Dudley and Larson, 1976). The water within Devils Hole is slightly supersaturated with respect to calcite. Therefore, instead of the water in Devils Hole eroding the carbonate rock away, it deposits calcite onto the walls of Devils Hole much like tree rings grow from the center of a tree. The calcite present on the walls can show major water-level fluctuations in Devils Hole (Szabo et al., 1994), but also lead Riggs et al. (1994) to believe that Devils Hole is formed from faulting rather than carbonate rock dissolution. If calcite is being deposited on the walls of Devils Hole, then calcite dissolution is not taking place or is less than growth. The rate of calcite growth in Devils Hole is high and the open fractures in Devils Hole should be filled with calcite; however, the fractures remain open. An explanation for this is that the fractures are opening at rates greater than calcite growth. If dissolution is the primary

factor forming Devils Hole, there should be more openings present and Devils Hole should not exhibit extensive calcite growth (Riggs et al., 1994).

This argument is expanded to include the dissolution of carbonate rock along a fault zone. Dudley and Larson's (1976) argument involves the faults present in Devils Hole and the general geometry in Devils Hole. This accounts for faulting and carbonate rock dissolution. An earlier study by Winograd and Thordarson (1975) supports their view with evidence from caverns within the carbonate rock aquifer. A general statement made by Winograd and Thordarson (1975) is that without the presence of caverns in the carbonate rock aquifer, spring lines could be more continuous. The results of hydraulic tests performed on the lower carbonate rock aquifer suggest that transmissivities vary widely within a well at different depths and between wells at similar depths in the aquifer (Winograd and Thordarson, 1975). The line of springs that exists to the west of Devils Hole trends to the northwest. The discharge from the springs is high. A maximum transmissivity of 11,177 m^2/d was measured on a fracture within the aquifer by Winograd and Thordarson (1975). Because of the tremendous discharge that occurs in the springs, it is postulated that flow occurs from large caverns of water through faults and fractures that have formed in the lower carbonate aquifer (Winograd and Thordarson, 1975).

CHAPTER II

GEOLOGY

2.1 REGIONAL GEOLOGY

The geology around and in Devils Hole is complex (Fig. 2-1). Many faults exist in the formations surrounding Devils Hole (Denny and Drewes, 1965). Two major periods of deformation occurred in the past in the Devils Hole area that helps explain the complex geology. The first was during the late Mesozoic, which folded and thrust faulted Precambrian and Paleozoic rocks. The second occurred in mid to late Cenozoic time, which created the basin and range topography through normal faulting. Both periods experienced strike-slip faulting (Winograd and Thordarson, 1975).

The major rock formations around Devils Hole are the Bonanza King Formation, the Alluvium, Alluvial fan deposits and Playa deposits (Denny and Drewes, 1965). The large outcrops that create the hills surrounding Devils Hole are the Amargosa ridges. The outcrop that holds the opening to Devils Hole is referred to as the Devils Hole ridge. The adjacent ridge to the southeast is Point of Rocks ridge. This naming convention is used in this thesis. Both ridges contain large sections of the Bonanza King Formation, which is part of the carbonate rock aquifer, and trend northwest (Carr, 1988).

2.1.1 Bonanza King Formation

The opening to Devils Hole resides in the Bonanza King Formation (Denny and Drewes, 1965). The Bonanza King Formation is part of a larger carbonate rock
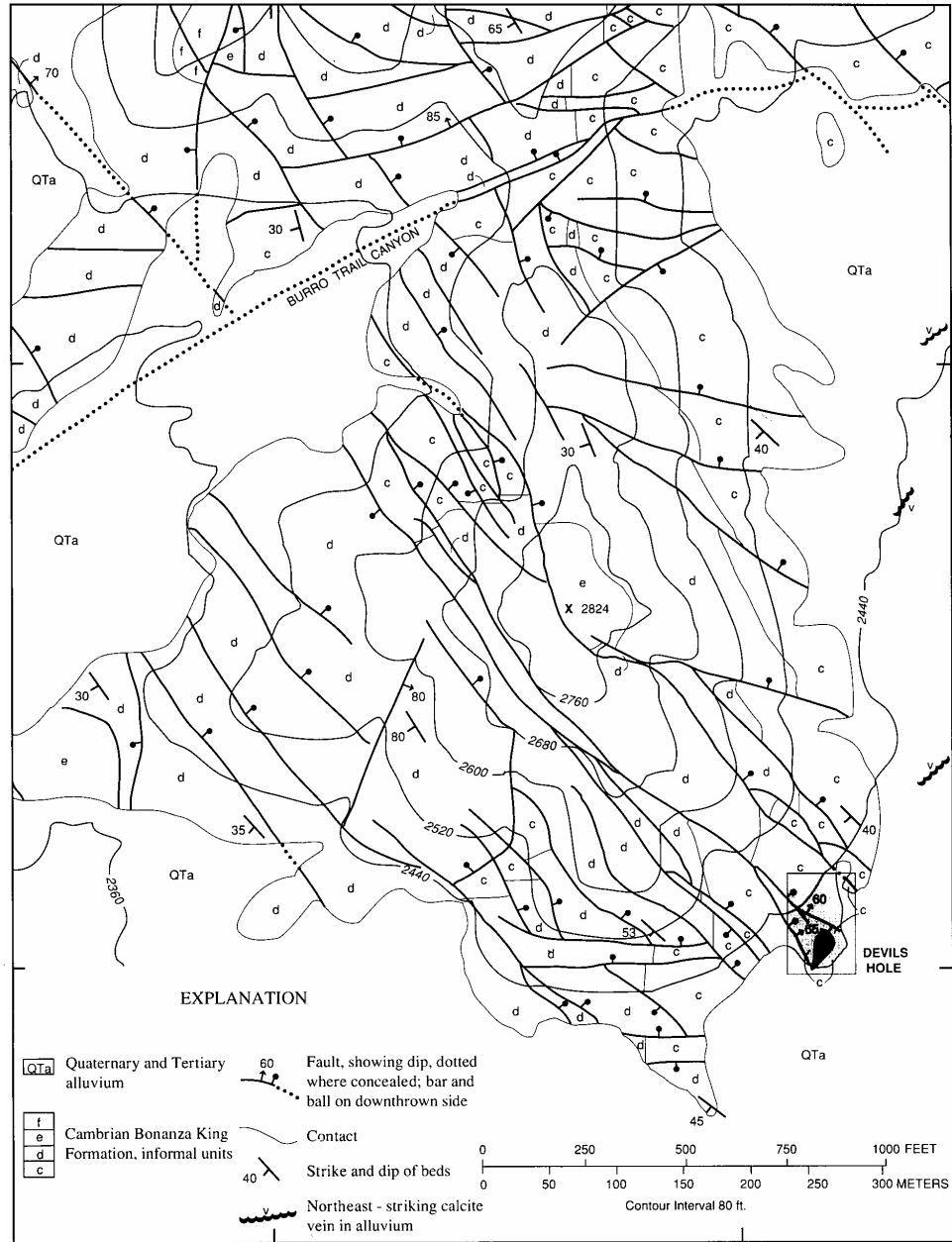
Figure 2-1. Faults and fractures in the Devils Hole area. A proposed fault follows the trend of the Burro Trail Canyon indicated on the figure. Figure taken from Carr (1988).

formation known as the lower carbonate rock aquifer (Carr, 1988). Denny and Drewes (1965) divide the formation into two layers, the upper and the lower, both of which are dated to the middle to upper Cambrian. The upper layer is classified as a banded limestone to dolomite consisting of light gray to medium gray bands with thicknesses from 183 m to 305 m (Hunt and Mabey, 1966). The basal unit of the upper layer is 30 m thick consisting of shale, red to brown siltstone, and fossiliferous limestone (Denny and Drewes, 1965). Hunt and Mabey (1966) state that the middle of the Bonanza King Formation consists of two light colored shaly sand zones 15 m thick or less that are separated from each other by 60 m. This is equivalent to the basal unit of the upper layer referred to by Denny and Drewes (1965). The upper of these zones is fossiliferous and contains trilobites (Hunt and Mabey, 1966). Atop the triolobite layer is another dark layer of dolomite which has a thickness of about 30 m. The lower layer is medium gray to dark gray limestone and dolomite with no reported thickness (Denny and Drewes, 1965; Hunt and Mabey, 1966). The total thickness of the lower carbonate rock aquifer is about 300 m to 400 m thick in the study area, but can reach over 1500 m in areas (Carr, 1988).

The outcrop of the Bonanza King Formation in which Devils Hole lies has multiple small faults (Fig. 2-1). The majority of the faults trend from southeast to northwest (Denny and Drews, 1965; Carr, 1988). The throw of the faults is typically 15 to 30 m, but can approach 60 m in some cases. Dips on the outcrop range from 20 to 45 degrees in the west to southwest directions. Strike and dip measurements taken in close proximity to Devils Hole indicate strikes of N 15 W and N 18 W with dips of 40 degrees west and 45 degrees west, respectively (Carr, 1988).

2.1.2 Alluvial Deposits

Menges (2005) mapped in detail the alluvial deposits around the Devils Hole and Point of Rocks ridges. Distinctions are made between young alluvial deposits, older young alluvial deposits, intermediate alluvial deposits, older intermediate alluvial deposits, and marl deposits (Fig. 2-2). All the alluvial fan deposits are composed of breccia, sand, silt and clay particles (Denny and Drewes, 1965). The particle size in the fans decreases with distance from the apex of the fan. On average, particle size decreases from 10.5 millimeters to 2.0 millimeters over the course of 5 km. The exposed top of the alluvial fans is typically coated with a dessert varnish from climatic effects (Denny and Drewes, 1965). Ages of alluvial deposits range from mid-Pleistocene to present (Menges, 2005; Carr, 1988).

Pleistocene and Pliocene are the dates given to the marl deposits (Menges, 2005) that are similar to the playa deposits documented by Denny and Drewes (1965) and the "Lake Bed" deposits by Carr (1988). These deposits extend into the Amargosa Desert from the Amargosa ridges and underlie the alluvial deposits (Menges, 2005; Carr, 1988). The boundary between the marl and alluvial fan deposits is where over half of the present material is sand, silt and clay. Those areas containing a majority of sand, silt and clay are the marl deposits (Denny and Drewes, 1965). The depositional environments for these deposits are shallow lakes, ponds, and playas (Hay et al., 1986). Sediments found in the marl deposits are fine grained clastic to clacareous sediments (Carr, 1988). In addition to the alluvial deposits discussed, basin fill sediments from the Miocene and eolian sand deposits from the Holocene are intermingled with these deposits farther into the Amargosa Desert (Menges, 2005).

Devils Hole Ridge

Devils Hole ★

Point of Rocks Ridge

Kilometers   2   3   4   5

N
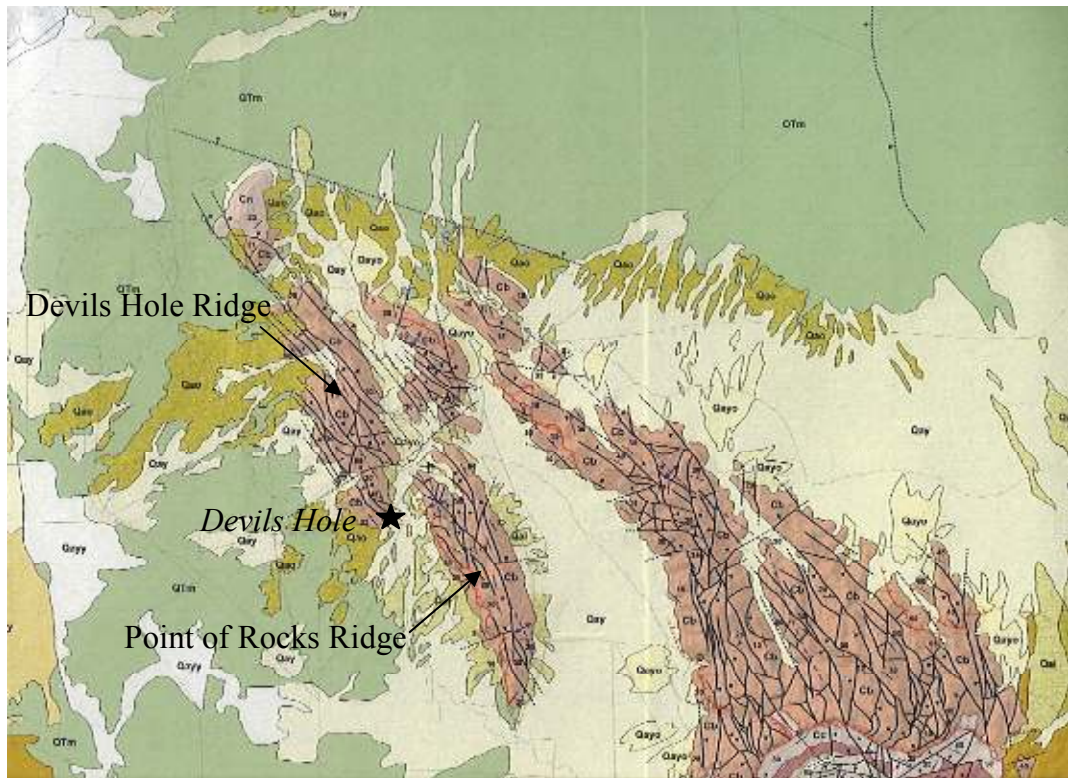
Qayy	Youngest alluvial deposits (Holocene)
Qay	Young alluvial deposits (Holocene)
Qayo	Older young alluvial deposits (middle and early Holocene)
Qai	Intermediate alluvial deposits (late and late-middle Pleistocene)
Qao	Older intermediate alluvial deposits (late(?) to early Pleistocene)
QTm	Marl deposits (Pleistocene and Pliocene)
Cn	Nopah Formation (Upper Cambrian)
Cb	Bonanza King Formation (Upper and Middle Cambrian)
Cc	Carrara Formation (Middle Cambrian)
——	Fault

Figure 2-2. Local geology in the Devils Hole area (Menges, 2005).

2.2 STRUCTURAL ELEMENTS

Two major fault zones are located in close proximity to Devils Hole, the Gravity Fault and the Ash Meadows fault zone. The locations of the fault zones are referenced on Figure 2-3. Both of these faults fall under the title of the Ash Meadows Fault System. The fault zones have large effects on the ground-water system as they can act as conduits or barriers to ground-water flow. The accepted understanding of the fault zones in the Devils Hole area is that they act as barriers to ground-water flow. The Gravity Fault and Ash Meadows fault zone are the principal locations where the lower carbonate rock aquifer is discontinuous and forces ground-water to the surface for discharge (Winograd and Thordarson, 1975).

The Gravity Fault is characterized as a large normal fault through the study area (Fridrich, 2005). It trends N 24 W for 30 km in the Ash Meadows area, then trends to the north at locations north of Ash Meadows (Schweickert and Lahren, 1997). The Gravity Fault terminates just north of the study area. The maximum offset is suggested as 1 km with a 60 degrees dip to the west. The carbonate rock aquifer is about 300 m to 400 m thick in the Ash Meadows area (Carr, 1988). The lower carbonate rock aquifer terminates into younger Quaternary sediments where hydraulic conductivities are not as great because of the offset caused by the Gravity Fault. The conductivity of the Gravity Fault is currently unknown. Efforts are currently being made by the NPS to estimate the conductivity.
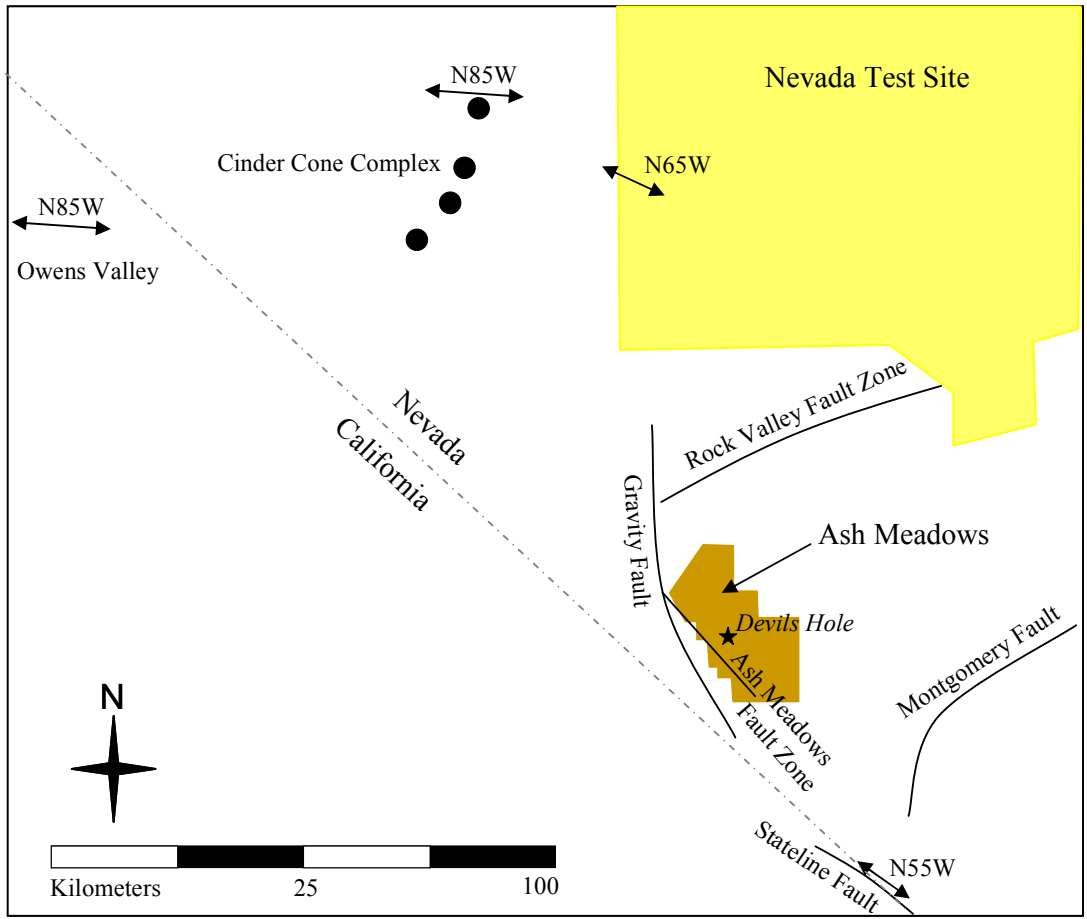
Figure 2-3. Locations of faults and strain measurements near Devils Hole. The Walker Lane Zone encompasses the area in the entire figure. Fault locations interpreted from Brocher et al. (1993) and Fridrich (2005).

The Ash Meadows fault zone is located in the eastern part of the Amargosa Desert in Nye and Inyo counties of Nevada and California, respectively, between Devils Hole and the Gravity Fault. The zone strikes N 24 W from south of the study area and continues north through Ash Meadows until it terminates into the Gravity Fault. The dip of the fault zone is to the west. Multiple small and discontinuous faults with normal faulting characterize the zone (Anderson et al., 1995). These faults are on the order of 4 km in length or less with at least 50 m of offset (Hay et al., 1986). Many scarp faces are present in the fault zone that exists on Pleistocene alluvium; therefore, activity on the fault line has been dated to the late Quaternary (Donovan, 1991). The Ash Meadows fault zone represents the first large barrier to ground-water flow that is encountered by ground-water flow originating in the Specter and Spring Mountains and traveling in the lower carbonate rock aquifer (Winograd and Thordarson, 1975). It is likely that the multiple small faults are causes for some of the spring discharges in the Ash Meadows area. The gaps between fault segments of this fault zone allow for ground-water to pass and continue towards the Gravity Fault area.

Other faults present in the study area are the Rock Valley fault zone and the Montgomery Fault (Fig. 2-3). The Rock Valley fault zone is located in the northern portion of the study area extending from the Ash Meadows Fault System to the northeast at about N 65 E. This fault zone is discontinuous allowing for ground-water to pass through it (Schweickert and Lahren, 1997). The Montgomery Fault is a low angle thrust fault that trends to the northeast in the southwest section of the study area. The quartzite that is uplifted by this fault marks the southern boundary to the

lower carbonate rock aquifer present in the study area. The uplifted quartzite acts as a ground-water divide where ground-water north of the fault travels into the study area; ground-water south of the fault travels into another drainage basin (Fridrich, 2005).

2.3 STRAIN ORIENTATION

The study area is located in an area of active tectonic strain. The Walker Lane Zone is a 700 km long zone of Cenozoic strike-slip (Bell et al., 1999), which incorporates the study area (Fig. 2-3). Orientations of strain were complied by Bellier and Zoback (1995) for different areas within the Walk Lane Zone. Those areas nearest to the study area exhibit values of N 85 W. These data are supported by the occurrence of a volcanic complex located to the northwest of the study area (Fig. 2-3). The volcanic complex is composed of four cinder cones in an arcing trend (Connor et al., 1998). If a curve is fit through the arc of the cinder cones, a perpendicular line to the arc at the northern most cinder cone can be fit that trends about N 85 W (Fridrich, 2005). Strain orientation south of the study area is revealed by an escarpment on the Stateline Fault that dates within the last 2,000 years. The trend of the escarpment is N 55 W (Fig. 2-3). The most realistic strain orientation for the study area is from the Nevada Test Site where an orientation of N 65 W is reported by the Global Positioning System (Wernicke et al., 1998; Savage, 1998).

2.4 GEOLOGY OF DEVILS HOLE

Devils Hole is a large opening in the lower carbonate rock aquifer adjacent to the contact between the Bonanza King Formation and the surrounding alluvium. The carbonate rock in this area is about 180 m thick (Riggs et al., 1994). The opening to

Devils Hole has three sides (Fig. 2-4). For the purposes of this thesis they will be named the west, north and east walls. The west wall trends N 26 E for about 25 m, the north wall trends N 47 W for about 5 m, and the east wall trends N 26.5 E for about 25 m (Carr, 1988). The southern end of the opening does not have a distinct border wall. The east and west walls come together to form a somewhat triangular shaped opening in the ground. The dimensions of the opening are roughly 25 m long by 8 m at the maximum extents (Carr, 1988).

The water level in Devils Hole is about 15 m below the surrounding ground surface. The water surface area measures about 3 m by 12 m with the reach trending from north to south (Worts, 1963). A roof covers the northern section of the water surface. The roof is visible from within Devils Hole and from the south (Fig. 1-4). The southern area of the pool is only 0.3 m to 0.6 m deep where a shelf has been created from falling rock debris or existing rock that is fractured and relocated (Riggs et al., 1994). The rocks creating the shelf have been wedged into place. An example of this is Anvil Rock, which marks the last rock on the northern edge of the floor (Fig. 2-5). Beyond Anvil Rock are unknown depths. Anvil Rock's origin is proposed as the location directly above its current location on the roof of Devils Hole. Other fallen rock fragments have been cemented to the walls of Devils Hole through calcite cementation due to the calcite rich waters. Riggs et al. (1994) show two dark layers of material on the tops of deposited rocks at the top of Devils Hole. These are areas where current surface runoff has carried sediments and small rocks into Devils Hole where they have been fixed by calcite growth.
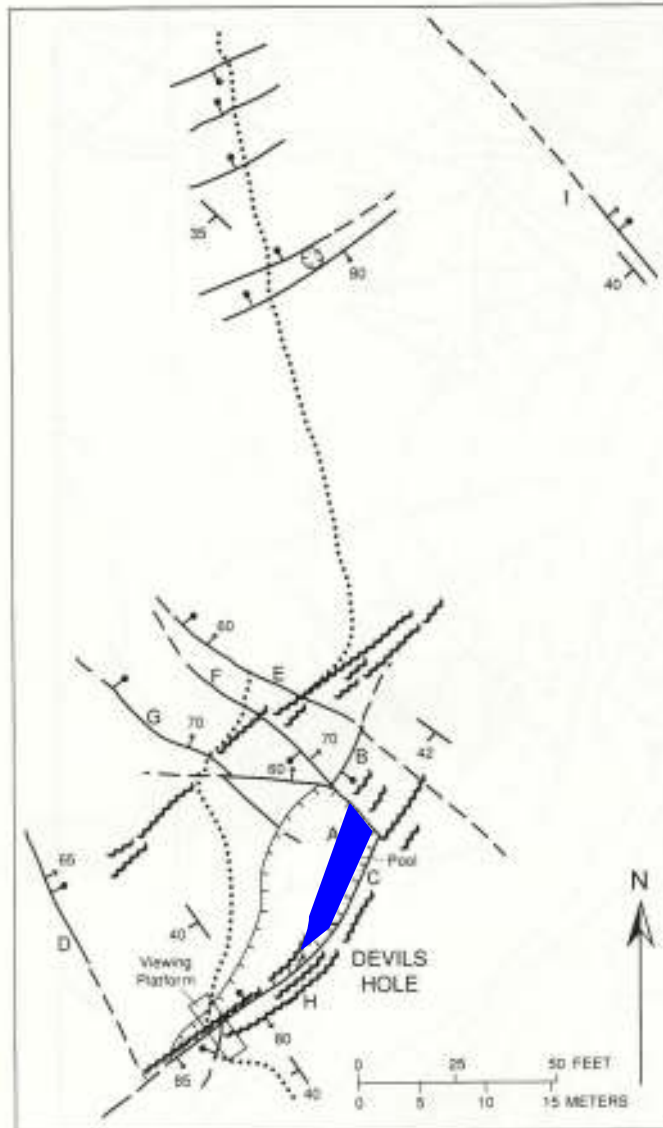
Figure 2-4. Local geology of Devils Hole interpreted by Carr (1988). Multiple calcite veins and faults trend in the northeast directions indicating that extension is in the northwest direction.
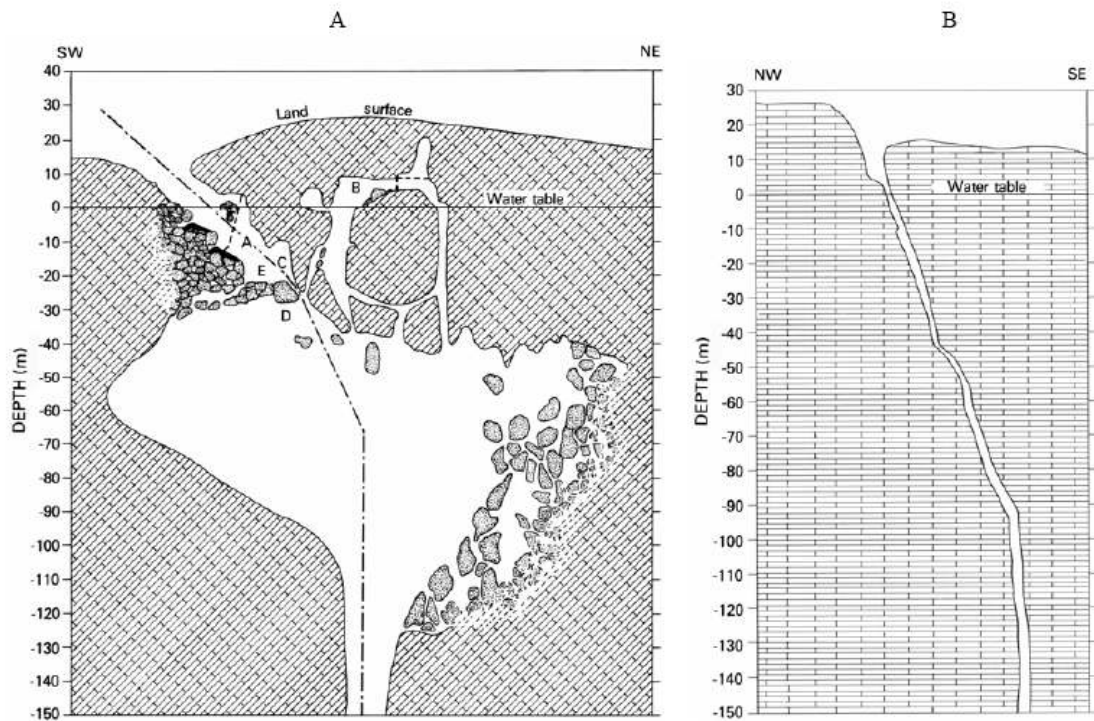
Figure 2-5. Cross sections through Devils Hole depicted by Riggs et al. (1988). Below 30 meters depth, cross sections are drawn from Riggs' memory. Horizontal scales in both cross sections are the same as vertical scales. A) Large amounts of carbonate rock are missing either from dissolution and/or faulting causing the rock to fall. Dark areas near A and E represent calcite deposits on fallen rock. Anvil rock is located above letter D and thought to have fallen from the area above letter C. B) Cross section that shows Devils Hole follows a relatively constant 70 to 80 degrees dip of a fault into the ground.

Inside the opening and present in the surrounding rock of Devils Hole are calcite veins. Calcite veins outside the east wall trend in the same direction as the east wall (Carr, 1988). It is noted that the fracture parallel to the east wall is open and contains a calcite vein. This indicates that the entire east wall of Devils Hole is unstable (Riggs et al., 1994) and that extension is occurring in the northwest direction. Calcite veins within Devils Hole are present in the center of the southern half of the opening. These calcite veins also trend along the same path as the calcite veins located outside of Devils Hole (Carr, 1988).

The dimensions inside of Devils Hole change drastically with depth. Following a 70 to 85 degree southeast dipping planar fissure, the dimensions of Devils Hole shorten in the first few meters from the surface (Riggs et al., 1994). After the contraction in dimensions, the length of Devils Hole increases with depth to a maximum of over 100 m at 70 m depth. Beyond 70 m depth, the opening narrows with depth to an average of less than 2 m for the remainder of the known depth. The total depth of the hole is unknown.

CHAPTER III

HYDROGEOLOGY

3.1 OVERVIEW

Devils Hole is located within the Great Basin, which incorporates most of Nevada and western Utah (Fig. 3-1). It is about 362,598 km^2 (Harrill and Prudic, 1998) and is underlain with consolidated rocks and unconsolidated to semi-consolidated deposits (Plume, 1996). The mountain ranges running through the Great Basin are characteristically parallel and trend north-south due to extension (Harrill and Prudic, 1998; Laczniak et al., 1996). The ranges are typically separated 8 km to 24 km apart (Harrill and Prudic, 1998) with elongated valleys between (Laczniak et al., 1996). Tertiary volcanism is responsible for the current topography in the Great Basin (Dudley and Larson, 1976). The ranges and valleys help to define hydrologic sub-basins within the Great Basin. A sub-basin is defined by ground-water recharge paths and flow paths to surface discharge (Fenelon and Moreo, 2002).   The boundaries are locations where ground-water movement is limited.   The sub-basin used to define the drainage to Ash Meadows is defined in Figure 1-3.

3.2 AQUIFERS

Several different aquifers are present in the region around Devils Hole (Fig. 3-2). The most prevalent of these in the vicinity of Devils Hole are the valley fill aquifer, the volcanic rock aquifer, and the lower carbonate rock aquifer. The valley fill aquifer is composed of alluvial fan and fluvial deposits that are unconsolidated to poorly consolidated. The valley fill aquifers are present in most locations

41
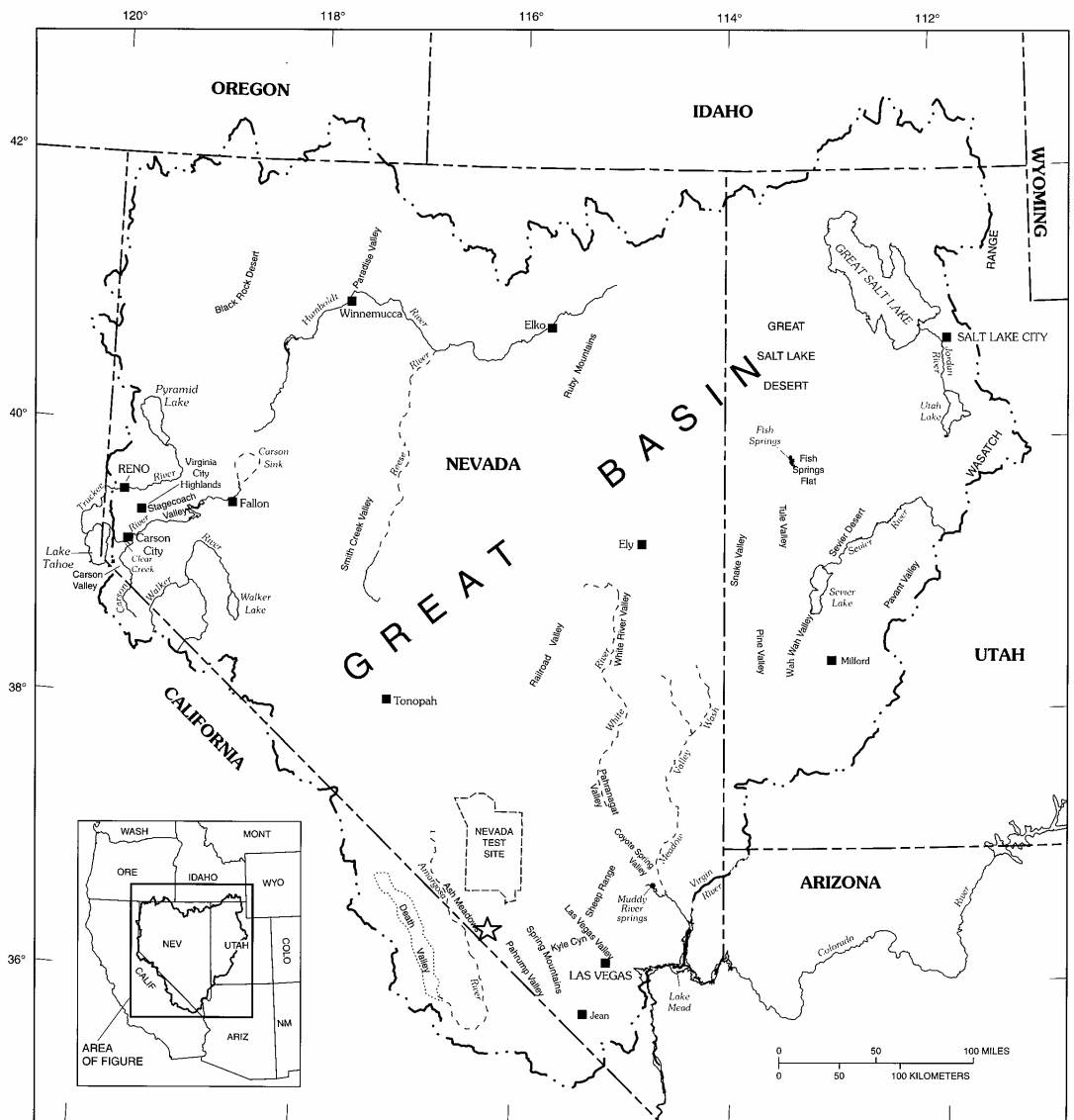
Figure 3-1. Location and extent of the Great Basin area defined by the dashed and dotted line. Ash Meadows is located in the southern part of the Great Basin at the star. Figure modified from Harrill and Prudic (1998).

System	Series	Stratigraphic Unit	Major lithology	Maximum thickness (m)	Hydrogeologic Unit
Quaternary and Tertiary	Holocene, Pleistocene, and Pliocene	Valley fill	Alluvial fan, fluvial, fanglomerate, lakebed, and mudflow deposits	600	Valley-fill aquifer
Tertiary	Pliocene	Basalt of Skull Mountain	Basalt flows	75	Volcanic rock aquifer
		Timber Mountain Tuff	Ash-flow tuff, moderately to densely welded	260	Welded tuff aquifer
	Miocene	Bedded tuff	Ash-flow tuff and fluvially reworked tuff.	305	Bedded tuff aquifer
		Wahmonie Formation	Lava-flow and interflow tuff and breccia; locally hydrothermally altered.	1220	Lava flow aquitard
		Salyer Formation	Breccia flow, lithic breccia, and tuff breccia, interbedded with ash-fall tuff, sandstone, silt-stone, and claystone.	610	Tuff aquitard
		Indian Trail Formation	Ash-flow tuff	760	
	Miocene and Oligocene	Tuff of Crater Flat	Ash-flow tuff, nonwelded to partly welded, interbedded with ash-fall tuff.	90	
Permian and Pennsylvanian		Tippipah Limestone	Limestone	1100	Upper caboante aquifer
Mississippian and Devonian		Eleana Formation	Argillite, quartzite, conglomerate, limestone.	2400	Upper clastic aquitard
Devonian	Upper	Devils Gate Limestone	Limestone, dolomite, minor quartzite.	>420	Lower carbonate aquifer
	Middle	Nevada Formation	Dolomite	>460	
Ordovician	Upper	Ely Springs Dolomite	Dolomite	90	
	Middle	Eureka Quartzite	Quartzite, minor limestone.	100	
	Middle to Lower	Antelope Valley Limestone	Limestone and silty limestone	460	
	Lower	Ninemile Formation	Claystone and limestone, interbedded.	108	
	Lower	Goodwin Limestone	Limestone	>275	
Cambrian	Upper	Nopah Formation	Dolomite, limestone	325	
	Middle	Bonanza King Formation	Limestone, dolomite, minor siltstone	745	
	Middle	Carrara Formation	Siltstone, limestone, interbedded	610	
Precambrian		Stirling Quartzite	Quartzite, siltstone.	1040	Lower clastic aquitard

Figure 3-2.   Stratigraphic column showing the principal rock units present in the study area. Modified from Winograd and Thordarson (1975).

surrounding outcropped rock. The confining layers for the valley fill aquifer are ancient lake beds and playa deposits, volcanic ash beds and mudflows (Fenelon and Moreo, 2002). The volcanic rock aquifer originates from lava flow deposits that occurred in the Cenozoic and underlie most basin alluvial deposits in the study area (Plume, 1996). The principal aquifer in the Ash Meadows area is the lower carbonate rock aquifer. The lower carbonate rock aquifer is very extensive and exists throughout the Ash Meadows sub-basin. It is typically confined at locations within basins and unconfined under ridges (Fenelon and Moreo, 2002).

3.2.1 Valley Fill Aquifer

The valley fill aquifer is present in most areas surrounding the Amargosa Ridges. It is composed of alluvial fan, fluvial, fanglomerate, lakebed and mudflow deposits (Winograd and Thordarson, 1975) of unconsolidated sediments including sand, silt, gravel and clay (Harrill and Prudic, 1998). The sediment clasts range in size from cobble sized rocks to clays (Winograd and Thordarson, 1975). Typically, the aquifer is unsaturated or locally saturated. The aquifer shows generalized poor sorting with poor stratification.

The connectivity of the valley fill aquifer to other aquifers varies throughout the Great Basin, but commonly the valley fill aquifer is hydraulically connected to the underlying lower carbonate rock aquifer (Harrill and Prudic, 1998). The hydraulic conductivity of the valley fill aquifer varies both vertically and laterally due to compositional changes of the deposit (Harrill and Prudic, 1998). Values range from 0.006 to 43 m/d with a mean of 24 m/d and a median of 25 m/d (Bunch and Harrill,

1984, 115-118). The transmissivity of the aquifer ranges from 9.9 m^2/d to 422.26 m^2/d (Winograd and Thordarson, 1975).

3.2.2 Volcanic Rock Aquifer

The volcanic rock aquifer is located under most alluvial deposits in the study area (Plume, 1996). Stratigraphic units of volcanic rock aquifer ranging from 6 m to 9 m thick are typically interbedded with basin fill deposits. Hydraulic conductivities in this aquifer range from 0.5 m/d to 5 m/d (Plume, 1996). Ground-water transmitted through this aquifer and stored in this aquifer typically progresses stratigraphically downward into the underlying lower carbonate rock aquifer with time (Winograd and Thordarson, 1975).

3.2.3 Lower Carbonate Rock Aquifer

The lower carbonate rock aquifer present in the Devils Hole area is pervasive throughout most of eastern Nevada and extending into western Utah (Harrill and Prudic, 1998). The Wasatch Range and Colorado Plateau bound this aquifer to the east; volcanic fields south of the Snake River Plain bound it to the north; the west is bounded by increased amounts of clastic rocks and chert through central Nevada; and the south is truncated onto Precambrian crystalline basement rock (Plume, 1996). The lower carbonate rock aquifer ranges from about 1,500 m to 9,150 m in thickness (Harrill and Prudic, 1998) and includes the following rock formations (Fig. 3-2): Carrara Formation, Bonanza King Formation, Nopah Formation, Goodwin Limestone, Ninemile Formation, Antelope Valley Limestone, Eureka Quartzite, Ely

Springs Dolomite, Nevada Formation and the Devils Gate Limestone (Winograd and Thordarson, 1975). In the Devils Hole area, the upper portion of the lower carbonate rock aquifer is not present. Only the upper portion of the Carrara Formation, the Bonanza King Formation and the Nopah Formation are present in the Ash Meadows area (Dudley and Larson, 1976). These account for roughly 2130 m of the aquifer. The base of the lower carbonate rock aquifer is marked by the contact with metamorphic, igneous, and sedimentary rocks dating to the Precambrian and Lower Cambrian (Harrill and Prudic, 1998).

The lower carbonate rock aquifer is dated to the Middle Cambrian to Devonian (Winograd and Thordarson, 1975; Plume, 1996). It is the principal means for ground-water flow in the Ash Meadows sub-basin. The saturated thickness of the lower carbonate rock aquifer ranges from hundreds to thousands of meters (Winograd and Thordarson, 1975). The aquifer is typically saturated except in areas of outcrop, where it is unsaturated. The Devils Hole ridge and the Point of Rocks ridge are both areas where the lower carbonate rock aquifer is unsaturated, but in Devils Hole it is saturated.

The lower carbonate rock aquifer is heavily fractured. The primary conduits of flow within the lower carbonate rock aquifer are the fractures and joints (Winograd and Thordarson, 1975; Dudley and Larson, 1976; Plume, 1996). The fractures and joints have probably been influenced by calcite dissolution where flow rates are high with transmissivities up to 10,000 m^2/d (Waddell et al., 1984). The sections of the aquifer that are not fractured have low transmissivities (Dudley and Larson, 1976). Plume (1996) defines solution widened fractures and joints as being less than a

centimeter to a few centimeters wide whereas solution channels are defined between centimeters to tens of meters. In exposed areas, chemical and physical weathering has increased the porosity of the fractures. The penetration depth of weathering ranges from meters to tens of meters dependent on the area (Winograd and Thordarson, 1975).

3.3 GROUND-WATER RECHARGE

Recharge to the ground-water system is mainly due to precipitation in the higher elevations northeast of the study area (Winograd and Thordarson, 1975; Harrill and Prudic, 1998; Fenelon and Moreo, 2002). Precipitation is more likely in higher elevations in the Ash Meadows sub-basin. Snow is unlikely at Devils Hole, but common during the winter months in the mountain ranges that comprise the northern portions of the Ash Meadows sub-basin. The spring melt of the snow infiltrates into the ground along with surface waters created by other precipitation events to recharge the ground-water system. Once water has entered the ground, it moves through the Ash Meadows sub-basin in the lower carbonate rock aquifer (Winograd and Thordarson, 1975). Recharge that occurs in the Ash Meadows sub-basin from the northeast is likely from beneath the Spring Mountains where the lower carbonate aquifer is highly fractured (Fenelon and Moreo, 2002; Laczniak et al., 1996). Other sources of recharge are minimal in comparison to precipitation. They include seepage of ground-water from the valley fill aquifer into the lower carbonate rock aquifer and flow from the northwest (Winograd and Thordarson, 1975; Fenelon and Moreo, 2002).

Precipitation in the desert basins also needs to be considered for the study area. Precipitation in these areas is the leading source for water in the alluvial aquifer. Historical precipitation data for locations throughout Nevada is managed by the Western Regional Climate Center (2006). Precipitation gauges are located at Amargosa Farms for desert basins in the Devils Hole area. Mountain precipitation rate is recorded in the Spring Mountains (Fenelon and Moreo, 2002). Yearly records of precipitation are plotted in Figure 3-3. There is a noticeable difference in the precipitation rates in the desert basins versus the mountain areas. Desert basins average 0.0002 m/d (Western Regional Climate Center, 2006) of precipitation where mountainous areas average 0.0015 m/d (Fenelon and Moreo, 2002) in the study area over the time span of 11 years.

3.4 GROUND-WATER DISCHARGE

Water exits the Ash Meadows area through evapotranspiration and to a larger extent through spring discharge (Winograd and Thordarson, 1975; Waddell et al., 1984; Fenelon and Moreo, 2002). Evapotranspiration occurs through low lying vegetation in the desert basins and on larger rock outcrops, and through bare soil (Fig. 3-4). Evapotranspiration is accountable for a large amount of ground-water loss. Walker and Eakin (1963) indicate that evapotranspiration can account for 1×10^7 m^3/d to 3×10^7 m^3/d of ground-water discharge from the study area. Evapotranspiration is estimated between 5×10^{-4} m/d and 7×10^{-3} m/d by Laczniak et al. (1999) for locations in the Ash Meadows area. The upper limit to these estimations is taken from an open water body; the majority of measurements are proximal to the lower limit. Rates of
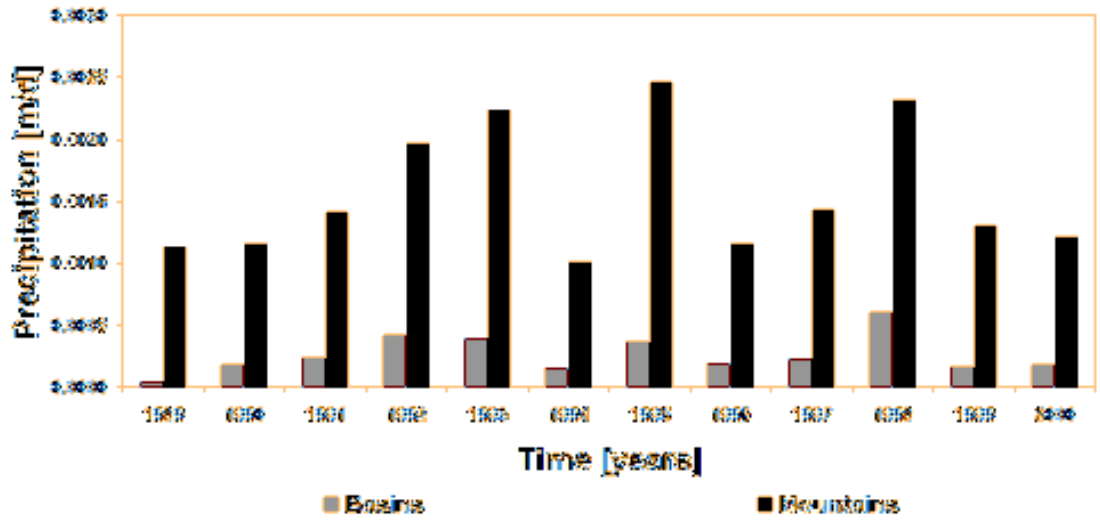
Figure 3-3. Daily precipitation rates recorded at Amargosa Valley for basin areas and the Spring Mountains for mountain areas derived from yearly averages (Fenelon and Moreo, 2002).

Figure 3-4. Vegetation present in the Devils Hole area where evapotranspiration occurs. Devils Hole is noted by the white arrow in the picture. Picture is taken looking to the northwest. The shrub in the foreground is about 1 m tall for scale. Photo taken May, 2005.

evapotranspiration in northern Nevada basins were computed by Robinson (1970) for two locations, which yielded results of 0.0005 ± 0.0001 m/d for evapotranspiration rates. Other studies were performed by Hines (1992) where values of evapotranspiration were calculated for vegetated and non-vegetated areas. Results of this study concluded that evapotranspiration rates varied between 0.00008 and 0.0007 m/d for vegetated areas, and 0.00008 and 0.0004 m/d with an average of 0.0001 m/d for non-vegetated areas.

A structural control on ground-water flow adjacent to Devils Hole is the occurrence of a natural spring line (Fig. 3-5). The spring line occurs where the highly conductive lower carbonate rock aquifer terminates into less conductive Quaternary sediments due to faulting (Fig. 3-6). Ground-water is forced to flow to the land surface through fractures and faults creating the spring line (Winograd and Thordarson, 1975). Two faults are responsible for the spring line, the Gravity Fault and the Ash Meadows fault zone. The spring line is roughly 13 km long and incorporates 25 to 30 springs along a trend of N 20 W to N 25 W (Winograd and Thordarson, 1975; Fenelon and Moreo, 2002; Laczniak et al., 1996). The spring line discharges about 2×10^7 m^3/yr of ground-water from the lower carbonate rock aquifer (Winograd and Thordarson, 1975). The boundaries of the spring line on the north and south ends are established by the lower clastic aquitard present in the sub-surface (Waddell et al., 1984). These boundaries continue from the spring line in a northeast direction towards the Specter Mountains essentially paralleling the ground-water flow path to Ash Meadows from the Specter Mountains (Waddell et al., 1984). Therefore, most of the ground-water discharge at Ash Meadows passes under the Specter
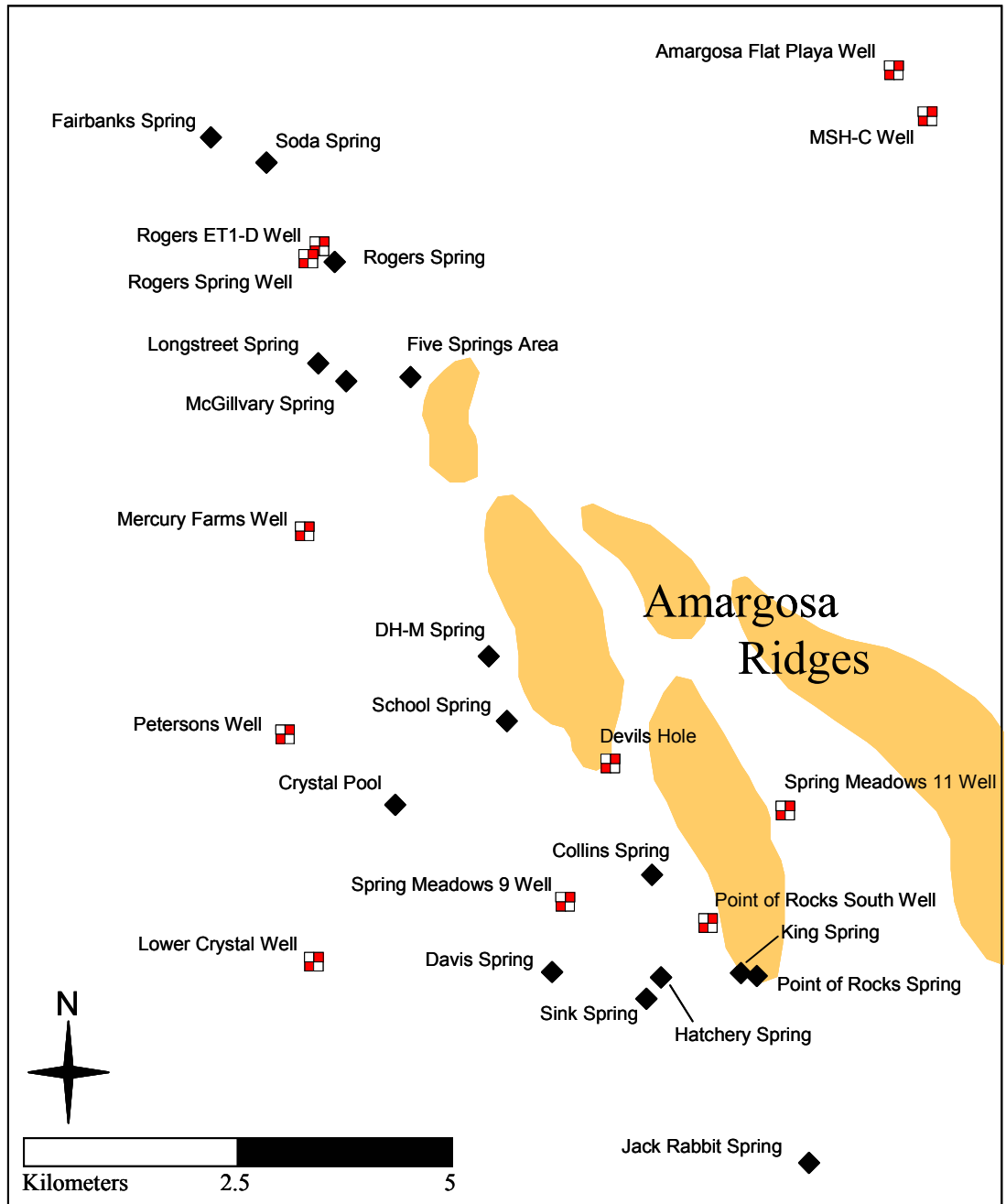
Figure 3-5. Locations of springs creating the Ash Meadows spring line. Springs are represented by diamonds. Observation wells are noted by red and white checkered squares.
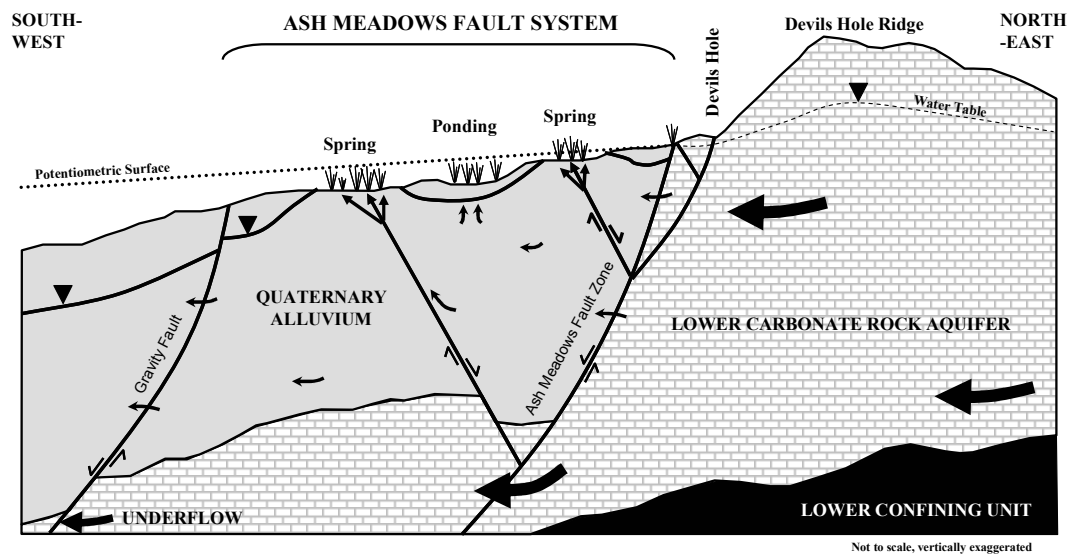
Figure 3-6. Cross section showing flow through the lower carbonate rock aquifer terminating into Quaternary sediments where the springs occur at Devils Hole. Springs discharge through fractures and faults present in the Ash Meadows fault system. Geological interpretation modified from Laczniak et al. (1996).

Mountains (Waddell et al., 1984). The largest measured discharge from the springs is at Crystal Pool, which has a measured discharge of about 5.8×10^6 m^3/yr (Laczniak et al., 1996).

The water that exits through the spring line is ground-water produced from the lower carbonate rock aquifer. This is supported by temperature data, hydraulic head differentials, and water chemistry (Winograd and Thordarson, 1975). Temperatures of spring waters adjacent and in close proximity to outcropped rock are greater than the temperatures of spring waters at greater distances from the outcropped rocks. Typically, spring waters close to outcropped rocks averages over 32.0˚C, while spring waters at greater distances from outcropped rocks are less than 32.0˚C (Winograd and Thordarson, 1975). The spring waters close to the outcrops do not have ample time to come into equilibrium with surrounding environmental temperatures and reflect temperatures closer to those temperatures measured within the lower carbonate rock aquifer. These are also locations where waters in the lower carbonate rock aquifer are nearest the surface. If water is being fed to the springs from the lower carbonate rock aquifer, it follows that discharging spring waters nearest to the ground-waters will have similar temperatures and spring waters at farther distances will not because of cooling due to travel distance. Spring water temperature is also reflective of discharge rate. Springs with discharge rates greater than 5,450 m^3/d tend to have temperatures between 27.0˚C and 33.0˚C; spring with lesser discharge rates yield temperatures between 23.0˚C and 34.5˚C (Winograd and Thordarson, 1975). Springs with greater discharge rates likely have better interconnectedness to the lower

carbonate rock aquifer and present temperatures representative of those in the lower carbonate rock aquifer.

An example of where spring temperature can indicate ground-water flow direction is in the Crystal Pool and School Springs areas where a large temperature anomaly has been observed (Fig. 3-5). Higher ground-water temperatures are found in the proximity of those springs (Winograd and Thordarson, 1975). This could indicate a large northeast trending fault in similar location to the Burrow Trail Canyon where ground-water flow is estimated to be enhanced (Winograd and Thordarson, 1975; Carr, 1988). This is supported by Carr (1988) who suggested a large fault exists with a northeast trend. The fault is aligned with the Burro Trail Canyon and strikes about N 60 E (Fig. 2-1). When the strike of the fault zone is projected to the southwest, it intersects School Spring and continues into Crystal Pool. Further, carbon-14 dating performed by Winograd and Pearson (1976) to date the age of the spring waters in the Ash Meadows discharge area indicates that waters at Crystal Pool have a carbon-14 content five times greater than other areas. The rational for this argument is that water must have a less obscured pathway to that spring from the northeast than to other springs.

CHAPTER IV

METHODOLOGY

4.1 CALCULATION OF VOLUMETRIC STRAIN

It is speculated that the water levels observed within Devils Hole may be under the influence of tectonic deformation caused by the stress field present throughout the Great Basin (Carr, 1988). The ground-water that fills Devils Hole originates from the northeast. Water enters the lower carbonate rock aquifer in areas of high elevation as infiltrating precipitation or yearly melt. From there, fracture and fault networks, and ground-water divides dictate the ground-water flow paths to Devils Hole and the remaining Ash Meadows spring line. The lower carbonate rock aquifer is heterogeneous and anisotropic. This is due to the tectonic forces acting on the rock matrix and changes in lithology. Fault and fractures open and close consistently through time altering the compartmentalization of the aquifer. It is postulated that the opening and closing of these faults and fractures affects ground-water flow over a geological time scale. Assuming this is true, the rate of water-level decline in Devils Hole is a measure of long-term water-level declines from tectonic deformation. Because the exact dimensions and locations of fractures and faults are not known, assumptions are necessary to account for strain induced tectonic deformation.

It is assumed that crustal strain affects the porosity of a matrix material. The current strain rate in the study area is 8 nanostrain/yr at N 65 W, which is equivalent to approximately 1.7 mm/yr of crustal elongation over 34 km in the N 65 W orientation (Wernicke et al., 1998). Volumetric strain is defined as the change in

length or volume from an initial length or volume (Yeats et al., 1997) and is calculated using the current strain rate and orientation. If the study area is discretized into a grid, the initial total volume, V_{total_i}, of a grid cell is determined using the cell dimensions. If principal axes of a frame of reference are aligned with grid cell orientations, cell dimension dx changes to $dx + \varepsilon sin\theta dx$ where θ is the orientation of strain and ε is strain, due to strain and cell dimension dy changes to $dy-\varepsilon cos\theta dy$ (Fig. 4-1). A new total volume, V_{total_n}, is computed per cell using,

$$V_{total_n} = (dx + \varepsilon \sin\theta dx) \times (dy - \varepsilon \cos\theta dy) \times dz \qquad (1)$$

where dx, dy and dz represent cell dimensions [L]. The difference between the initial total volume and the new total volume is the volume change due to strain. Therefore, volumetric strain, ε_v, is calculated using the following equation:

$$\varepsilon_v = \frac{\Delta V_{total}}{V_{total_i}} \qquad (2)$$

The value of dz is assumed to be a constant in equation (1). In nature, dz is incorporated into the volumetric strain change. For the purpose of this study, a constant value for dz is used for each grid cell. It is assumed that horizontal length changes from strain will portray the effects of strain on the ground-water system and that adding a vertical dimension will only increase the effects. This is justified as the magnitude of change in the horizontal direction far exceeds vertical change.
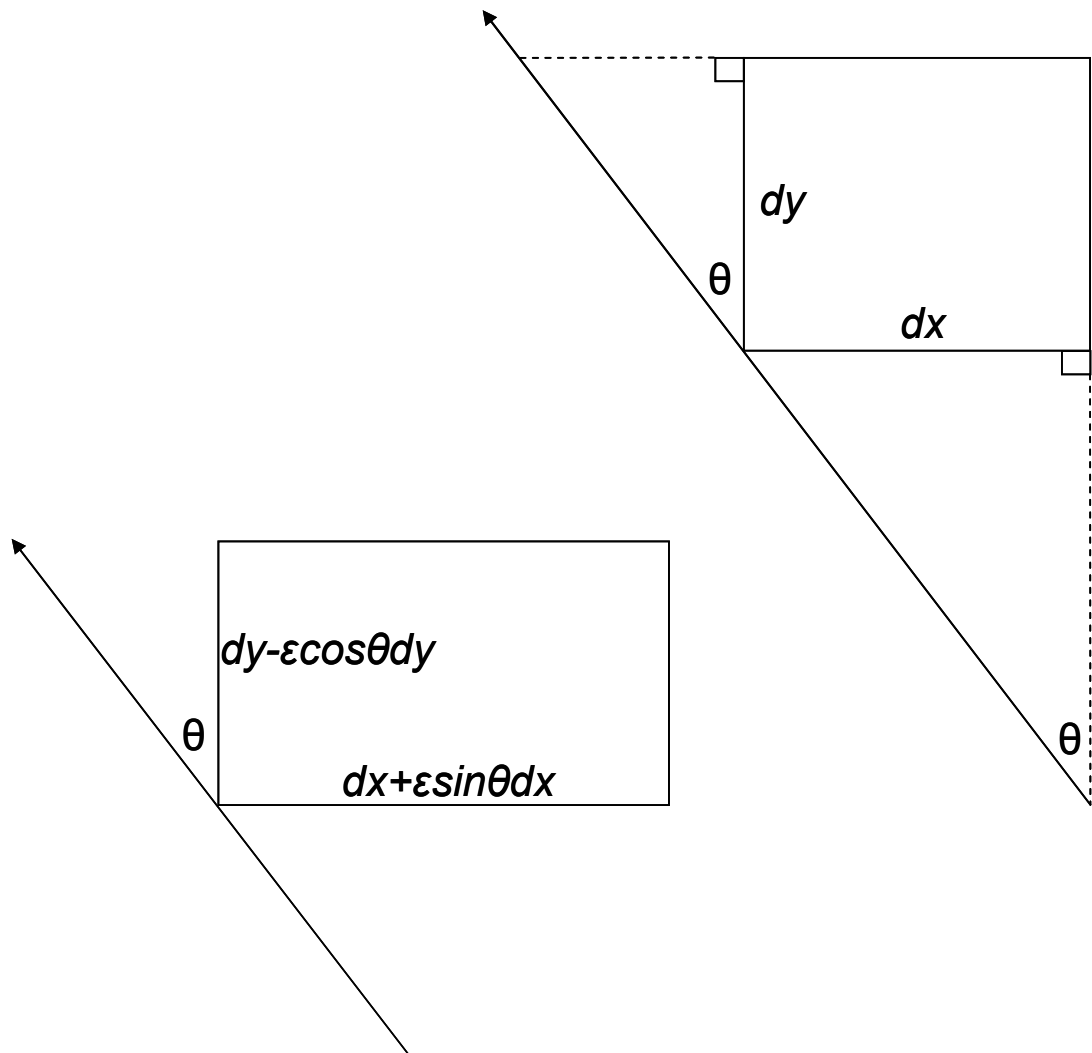
Figure 4-1. Plan view schematic of a grid cell. Strain orientation is represented by θ.

4.2 STRAIN AFFECTING POROSITY

Porosity is defined as the ratio of void volume (V_{void}) to total volume (V_{total}). It is assumed that compression or extension only alters the pore space within a cell and that grain mass in a cell remains constant. In order to maintain initial cell dimensions while strain is imposed on the system for modeling purposes, grain mass in a cell must be added or discarded. In this sense, porosity values change according to the change in void volume in a cell. Initial void volume is determined using an initial porosity, n_i, for each cell, and grid cell data in the format of equation (1).

$$V_{void_i} = n_i \times V_{total_i} \qquad (3)$$

The difference between the initial total volume and the new total volume is the volume change due to volumetric strain. Since it is assumed that volumetric strain only impacts the void volume, the change in total volume is subtracted from the initial void volume to generate a new void volume. The new void volume is then divided by the initial total volume to generate a new porosity.

Porosity is reflected in specific storage values, S_s, where:

$$S_s = \rho_w g(\alpha + n\beta) \qquad (4)$$

where ρ_w is the density of water [M L^{-3}], g is the gravitational constant [L T^{-2}] , α is matrix compressibility [L T^2 M^{-1}], n is porosity, and β is the compressibility of water [L T^2 M^{-1}]. It is assumed that matrix compressibility, water density, gravity, and the

compressibility of water remain constant through time. A decrease in porosity influences diffusivity values by decreasing specific storage. Diffusivity is defined as:

$$D = \frac{K}{S_s} \tag{5}$$

where D is diffusivity [$L^2\ T^{-1}$] and K is hydraulic conductivity [$L\ T^{-1}$]. Equation 5 shows that diffusivity is directly proportional hydraulic conductivity and thus permeability of a rock medium; it is inversely proportional to specific storage. To create faster movement of fluid in a rock medium, higher permeability, reflected in conductivity values, are required. Alternatively, increased specific storage values require that more fluid be moved through the rock medium.

4.3 STRAIN AFFECTING HYDRAULIC HEAD

Tectonic deformation can be approached by modeling the effect of strain as hydraulic head changes. This is done by calculating pore pressure changes in a rock matrix due to strain and converting those changes to hydraulic head changes. It is assumed that volumetric strain has great effects on pore pressure in a rock matrix. If volumetric strain is imposed on a matrix, then the pore pressure within the matrix will vary if the properties of the porous media are considered (Biot, 1941):

$$\Delta P = C\varepsilon_v \tag{6}$$

where ΔP is fluid pressure change [M L^{-1} T^{-2}], and C is a function of the properties of the porous media [M L^{-1} T^{-2}]. The pore space typically occupied by air is replaced by water in saturated rock; therefore, the pressure exerted on the surrounding matrix from the pore space is a fluid pressure. Furthermore, if the rock matrix is saturated, a pure stiffness case can be assumed where the medium is undrained and the fluid pressure and rock matrix are both resisting volumetric strain (Wang, 2000). This is reflected by rapid changes in pore pressure when strain is applied to the medium. The variable C is defined by Rice and Cleary (1976) as:

$$C = -BK \qquad\qquad (7)$$

where B is Skempton's coefficient and K is the bulk modulus [M L^{-1} T^{-2}]. For undrained conditions, Skempton's coefficient is defined as the ratio of induced pore pressure to the change in applied stress. More simply stated, it "is a measure of how the applied stress is distributed between the skeletal framework and the fluid" (Wang, 2000, p. 21). It has values between zero and one. Typical values of Skempton's coefficient for fluid-saturated rock are between 0.5 and 1.0 (Wang, 2000). The negative sign associated with Skempton's coefficient is emplaced to correct for the sign convention for stress. An increase in compressive stress, which causes pore pressure to increase, is in the negative direction. The bulk modulus, K, is defined by Turcotte and Schubert (2002) as:

$$K = \frac{1}{\alpha} \qquad\qquad (8)$$

where α is matrix compressibility [L T^2 M^{-1}]. Fluid pressure change, derived in equation 6, is used to define a hydraulic head change in the following equation if it is assumed that pore pressure is an undrained response to volumetric strain (Domenico and Schwartz, 1990):

$$\Delta h = \frac{\Delta P}{\rho_w g} \qquad (9)$$

where Δh is hydraulic head change [L]. The resulting value for Δh is positive or negative depending upon the value of ΔP, which is determined from the volumetric strain. In a model simulation, the value of Δh is added to the original hydraulic head in a cell to represent water level response to volumetric strain.

A first-order calculation can be performed to estimate maximum hydraulic head change due to volumetric strain using the methods above. Volumetric strain is calculated using grid cell dimensions with equation 2, and the current strain rate and orientation of 8 nanostrain/yr at N 65 W (Wernicke et al., 1998). The resulting volumetric strain value is -3.87x10^{-9}. Setting Skempton's coefficient to 1.0 to maximize pore pressure in equation 6; using a value of 4x10^{-10} m^2/N for matrix compressibility (Bredehoeft, 1992); and using conventional values for the density of water and gravity of 1000 kg/m^3 and 9.8 m/s^2, respectively, a Δh value of -0.1 cm results. This result places an upper bound on numerical simulations and on simulated water-level changes.

The effects of volumetric strain on hydraulic head is considered as a `fluid source' through the equation for the conservation of fluid by Domenico and Schwartz (1990):

$$K_{xx}\frac{\partial^2 h}{\partial x^2} + K_{yy}\frac{\partial^2 h}{\partial y^2} + K_{zz}\frac{\partial^2 h}{\partial z^2} - \frac{\partial \varepsilon_v}{\partial t} = S_s\frac{\partial h}{\partial t} \qquad (10)$$

where h is hydraulic head [L], and t is time [T]. The volumetric flux per unit volume term used to represent sources and/or sinks of water is replaced with a volumetric strain term, $\frac{\partial \varepsilon_v}{\partial t}$, in equation 10. Volumetric strain causes pore pressure to increase or decrease respective of the magnitude of volumetric strain. The change in pore pressure is considered an excess pressure. The lower carbonate rock aquifer matrix is saturated in the study area; therefore, pore pressure can be considered as a fluid pressure. According to equation 9, fluid pressure change is interpreted as a hydraulic head change. Hydraulic head change is representative of the volumetric flux term where an increase or decrease in hydraulic head is reflective of an increase in sources or sinks of water, respectively.

CHAPTER V

NUMERICAL MODEL

5.1 OVERVIEW

A numerical model was constructed to better predict alterations in ground-water flows because of the unique and complex ground-water flow system present in the study area. The three dimensional numerical model was constructed using Visual MODFLOW (Schlumberger, 2005). Visual MODFLOW (Schlumberger, 2005) is a three dimensional model interface that allows for geological modeling and petrophysical modeling. It is coupled with MODFLOW-2000, which is a ground-water flow and transport simulator (Harbaugh et al., 2000).

5.2 MODEL DOMAIN

The study area chosen for this investigation is based on natural boundary conditions present in the Great Basin. The width of the study area is 33.6 km; the length is 27.2 km (Fig. 5-1). The total area is 913.4 km^2. The Ash Meadows Fault System comprises the western boundary and a section of the southern boundary of the study area. The Ash Meadows Fault System is understood to be a large barrier to ground-water flow, although conclusive tests of the faults hydraulic conductivity have not been performed. The Ash Meadows Fault System represents a distinct termination point of the lower carbonate rock aquifer, which is why it is interpreted as such a large barrier to ground-water flow. The Spring Mountains are used to distinguish a large portion of the eastern boundary and the remaining section of the southern boundary not covered by the Ash Meadows Fault System. The Montgomery Fault that trends to the northeast is present in the Spring Mountains. This is a low
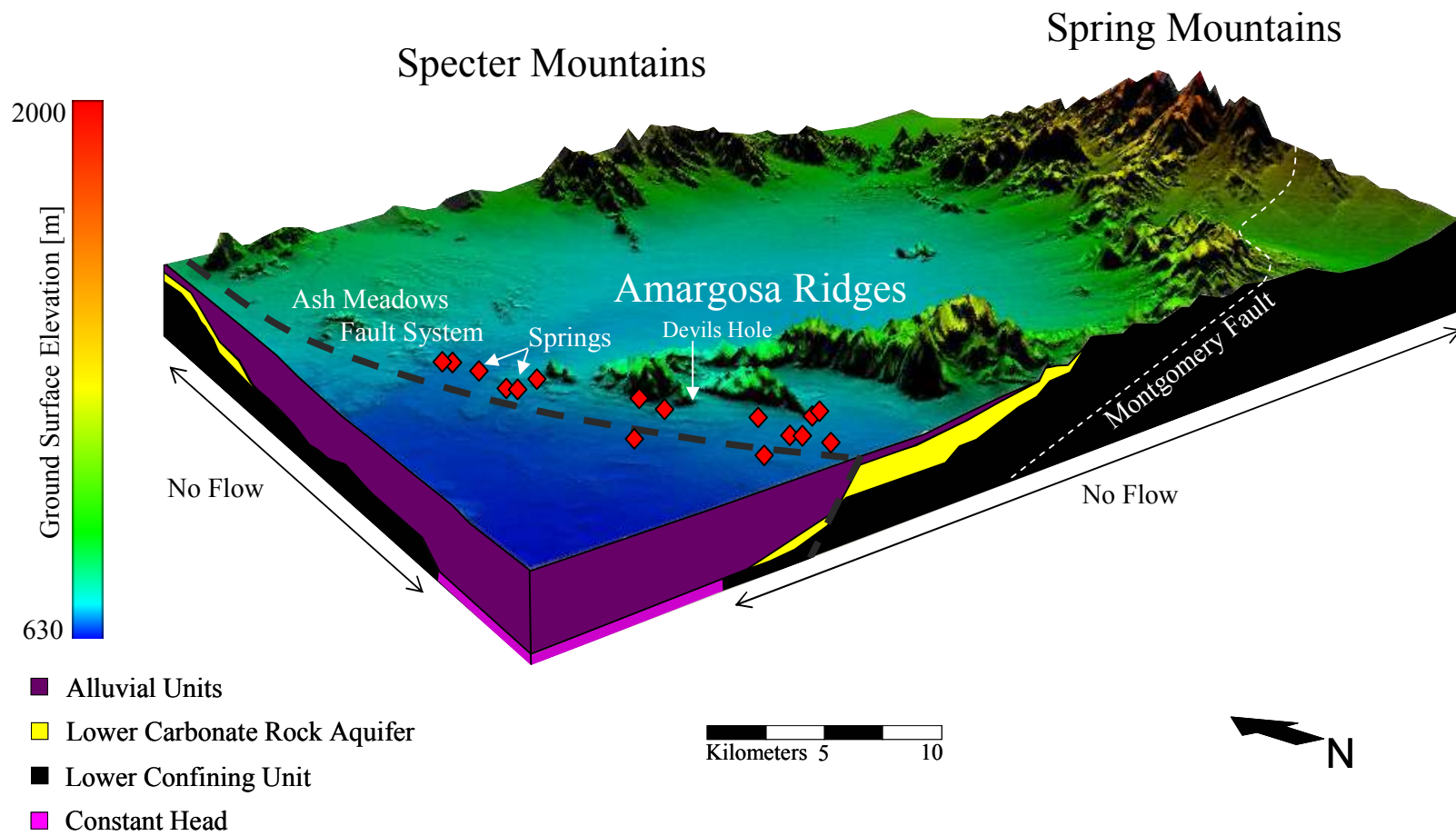
Figure 5-1. Block diagram of steady-state and transient models.

angle thrust fault that acts as a ground-water flow divide. The northern border and southeast corner of the study area are represented by constant hydraulic head boundaries as those are the areas where ground-water enters from outside the study area.

Devils Hole is located in the southwest quarter of the study area. Typically, the focus of a model is centered in the model domain. The reason for Devils Hole's location in the southwest quarter is due to the boundary conditions used to define the study area. The boundary conditions of the study area will be explained later in this thesis. The study area does not extended farther to the northeast to limit the effects of ground-water flowing to other drainage basins. By confining the extents of the study area to the local Devils Hole area, the assumption is made that all ground-water flow entering from the northeast passes through the Ash Meadows area.

All of the values used in the model were influenced from literature and/or by a larger model by Belcher (2004). The model created by Belcher (2004) is a three dimensional transient ground-water flow model for the Death Valley regional ground-water flow system. The model of Belcher (2004) is a very detailed model designed primarily to understand the effects of the Nevada Test Site on ground-water flow. The Belcher (2004) model was developed by the United States Geological Survey under the request of the Department of Energy.

5.3 GRID DISCRETIZATION

The model created is three dimensional (Fig. 5-1). 120 columns divide the model domain in the east-west orientation, 100 rows in the north-south orientation to

maintain square grid cells in the horizontal plane (Fig. 5-2). Each grid cell is 279.9 m east-west and 271.9 m north-south. The model consists of six layers, which are chosen to represent lithologic layers described and used by Belcher (2004). The layers represented in the model from youngest to oldest are the alluvial aquifer, the alluvial confining unit, the volcanic rock aquifer, the upper confining unit to the lower carbonate rock aquifer, the lower carbonate rock aquifer, and the lower crustal confining unit. The process to determine layer thickness is discussed below.

5.4 ROCK LITHOLOGIES AS MODEL LAYERS

ArcGIS software was used to create the data used to define the six layers present in the numerical model. A detailed description of layer elevation determination is found in Appendix A. The following layer elevations were brought into the numerical model: ground surface, top of the lower carbonate rock aquifer, and the top of the lower crustal confining unit. Elevations for the tops of layers 2 through 4 were not used because of cell to cell inconsistency in elevation (Fig. 5-3). Cell to cell inconsistency refers to adjacent cells not overlapping by at least 50 percent in the vertical plane. It is not recommended by Visual MODFLOW to incorporate such cell inconsistencies into a model as errors in processing numerical equations will occur (Schlumberger, 2005). Rather, the thickness between the top of the lower carbonate rock aquifer layer and the ground surface was equally divided into four layers (Fig. 5-2). Using this technique, the upper four layers of the model could be represented to a greater horizontal extent in the model domain. This assumption can be a possible source of numerical error. However, the overall combined thickness of the four top
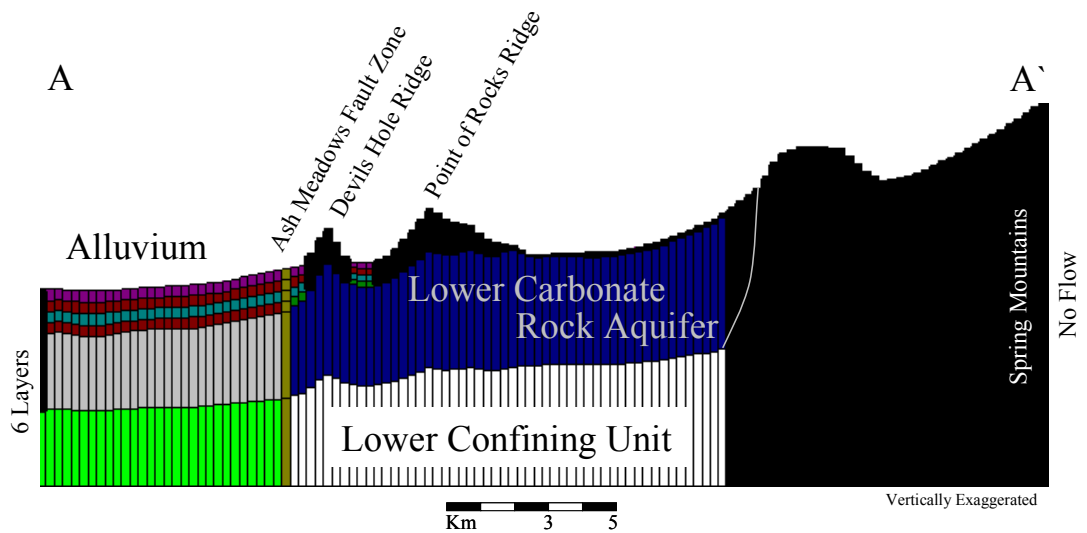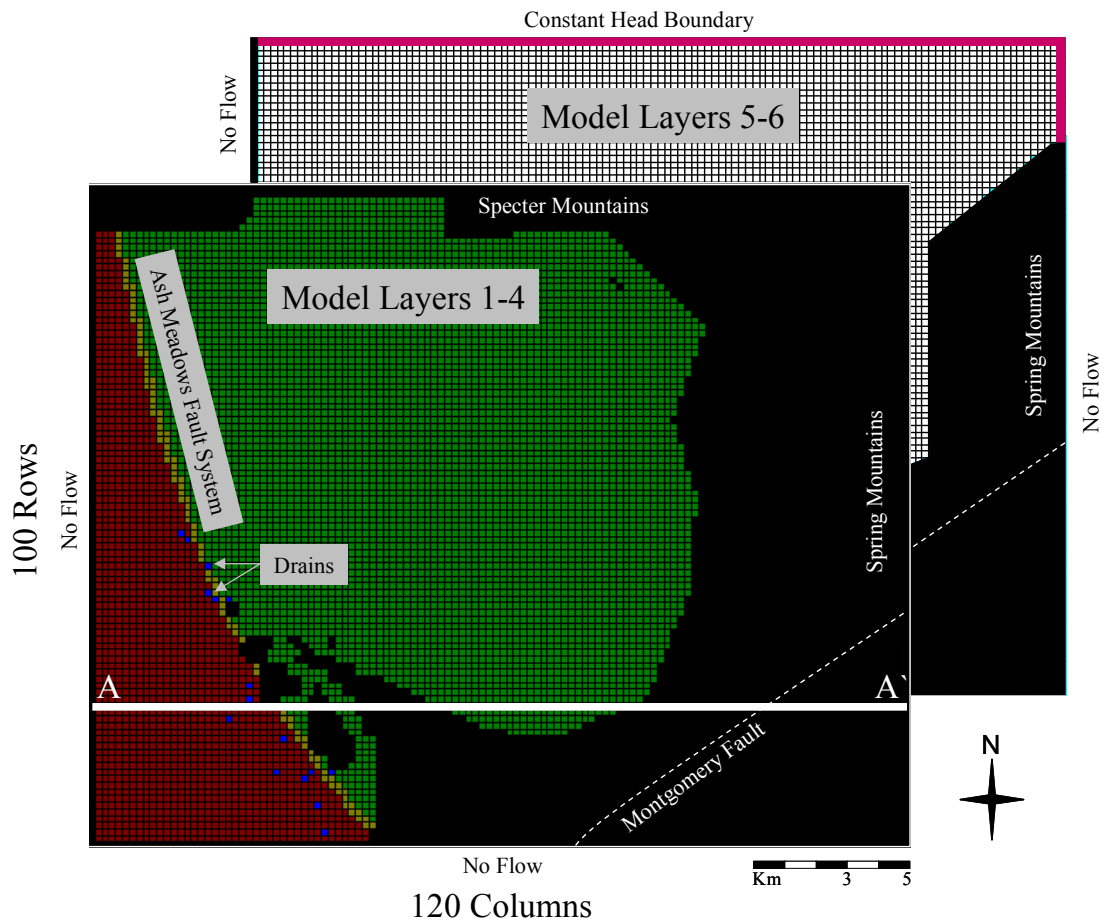
Figure 5-2. Model grid with boundary conditions labeled. Top figure is in plan view. Bottom figure is cross-section from A to A`.
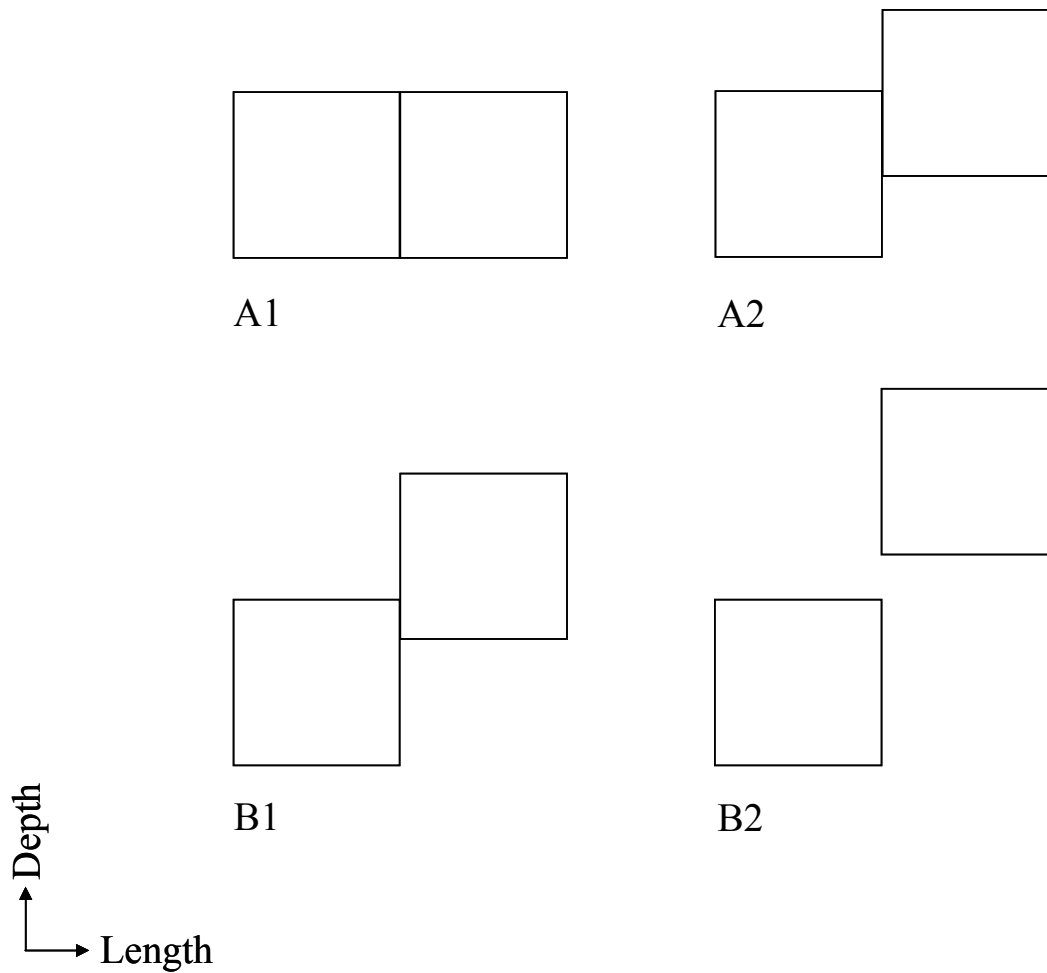
Figure 5-3. Examples of adjacent grid cell scenarios. A1 and A2 represent good cell to cell overlap, B1 and B2 show poor cell to cell overlap. Poor cell overlap may result in an inability of the program to process numerical calculations.

layers remained true to estimated natural conditions. The majority of the ground-water flow occurs in the lower carbonate rock aquifer and the effects of alluvial layers with altered vertical dimensions are assumed to be minimal to the ground-water flow occurring in the lower carbonate rock aquifer and throughout the model domain. Additionally, allowing the top four layers to extend to realistic extents in the model domain likely yielded better results than a model with little to no alluvial layers.

5.5 BOUNDARY CONDITIONS

5.5.1 Areas of No Flow

Cells in the model domain that are not considered in numerical calculations in MODFLOW-2000 are termed inactive cells (Harbaugh et al., 2000). They were used along the Montgomery Fault and overlying Spring Mountains in the southeast portion of the model domain where a ground-water divide exists (Fig. 5-2). Inactive cells were assigned in the top four layers of the model to specific cells that met the criteria described above for inaccuracies in numerical calculations. This occurs primarily in the mountainous areas of the model domain. Inactive cells were assigned to the majority of the western borders of all layers in the model. The Ash Meadows Fault System is the primary boundary to the western side of the model, however the proximity of the Ash Meadows Fault System to the Ash Meadows spring line is too close to represent the Ash Meadows Fault System by inactive cells where ground-water flow would be influenced by the inactive cells. A more realistic scenario is achieved by representing the Ash Meadows Fault System with low hydraulic

conductivities and using inactive cells as a boundary condition at an arbitrary distance west of the Ash Meadows Fault System.

5.5.2 Constant Hydraulic Head

Assigned constant hydraulic head cells maintain a specified hydraulic head value throughout model simulation using the MODFLOW-2000 simulator (Harbaugh et al., 2000). A large body of standing water (i.e. river or lake) is typically represented as a constant hydraulic head boundary condition. In the study area, two boundaries were designated as constant hydraulic head boundaries, the northern boundary and the southwest corner (Fig. 5-2). At the northern boundary, which includes the northeast corner, hydraulic head was specified as 800 m in the lower carbonate rock layer and lower crustal confining unit of the model. The upper four layers did not have a constant hydraulic head values assigned as they were inactive. The Spring Mountains located east of the model domain have an estimated hydraulic head value of 915 m (Prudic et al., 1995). The distance from the Spring Mountains to the northeast corner of the model is about 30 km (Waddell et al., 1984). If a hydraulic gradient of 1.1 m/km is used (USGS, 1971), hydraulic head at the northeast corner of the model domain is estimated at 882 m. Past contour maps of hydraulic head indicate that hydraulic head values are approximately 760 m in the area of the northern and northeast corner boundaries (Burbey and Prudic, 1991). The constant hydraulic head boundary assigned is within the constraints of these values. It is recognized that seasonal variation of the hydraulic head equipotential at these locations probably occurs. Uncertainties associated with this boundary condition are explored later in this thesis.

The mass balance of the Ash Meadows ground-water system suggests that underflow out of the lower carbonate rock aquifer accounts for roughly 10,000 m^3/d (Winograd and Thordarson, 1975). Underflow is considered ground-water passing through the Ash Meadows Fault System, at depth, into the remainder of the lower carbonate rock aquifer on the western side of the Ash Meadows Fault System (Fig. 3-6). This could occur through horizontal diffusion of ground-water at depth or through vertical diffusion down along the dip plane of the fault. The value given to this flux is an estimate and is subject to error.

The constant hydraulic head boundary assigned to the southwest corner of the model domain in layer six was used to simulate seepage of ground-water through the Gravity Fault from the lower carbonate rock aquifer. A constant hydraulic head boundary condition was used so that the flux out of the ground-water system could be quantified and compared to estimated values. Values for hydraulic head were assigned individually to each cell on the border of the southwest corner, which were equal to the mean hydraulic head at that location. Values were determined from interpolated data of observed water table elevations in the model domain taken from the USGS (2005).

5.5.3 Recharge

Recharge to the ground-water system of the Ash Meadows area is primarily due to precipitation. Percentages of averaged recorded annual precipitation values for mountain areas were used as recharge for the model. Recharge is estimated at less than two percent of average annual precipitation (Hevesi et al., 2003). An average annual net infiltration of 7.7×10^{-6} m/d is reported by Belcher (2004) for the study

area. Recharge values used in the model were between 1.6×10^{-7} m/d to 7.8×10^{-5} m/d, which accounts for 0.01 percent to 5 percent of annual precipitation in the Spring Mountains, respectively. Recharge was assigned to the upper most active cells of the model.

5.5.4 Evapotranspiration

A large amount of ground-water loss occurs through evapotranspiration in the low lying desert plants and directly through the soil (Fig. 3-4). The value for evapotranspiration used in the model was 0.0001 m/d. This value is within the constraints of the experiments performed by Robinson (1970), Hines (1992), and Laczniak et al. (1999), where rates of 0.00008 m/d to 0.007 m/d were reported. The low lying plants are not deep rooted. For this reason, a maximum extinction depth of evapotranspiration was set at 1 m below ground surface in layer 1. It is unlikely that root systems extend beyond that depth in the model domain.

5.5.5 Drains

The spring line present in Ash Meadows was represented by drains in the model (Fig. 5-2). In total, 16 drains were assigned. Information on the drains is summarized in Table 5-1. A drain is assigned to a particular grid cell in the numerical model. Once location is established, a drain elevation value is assigned. If ground-water levels rise above the assigned drain elevation point in the respective cell, ground-water is discharged out of the ground-water system through the drain (Harbaugh et al., 2000). Ground-water remains in the ground-water system if ground-water levels do not reach the drain elevation. In addition to assigning a drain elevation for each drain, a drain conductance value needs to be assigned. This value

Drain	Northing [m]	Easting [m]	Surface Elev. [m]	Drain Elev. [m]	Conductance [m^2/d]
Collins Spring	563207	4030110	707	696	8205679
Crystal Pool	560973	4030920	676	676	8205679
Davis Spring	562905	4028700	688	682	8205679
DH_M	561819	4032250	709	699	8205679
Fairbanks Spring	559001	4038530	697	686	8205679
Five Springs Area	560974	4035830	713	713	8205679
Hatchery Spring	564314	4028700	701	694	8205679
Jack Rabbit Spring	564616	4027360	694	688	8205679
King Spring	565180	4028720	716	697	8205679
Longstreet Spring	560108	4036070	698	698	8205679
McGillvary Spring	560410	4035770	703	703	8205679
Point of Rocks Spring	565441	4028720	723	698	8205679
Rogers Spring	560128	4037160	691	691	8205679
School Spring	561799	4031680	701	693	8205679
Sink Spring	564053	4028440	695	691	8205679
Soda Spring	559303	4038240	689	687	8205679

Table 5-1. Properties of the Ash Meadows spring line represented as drains in the numerical model. Values for conductance were based off those used by Belcher (2004).

represents the conductivity of the drain and is influenced by drain shape, root systems, sediment type, drain wall roughness, etc. The conductance value for all drains assigned was 8.2×10^6 m^2/d, which is based off grid cell dimensions and a conductance per unit length value. The conductance per unit length value of 107.8 m/d was taken from Belcher (2004) for drains in gravelly sediments, which is the depositional environment of the spring line in Ash Meadows.

5.6 INITIAL CONDITIONS

5.6.1 Hydraulic Conductivity

Values for hydraulic conductivity were based on Belcher's (2004) model, which uses estimates made by Belcher et al. (2001). Hydraulic conductivity values are referenced in Table 5-2. Layers 1 through 3 had uniform hydraulic conductivities assigned across the model domain, with exception to the presence of the fault systems. The lithologies represented by these layers do not have substantial depths in the study area and are assumed not to have been greatly affected by faulting in the Ash Meadows area. The Ash Meadows Fault System was established in the model by a line of low hydraulic conductivity in comparison to surrounding hydraulic conductivities. It is present in all layers of the model and follows the path of the Ash Meadows Fault System. To the west of the fault, layers 4 through 6 were assigned different values of hydraulic conductivity that were proportional to the values of hydraulic conductivity used for alluvial sediments. This was done to reflect the offset caused by faulting in the Ash Meadows area and create a barrier to ground-water flow.

Model Layer	Hydraulic Conductivity [m/d]
1	0.045 - 0.0045
2	0.046 - 0.0046
3	0.0412
4	0.0038 - 0.00038
5	0.1 - 100
6	0.0001 - 0.2
Ash Meadows Fault System	0.0001 - 10.0
Drain Fractures	1.0 - 4.0

Table 5-2. Hydraulic conductivity of model layers and other structural features used in numerical model simulations (Winograd and Thordarson, 1975; Belcher, 2004).

The lower carbonate rock aquifer is the primary conduit for ground-water flow into the Ash Meadows area. For this reason, more attention was directed to the hydraulic conductivity of that model layer. It is documented that the lower carbonate rock aquifer is highly fractured under the Specter Mountains and Spring Mountains (Dettinger et al., 1995). This was represented in the model by using larger values of hydraulic conductivity in the mountainous areas of the model domain in layer 5. Throughout the basin area of the model domain, a lower value of hydraulic conductivity was used to represent an un-fractured lower carbonate rock aquifer.

The locations of springs are tied to the presence of faults and fractures. Fractures and faults present in the lower carbonate rock aquifer provide conduits of flow for ground-water to pass easily through and exit. For this reason, a high hydraulic conductivity was assigned to each drain. For model layers 1 through 4, high vertical hydraulic conductivity was assigned to the cells under the drain. In model layer 5, the cell below the drain was assigned this high hydraulic conductivity and an arbitrary number of cells in the northeast direction until the un-fractured hydraulic conductivity zone of the lower carbonate rock aquifer was reached. For drains in the un-fractured zone, no extrapolation in the northeast direction was required. For drains west of the fault zones, extrapolation was required. A northeast direction of extrapolation was used because extension in the Ash Meadows area is to the northwest, therefore, fractures and faults should open in the northwest direction.

5.6.2 Storage Zones

Four specific storage zones were assigned for transient simulations. Zone 1 only represented layer 1 of the model. This was because layer 1 was unconfined and

dependent upon specific yield rather than specific storage. Layers 2 though 4 were all considered as one storage zone. The initial value of storage assigned for this zone was 4.5×10^{-5} m^{-1}. Model layer 5 and 6 were both assigned to individual storage zones to separate the lower carbonate rock aquifer from other layers of the model. Initial values for both of these zones were 1.5×10^{-5} m^{-1}. Belcher (2004) defines a range of specific storage for similar layers. The values used in this study are within those constraints.

5.7 STEADY-STATE MODEL SIMULATION

MODFLOW-2000 was the flow simulator used to model the steady-state conditions (Harbaugh et al., 2000). The top layer of the model was defined as an unconfined aquifer; the remaining layers were modeled as confined. For confined aquifers, transmissivity remain constant through time. A rewetting condition was applied to the model where dry cells could become re-saturated if the cell below the dry cell had an excess of 0.1 m of hydraulic head. The steady-state model was run using the WHS solver in Visual MODFLOW (Schlumberger, 2005). A hydraulic head change criterion of 0.001 m was used.

Steady-state model calibration was performed using 12 observation wells present throughout the model domain, and the mass balance of flow for the Ash Meadows area. Observation wells were georeferenced in the model to their actual locations. Locations of the observation wells are listed in Table 5-3. The center of the screened interval for each observation well was placed in the lower carbonate rock aquifer. The lower carbonate rock aquifer is the principal transmitter of ground-

Observation Well	Latitude [m]	Longitude [m]	Land Surface Elevation [m]	Observed Water Elevation [m]	Calibrated Water Elev. [m]
Devils Hole	563499	4031373	774.61	719	718
Amargosa Flat Playa	566432	4038900	708.57	706	713
Rogers ET1-D	559612	4037524	687.31	687	688
Lower Crystal Well	559602	4029165	658.53	655	658
Point of Rocks South	564833	4029167	724.66	709	709
Spring Meadows 9	562487	4029588	685.19	679	686
Spring Meadows 11	565540	4031059	744.32	n/a	723
MSH-C Well	565373	4039902	710.18	n/a	708
Peterson Well	559396	4033696	675.13	674	677
Rogers Spring Well	559966	4037613	690.65	690	690
Mercury Farms Well	559212	4031476	663.85	662	662

Table 5-3. Locations and elevations of observation wells used in steady-state model calibration. Information gathered from Laczniak et al. (1999).

water in the study area. Observed water levels for each observation well are presented in Figure 5-4 with the calibrated model results for hydraulic heads (Fig. 5-5).

The mass balance of ground-water flow for the Ash Meadows area fluctuates annually and is very difficult to quantify. For this reason, average values for major sources and sinks into and out of the model domain were used. An annual estimate of the total input to the ground-water system of 9.3×10^4 m^3/d was made by Winograd and Thordarson (1975). The sources of ground-water into the steady-state simulation were the constant hydraulic head boundaries assigned across the northern boundary and northeast corner of the model domain, and recharge. A value of 9.2×10^4 m^3/d was produced upon calibration, which is in strong agreement with the estimated observed input value. The total estimated ground-water discharge from Ash Meadows can be broken down into components of spring discharge, underflow and evapotranspiration, where values of 5.4×10^4 m^3/d, 1.0×10^4 m^3/d and 5.5×10^4 $\pm$ 2.5×10^4 m^3/d are reported, respectively (Winograd and Thordarson, 1975). Discharge occurs through drains, underflow in the southwest, and evapotranspiration in the model. Calibrated results for these values are 4.6×10^4 m^3/d, 9.6×10^3 m^3/d, and 3.5×10^4 m^3/d, which are also in agreement with observed values. Results of model calibration to observed values are shown in Table 5-4.
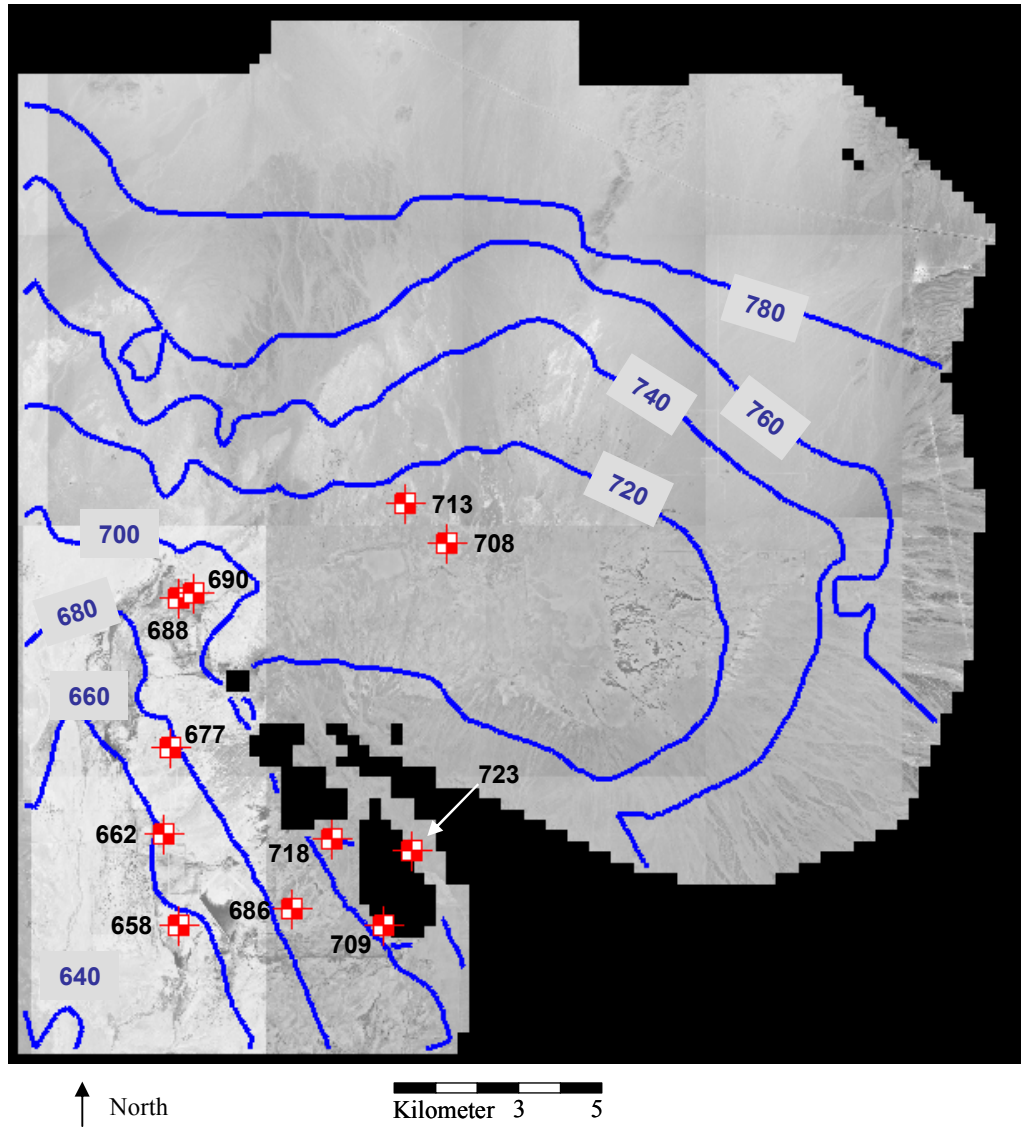
Figure 5-4. Layer 1 hydraulic head equipotentials produced from the numerical model with reported observation well hydraulic heads (Laczniak et al., 1999).
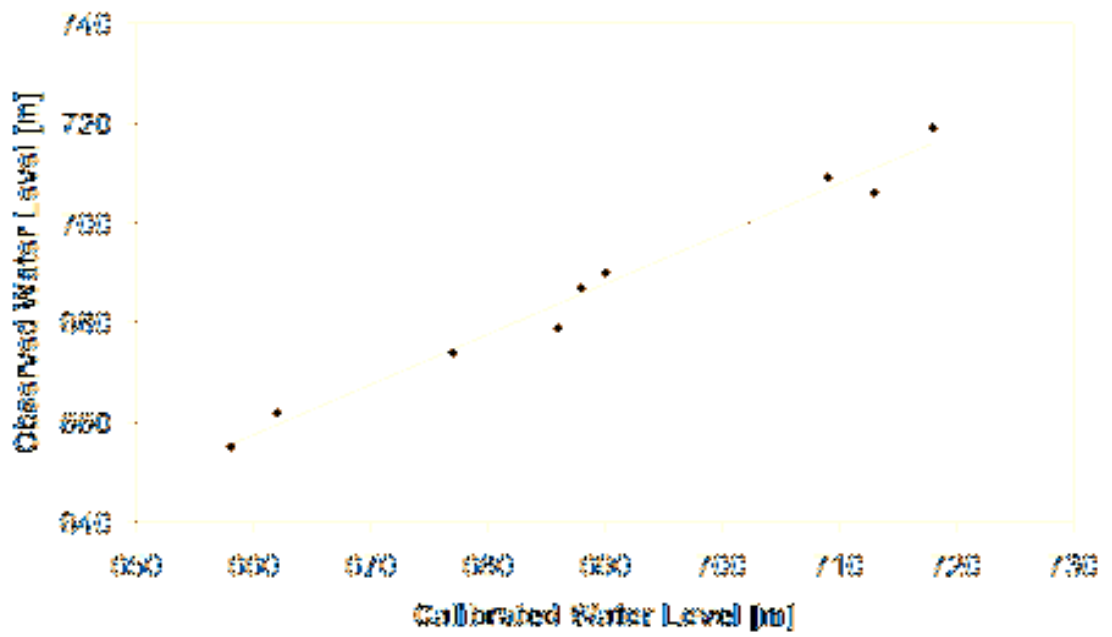
Figure 5-5. Calibrated versus observed water level.

Source/Sink	Observed [m^3/d]	Calibrated [m^3/d]
Total In	92934*	91555
Out - Springs	53964*	46405
Out - Underflow	10138*	9583
Out - Evapotranspiration	28832 to 81106*	35280

* Values subject to seasonal variation. Taken from Winograd and Thordarson, 1975

Table 5-4. Comparison of observed to calibrated mass balance of flow in and out of the Ash Meadows flow system.

CHAPTER VI

ANALYSES AND RESULTS

6.1 STEADY-STATE MODEL ANALYSES AND RESULTS

6.1.1 Overview

Initial sensitivity analyses were performed on the steady-state model after calibration to examine the effects of boundary conditions and hydraulic conductivities on model results. Calibrated hydraulic conductivities for different zones and calibrated water levels are shown in Table 6-1. The calibrated water levels are used for comparison during sensitivity analyses. The different sensitivity analyses are described in the following sections. Sensitivity analyses were performed to address the uncertainties associated with assumptions made in defining system parameters.

6.1.2 Constant Hydraulic Head Boundary

The constant hydraulic head boundary condition assigned to the north and northeast corner of the model was estimated at 800 m, which is between reported values of 760 m and 882 m from Burbey and Prudic (1991) and Prudic et al. (1995), respectively. A sensitivity analysis was performed to examine the effects of decreasing or increasing the constant hydraulic head boundary condition to the reported values. If a value of 760 m is assigned as the boundary condition, the total volume into the system decreases to 5.8×10^4 m^3; if a value of 882 m is assigned, the volume into the system increases to 1.7×10^5 m^3. Correlated hydraulic head values to these conditions at Devils Hole are 710 m and 740 m, respectively. The large fluctuations observed are not realistic to observed fluctuations in the water level in Devils Hole. Variation for this boundary condition is likely much less and will be

Zone	Conductivity [m/d]			Water Level [m] - Calibrated							
	Kx	Ky	Kz	Devils Hole	Amargosa Playa Well	Lower Crystal Well	Point of Rocks South Well	Rogers ET1-D	MSH-C Well	Spring Meadows 9	Spring Meadows 11
Ash Meadows Fault System	0.01	0.01	0.1	720	708.5	658	710	688	713	686.5	723
Carbonate Aquifer - Fractured	2.9	2.9	2.9								
Carbonate Aquifer - Unfractured	2.4	2.4	2.4								
Drain Fractures	2.5	2.5	2.5								

Table 6-1. Values for hydraulic conductivity of specified zones with corresponding water levels at monitoring wells for calibrated steady-state model.

condition is likely much less and will be investigated through annual recharge values rather than constant hydraulic head values.

6.1.3 Conductivity of Model Layers and Features

Sensitivity analyses were performed on hydraulic conductivity values in the steady-state model for the fractured and un-fractured lower carbonate rock aquifer conductivities, the Ash Meadows Fault System conductivity, and the drain fracture conductivity. Values for each sensitivity analysis were recorded in water levels at the observation wells and overall mass flux of flow into the ground-water system (constant hydraulic head and recharge). Calibrated hydraulic conductivities and water levels are shown in Table 6-1 for comparison to sensitivity analyses. Overall mass flux into the ground-water flow system is shown in Figure 6-1.

The hydraulic conductivity of the un-fractured lower carbonate rock aquifer primarily controls the total amount of mass flux into the ground-water system. Results plotted in Figure 6-2 show that for increasing values of hydraulic conductivity in this zone, there is a steady increase of water levels in observation wells. For values of hydraulic conductivity in the fractured zone of the lower carbonate rock aquifer less than those of the un-fractured zone, the fractured zone will govern the amount of mass flux entering the system (Fig. 6-1). Once values of hydraulic conductivity are above those of the un-fractured zone, the hydraulic conductivity of the un-fractured zone dominates mass flux. This is also recognized in the water levels in Figure 6-3 by a flattening of the water level curves for hydraulic conductivity values over 5 m/d.

The hydraulic conductivity of drain fractures is also controlled by the hydraulic conductivity of the un-fractured zone. Increasing vertical hydraulic
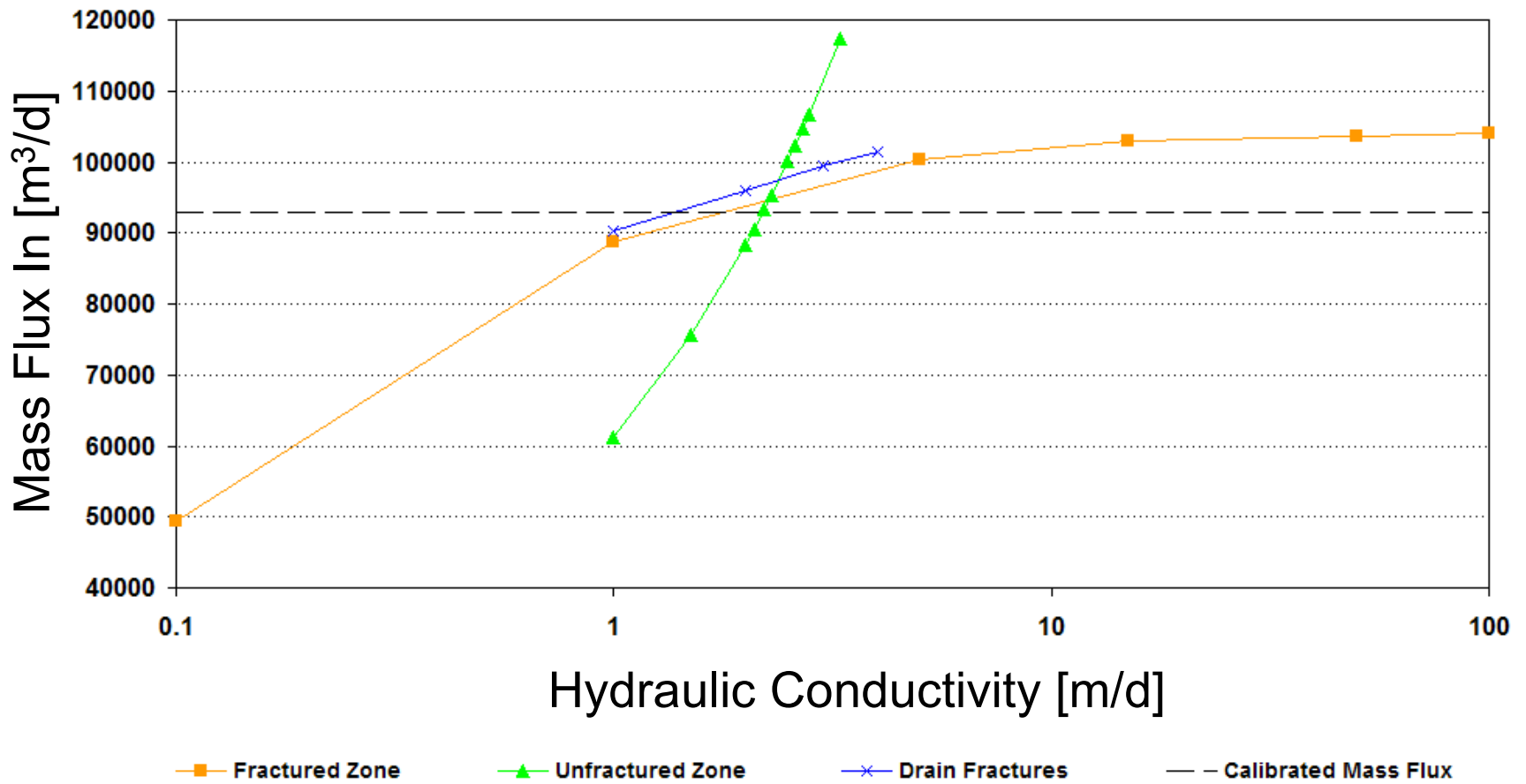
Figure 6-1. Total overall mass flux of ground-water entering the Ash Meadows ground-water system for different values of hydraulic conductivity.

Lower Carbonate Aquifer - Unfractured Zone			
Trial	Conductivity		
	Kx	Ky	Kz
1	1	1	1
2	1.5	1.5	1.5
3	2	2	2
4	2.1	2.1	2.1
5	2.2	2.2	2.2
6	2.3	2.3	2.3
7	2.6	2.6	2.6
8	2.8	2.8	2.8
9	2.7	2.7	2.7
10	2.8	2.8	2.8
11	3.3	3.3	3.3

Water Levels [m] - Calibrated							
Devils Hole	Amargosa Playa Well	Lower Crystal Well	Point of Rocks South Well	Rogers ET1-D	MSH-C Well	Spring Meadows 9	Spring Meadows 11
720	708.5	658	710	688	713	686.5	723

Figure 6-2. Sensitivity analysis results for the un-fractured zone of the lower carbonate rock aquifer in the steady-state simulation. The plot represents the conditions listed in the 'conductivity table'. Calibrated water levels are listed in the lower table for comparison.   Hydraulic conductivity has units of m/d.

Lower Carbonate Aquifer - Fractured Zone			
Trial	Conductivity		
	Kx	Ky	Kz
1	0.1	0.1	0.1
2	1	1	1
3	3	3	3
4	10	10	10
5	50	50	50
6	100	100	100

Water Levels [m] - Calibrated							
Devils Hole	Amargosa Playa Well	Lower Crystal Well	Point of Rocks South Well	Rogers ET1-D	MSH-C Well	Spring Meadows 9	Spring Meadows 11
720	708.5	658	710	688	713	686.5	723

Figure 6-3. Sensitivity analysis results for the fractured zone of the lower carbonate rock aquifer in the steady-state simulation. The plot represents the conditions listed in the 'conductivity table'. Calibrated water levels are listed in the lower table for comparison. Hydraulic conductivity has units of m/d.

conductivity in drain cells does take more ground-water out of the system (Fig. 6-4). However, the amount of ground-water entering the system to maintain a mass balance to the increased flow out through drains is governed by the conductivity of the un-fractured zone. Figure 6-1 shows that the mass entering the system due to increased vertical hydraulic conductivity in drain cells is similar to the mass flux curve for the un-fractured zone.

The Ash Meadows Fault System is shown not to have large effects on the ground-water system for different values of vertical hydraulic conductivity (Fig. 6-5). For variation in hydraulic conductivity in the horizontal dimension, the fault system does have a large influence on the mass flux exiting the ground-water system. This is recognized in Figure 6-5 by declining water levels in observation wells with proximity to the fault system.

6.1.4 Devils Hole as Open Water Surface

The shape and nature of Devils Hole in the study area is quite unique. It is a pool feature that extends vertically down through the model domain. Realistically, the vertical hydraulic conductivity in Devils Hole is very high. In model simulations, no special hydrogeologic distinctions were given to Devils Hole due to the very small area that it encompasses within a grid cell. A sensitivity analysis was performed to examine the effects of raising the value of vertical hydraulic conductivity for the Devils Hole cell. This was accomplished using a vertical hydraulic conductivity of 1×10^{10} m/d in grid cells that contain Devils Hole from layer 1 to layer 5. Horizontal conductivities remained unchanged with respect to surroundings. Results of this

Water Levels [m] - Calibrated							
Devils Hole	Amargosa Playa Well	Lower Crystal Well	Point of Rocks South Well	Rogers ET1-D	MSH-C Well	Spring Meadows 9	Spring Meadows 11
720	708.5	658	710	688	713	686.5	723

Figure 6-4. Sensitivity analysis results for drain fracture zones in the steady-state simulation. The plot represents the conditions listed in the 'conductivity table'. Calibrated water levels are listed in the lower table for comparison. Hydraulic conductivity has units of m/d.
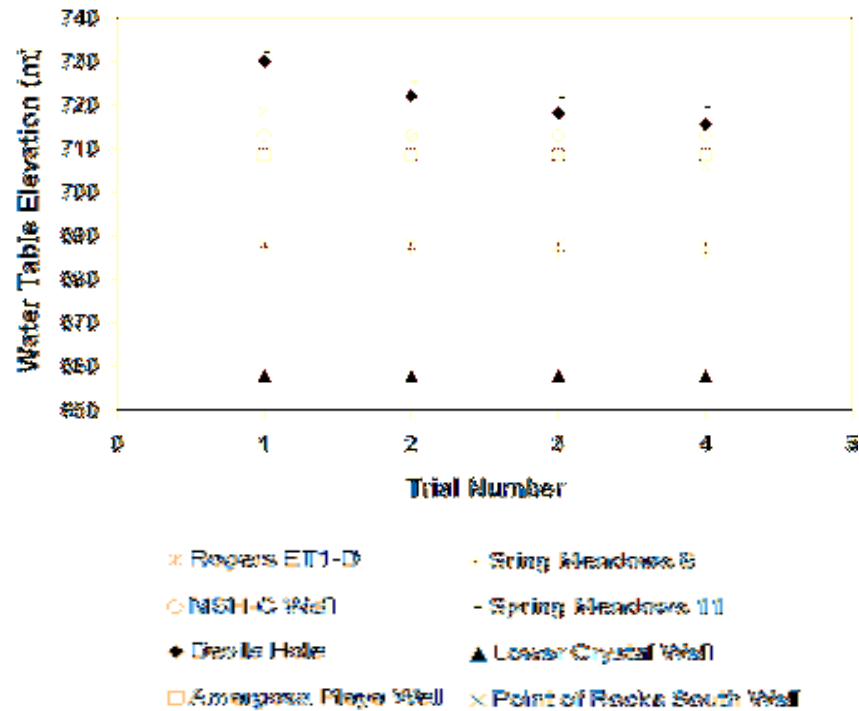
Ash Meadows Fault System			
Trial	Conductivity		
	Kx	Ky	Kz
1	0.01	0.01	0.001
2	0.01	0.01	0.01
3	0.01	0.01	1
4	0.01	0.01	10
5	0.0001	0.0001	0.1
6	0.001	0.001	0.1
7	0.1	0.1	0.1
8	1	1	0.1

Water Levels [m] - Calibrated							
Devils Hole	Amargosa Playa Well	Lower Crystal Well	Point of Rocks South Well	Rogers ET1-D	MSH-C Well	Spring Meadows 9	Spring Meadows 11
720	708.5	658	710	688	713	686.5	723

Figure 6-5. Sensitivity analysis results for the Ash Meadows Fault System in the steady-state simulation. The plot represents the conditions listed in the 'conductivity table'. Calibrated water levels are listed in the lower table for comparison. Hydraulic conductivity has units of m/d.

analysis indicate that changes in vertical hydraulic conductivity have little to no effect on the water level in Devils Hole. It is also noted that vertical hydraulic conductivity was assigned to the entire cell dimensions containing Devils Hole which is an area 72,500 m^2 larger than the actual pool in Devils Hole. Therefore, results would be of greater similarity if a smaller grid mesh was utilized.

6.2 TRANSIENT MODEL ANALYSES AND RESULTS

6.2.1 Overview

Two transient models were developed to investigate the effects of tectonic strain on the water level in Devils Hole. Both transient models differ from the steady-state model by the incorporation of specific storage values and evolving recharge values. The two transient models are differentiated from each other by run time. The first transient model, which was used to model the effects of altering recharge values through time and tectonic deformation through storage values, runs for 11 years where each year was a new stress period composed of 100 time steps. The 11-year duration was selected because of the availability of the water level data from Devils Hole. In this model, recharge values were updated yearly according to observed precipitation values and storage was altered once for the entire model simulation to simulate tectonic deformation. The second transient model also ran for 11 years, but was not continuous. The 11-year transient run was accomplished by coupling 11 one-year simulations together. Each one-year simulation was a stress period also composed of 100 time steps. For each one-year simulation, the appropriate recharge value was assigned, and the hydraulic head output from the previous stress period was

used as initial hydraulic heads for the current stress period. The reason for using a coupled model was that hydraulic head output could be altered due to strain prior to the next stress period where it as used as initial hydraulic heads. This modeling technique was used to simulate tectonic deformation through changes in specific storage values or hydraulic head values.

6.2.2 Precipitation Rates to Observed Water Level

Devils Hole is located at the contact of a desert basin with mountains. Precipitation rates gathered for modeling purposes were taken from both basin and mountain locations. Precipitation records for both mountain and basin areas were plotted against yearly averaged observed water levels in Devils Hole (Fig. 6-6). Precipitation from the mountain areas matched the curve of the observed water level better and was used in model simulations. The percentage of precipitation that was assumed to be recharge to the ground-water flow system was varied between 0.01 and 0.1 percent. Results of this variation are shown in Figure 6-7. The shapes of the curves do not change, only the ground-water level in the system is affected. For the purpose of this study, a 0.05 percentage was used to best fit the observed water-level data in Devils Hole and because the volume of water is more realistic.

Model simulations were performed that included both mountain and basin precipitation as recharge to the ground-water system. The results of those simulations were similar to simulations of only mountain recharge. If the percentages of precipitation were raised for recharge values, a larger volume of ground-water entered the system; if percentages decreased, less volume was added. Differences in these simulations were in the overall trend of water levels to observed water levels. When
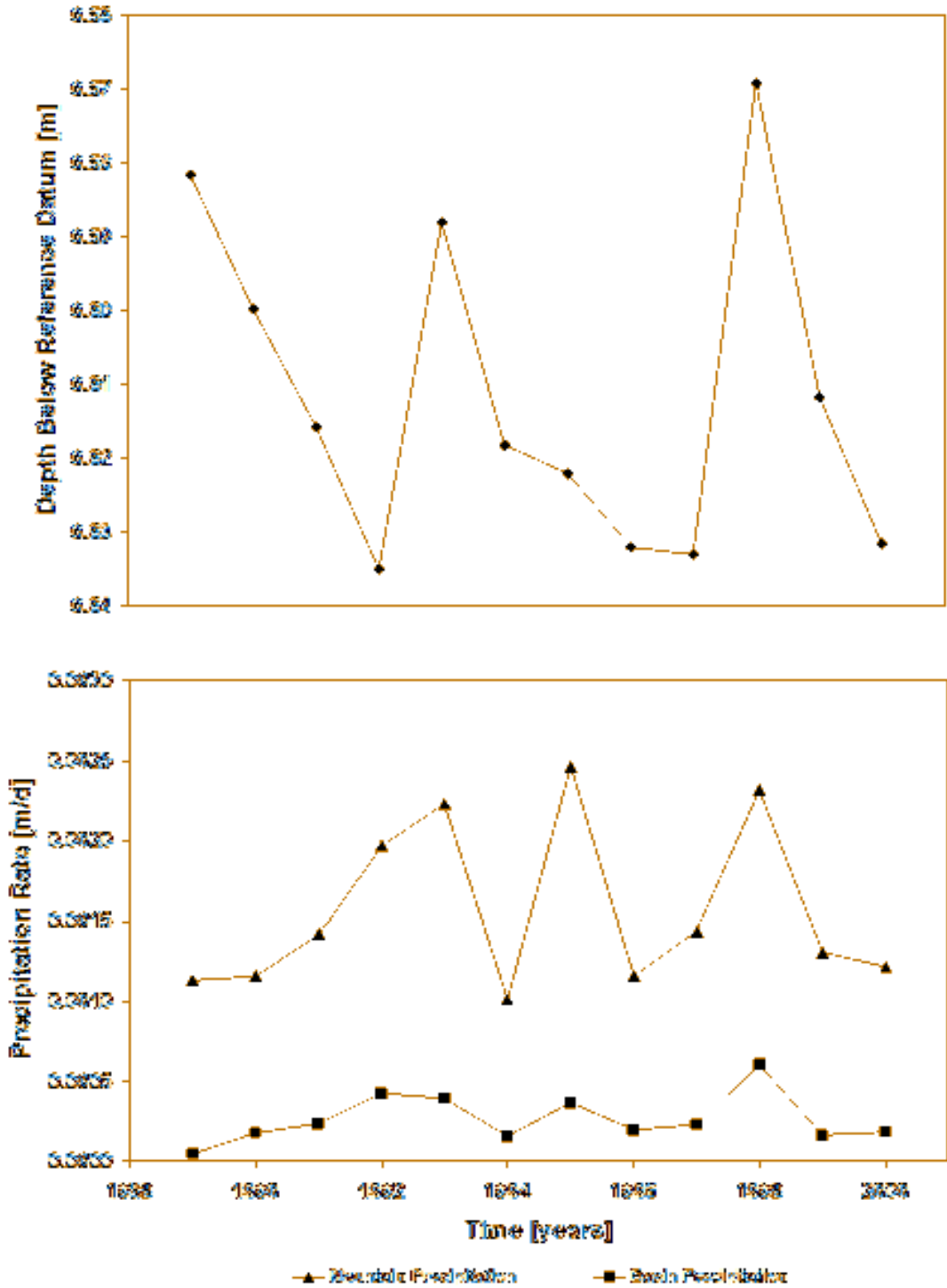
Figure 6-6. Top: Yearly average water level in Devils Hole. Bottom: Basin and mountain daily precipitation rates reported as yearly values. Mountain precipitation shows a better match to observed water levels with a peak in 1993 and a declining trend from 1999 to 2000. Precipitation data from Fenelon and Moreo (2002) and Western Regional Climate Center (2005).
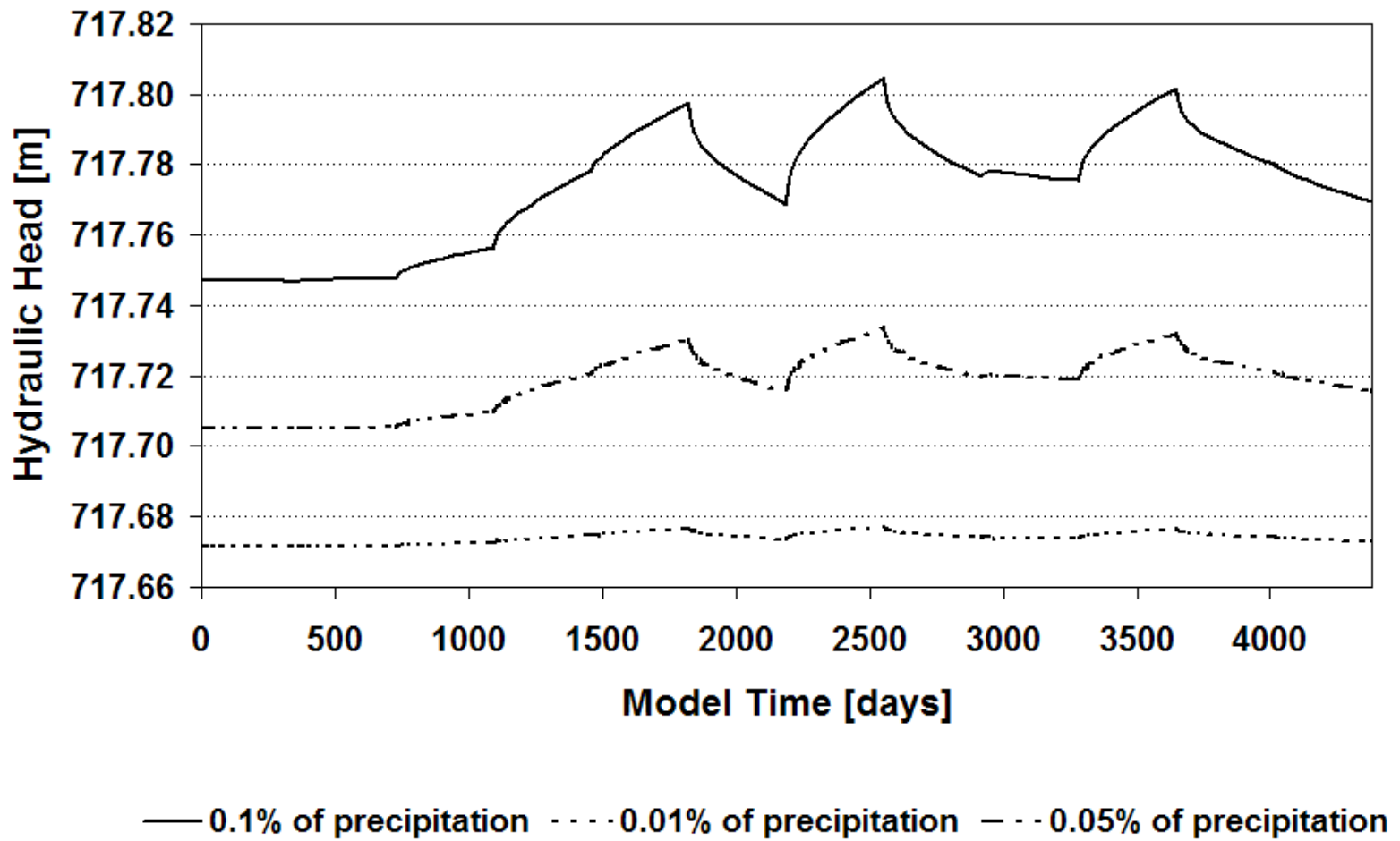
Figure 6-7. Hydraulic head in Devils Hole produced from varying rates of recharge determined through different percentages of recharge due to precipitation in the Spring Mountains (Fenelon and Moreo, 2002).

a basin recharge value was assigned, figured from basin precipitation, the simulated water levels in Devils Hole did not match the trend of the observed water levels. This is supported by Figure 6-6, where basin precipitation was plotted against observed water levels. Additionally, this indicates that mountain precipitation dominates for recharge into the Devils Hole area and basin precipitation may be relatively insignificant or that mountain precipitation rates may extend farther into the desert basins than assumed.

6.2.3 Strain Incorporated into Specific Storage

Tectonic deformation was first imposed on the model domain through porosity changes reflected in specific storage values. This was accomplished by determining a volumetric change in grid cells due to strain present in the study area, which was interpreted as a change in void volume of a grid cell. The new void volume was used to calculate a new porosity value to be incorporated into specific storage values. Refer to Chapter IV for a detailed explanation.

Multiple scenarios were run for various strain orientations and magnitudes. Strain orientations varied from N 55 W to N 95 W; strain rates between 8 and 50 nanostrain/yr were used. The extents of the strain orientations simulated were determined by geological features near the study area. The orientation of N 55 W was determined from the scarp face on an outcrop of rock located south of the study area on the Stateline Fault (Fig. 2-3). This orientation is probably greatly influenced by the orientation of faulting, but provides a reasonable orientation for analysis. The orientation of N 85 W was supported by strain orientations is the southeast portion of the Walker Lane Zone (Bellier and Zoback, 1995) and by the occurrence of a caldera

complex located to the northwest of the study area (Fig. 2-3). The reported strain orientation in proximity to the study area is N 65 W, as reported at the Nevada Test Site through GPS equipment. The strain rates of 8 to 50 nanostrain/yr used in simulations were also recorded by this equipment.

In model simulations, a constant storage value for each storage zone was used for the entire simulation time of the model – 11 years. This was done because MODFLOW-2000 does not allow for specific storage values to change during simulation time (Harbaugh et al., 2000). Results of tectonic deformation simulations for altered storage values are shown in Figure 6-8 where little to no overall change in the water level in Devils Hole was found. In all cases, recharge dominated curve shape and re-established a 'no strain' case through time. The magnitudes of the changes in specific storage resulting from strain were not significant enough to cause noticeable changes in the water level. The result of imposing strain caused storage values to change on the order of 10^{-8} m^{-1} to 10^{-9} m^{-1}. The values of hydraulic conductivity in the study area are on the order of 10^{-3} m/d to 10^{2} m/d and initial specific storage values are on the order of 10^{-5} m^{-1} to 10^{-3} m^{-1}. The large difference in magnitude of the initial specific storage values and hydraulic conductivity terms to the change in specific storage values renders the changes in specific storage and diffusivity insignificant.

A more realistic simulation was performed where the specific storage change due to tectonic deformation was additive through time. This was accomplished using the second transient model (coupled model). Values of specific storage change were determined using the methodology described in Chapter IV for strain trending N 65
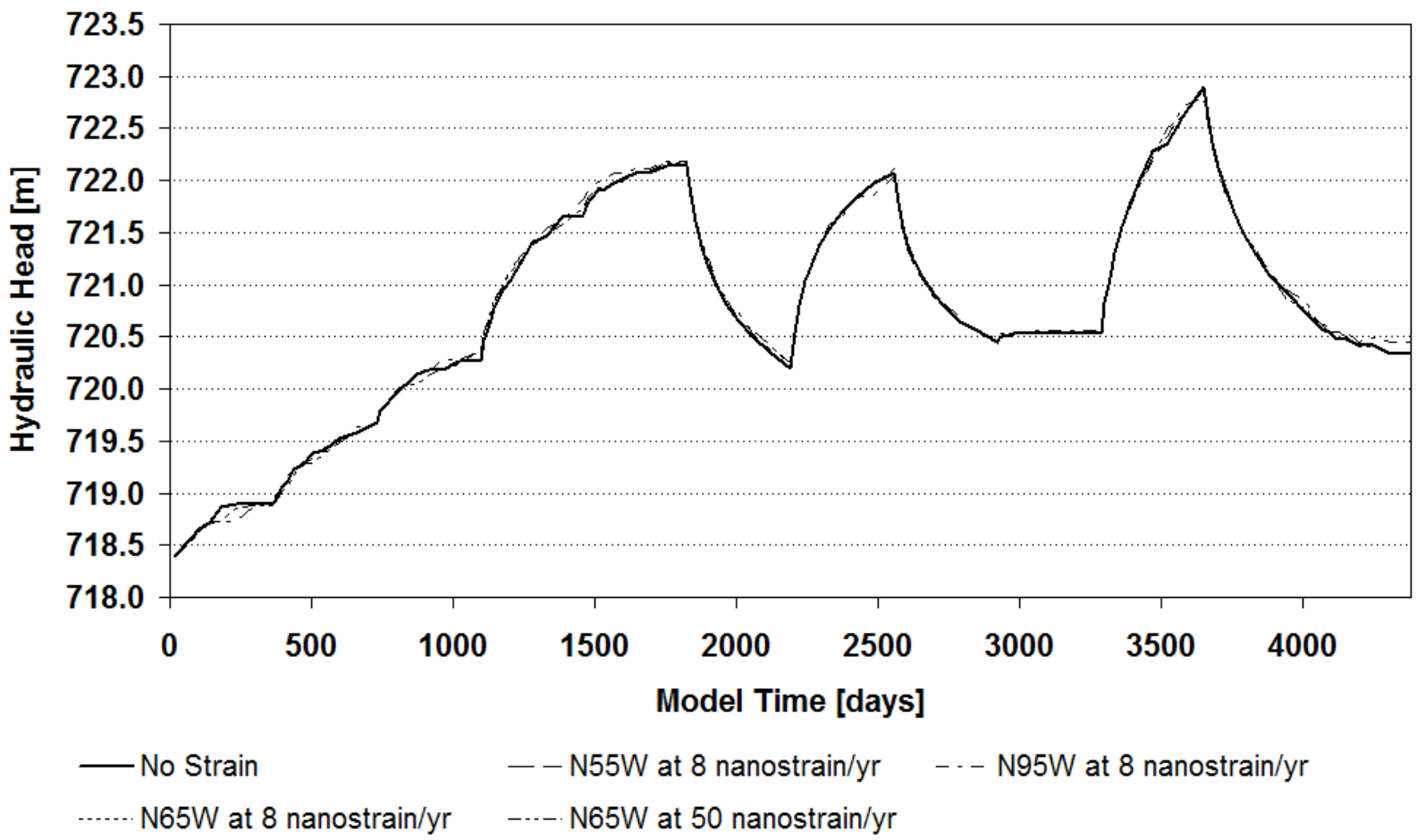
Figure 6-8. Hydraulic head at Devils Hole resulting from modeling strain through storage values for different magnitudes and orientations of strain.

W. The values were added to the values of specific storage used in the first stress period to create the values of specific storage for the second stress period. This process continued in fashion where a new specific storage values were used for each stress period that were greater than the previous stress period by the calculated amount.   Recharge values were also updated accordingly for each stress period through the simulation. Results of this simulation indicated no long term effects in water level and were similar to previous simulations.

To noticeably effect water levels in Devils Hole using the numerical model, specific storage values need to be altered by values of 10^{-4} m^{-1} or more. The values of specific storage determined through changes in tectonic deformation are not within these magnitudes. Potentially over a much longer time scale, the additive amount of specific storage due to strain would resemble a value closer to these that can alter water levels. However, the year to year change would still remain small and would be reflective of the results compiled in these simulations.

6.2.4 Strain Incorporated into Hydraulic Head

Hydraulic head values can be affected by strain as described in Chapter IV. In this approach, volumetric strain is used in conjunction with properties of the porous media to create a pore pressure change. The pore pressure change is interpreted as a hydraulic head change using the equation for hydrostatic pressure. A detailed explanation of this approach is found in Chapter IV. This method has been used by Cutillo and Ge (in press) to explore the effects of poroelastic responses to earthquakes in the Devils Hole area.

The coupled transient model was used to examine the effects of tectonic deformation through hydraulic head values. Between each stress period, initial hydraulic head values were updated to account for volumetric strain by subtracting away a change in hydraulic head determined though calculations using equation 9. In total, hydraulic head was updated ten times over the course of 11 years to simulate tectonic deformation. Extension dominates in the study area, so values of hydraulic head change are subtracted from output hydraulic head values of the previous time step. The value subtracted away, 0.001 m/yr, represents a maximum scenario of hydraulic head change due to extension. This is because Skempton's coefficient was assumed to be one to maximize pore pressure change and matrix compressibility was on the lower extents of values determined by Bredehoeft (1992). A maximum case scenario was used to explore the extent of tectonic deformations impact on the water level in Devils Hole. It is assumed that volumetric strain does not change over 11 years; therefore, alterations in Skempton's coefficient and/or matrix compressibility would alter the value of hydraulic head change. Recall that Skempton's coefficient is a value between 0.5 and 1.0 for saturated rocks. Reducing Skempton's coefficient would decrease pore pressure according to equation 6, Chapter IV. Matrix compressibility is proportional to the inverse of the bulk modulus, which is subject to variation. The value used for matrix compressibility was a low, increasing the value would reduce hydraulic head change according to equation 9, Chapter IV. Averaged annual results of the transient simulation are shown in Figure 6-9. During the transient simulation, recharge was updated
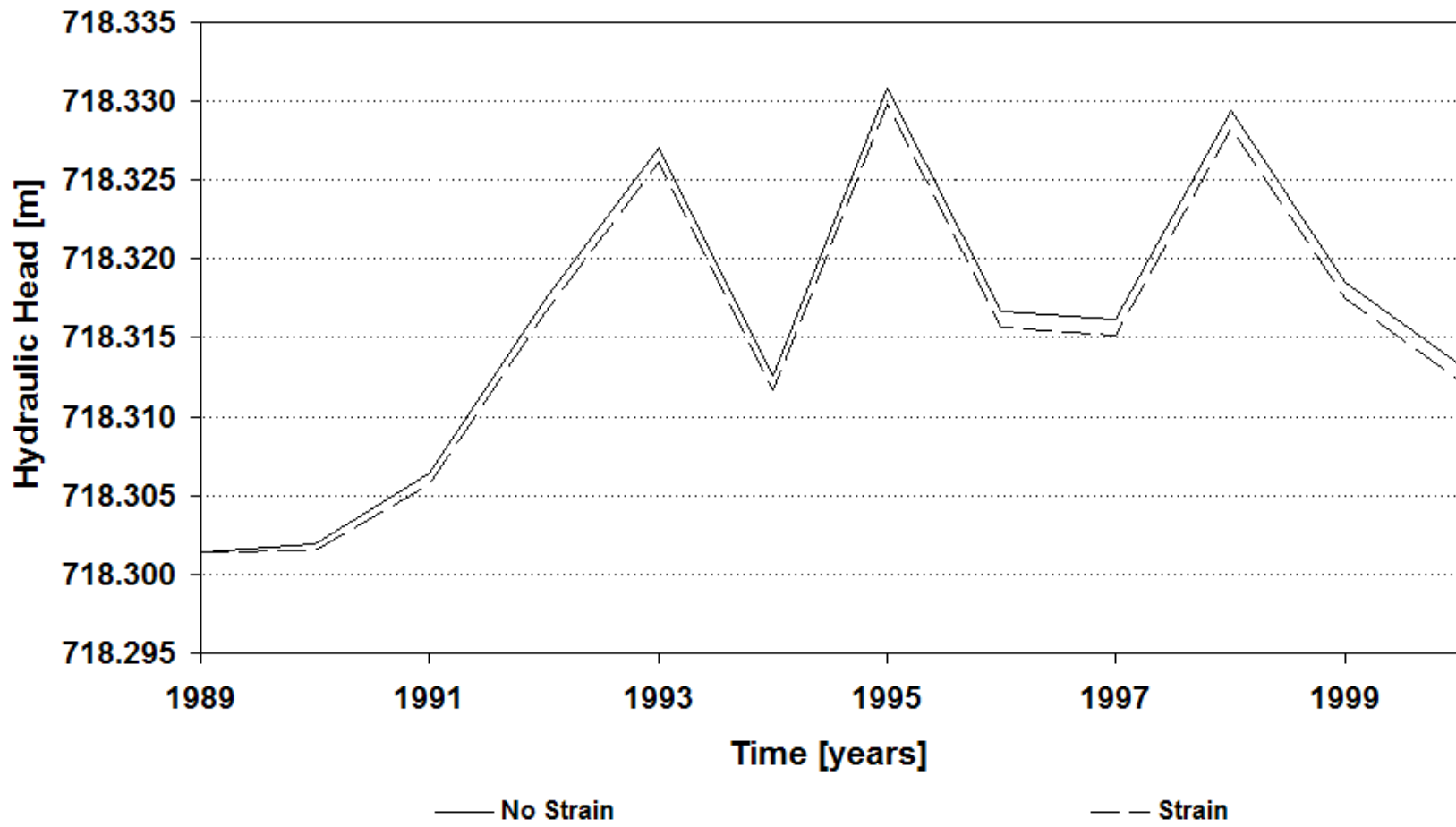
Figure 6-9. Hydraulic head at Devils Hole reported as the final time steps of each stress period for no strain and maximum strain scenario. Two millimeters of hydraulic head change results over the course of 11 years. During high recharge years, 1994 to 1995, the strain curve moves closer to the no strain curve; the opposite is true for low recharge years, 1996 to 1997.

accordingly for each stress period.

The results of the transient simulation show that water level in Devils Hole is affected by tectonic deformation. A rate of 0.001 m/yr of hydraulic head change over 11 years was imposed on the numerical model. Results show an average rate of 0.00018 m/yr of water-level decline as a result of the imposed rate of decline. This results in a difference of only 0.2 cm at the conclusion of simulation. The reasoning for the discrepancy is that recharge takes precedence in determining hydraulic head values in each stress period over the effects of strain. Notice that during times of increasing recharge, the strain curve moves closer to the no strain curve in Figure 6-9. Alternatively, during times of decreasing recharge, strain is allowed to have a greater influence on the ground-water system (Fig. 6-9). Because of the priority of recharge over strain, hydraulic head values will be determined to a greater degree by recharge then strain. The 0.2 cm of hydraulic head change resulting at the end of the last stress period is attributed to strain.

The water levels for the strain with recharge simulation are plotted with the observed water levels in Devils Hole in Figure 6-10. The simulated water levels are reported for every time step of every stress period in the model to show the evolution of the water levels within each stress period. The observed water levels are reported as monthly means. The long term decline in the observed water level is not realized, only small perturbations (Fig. 6-10). This indicates that there must be other factors affecting the water level in Devils Hole.
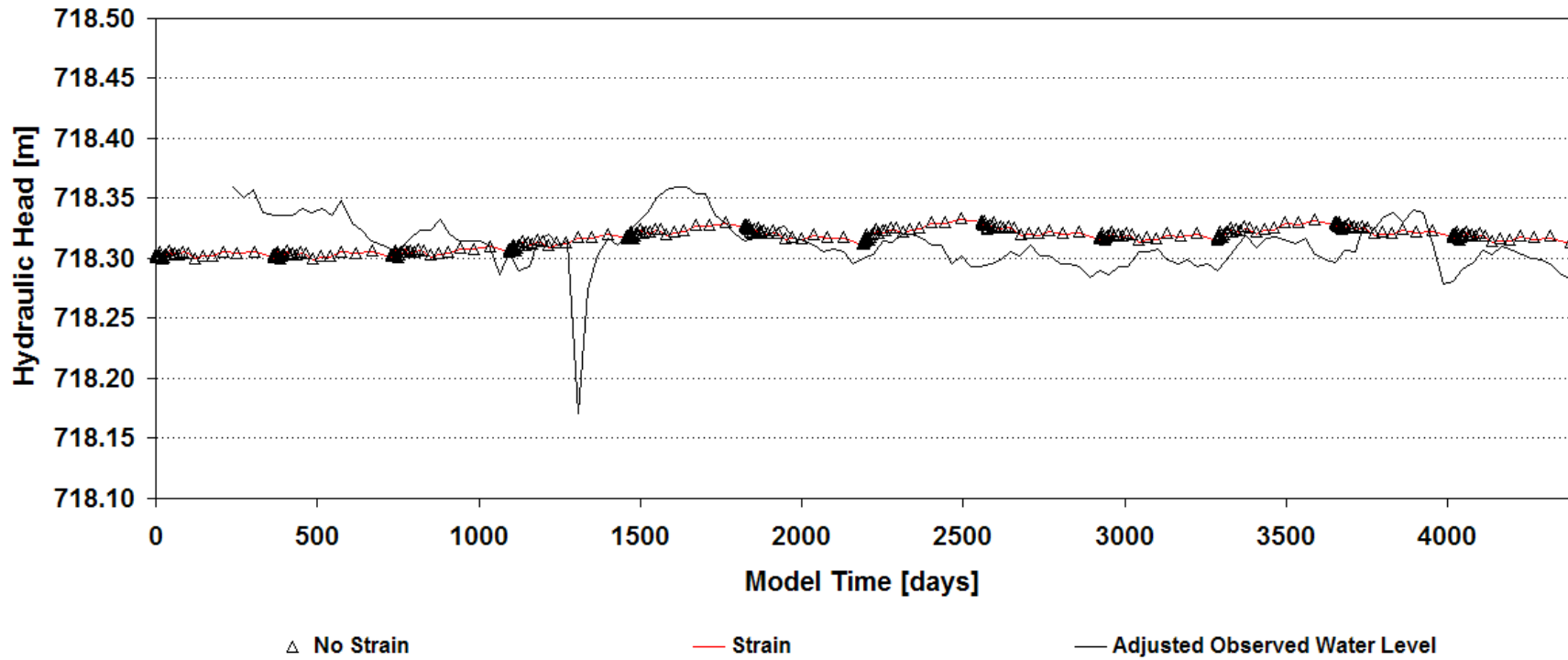
Figure 6-10. Simulated water levels in Devils Hole for no strain and strain cases plotted against the observed water level in Devils Hole. The data of observed water level have been adjusted to be consistent with the model. The large spike in the observed water level at 1250 days is due to an earthquake.

CHAPTER VII

DISCUSSION AND CONCLUSIONS

The impact of tectonic deformation was investigated as a source of water-level decline in Devils Hole. This was performed by creating models that simulated tectonic deformation through porosity and hydraulic head values. Porosity values were reflected in specific storage values for model simulations, hydraulic head values were updated yearly to account for strain. Little to no alteration in water level was reported for strain calculated through porosity values. Strain through hydraulic head was shown to have an effect on the water level in Devils Hole at very small scales. The leading factor in the water level changes in Devils Hole, as determined through transient simulations, was recharge.

In the course of this study, two factors were identified that have large impacts on the water-level changes in Devils Hole – ground-water pumping and precipitation. According to Bedinger and Harrill (in press), the long term declining trend in the water level in Devils Hole may be caused from distant ground-water pumping located in the primary recharge path to Devils Hole (Bedinger and Harrill, in press). Ground-water pumping in large volumes occurred in the Army 1 Well from the period of 1988 to 1995. During this time, the water level in Devils Hole experienced overall declines. When pumping was reduced from 1997 to 1995, the year to year change of water level in Devils Hole became more reflective of the annual precipitation rate than pumping, indicated in Figure 7-1 by the decrease in distance from the precipitation curve to the annual change in water-level curve for a given year. After
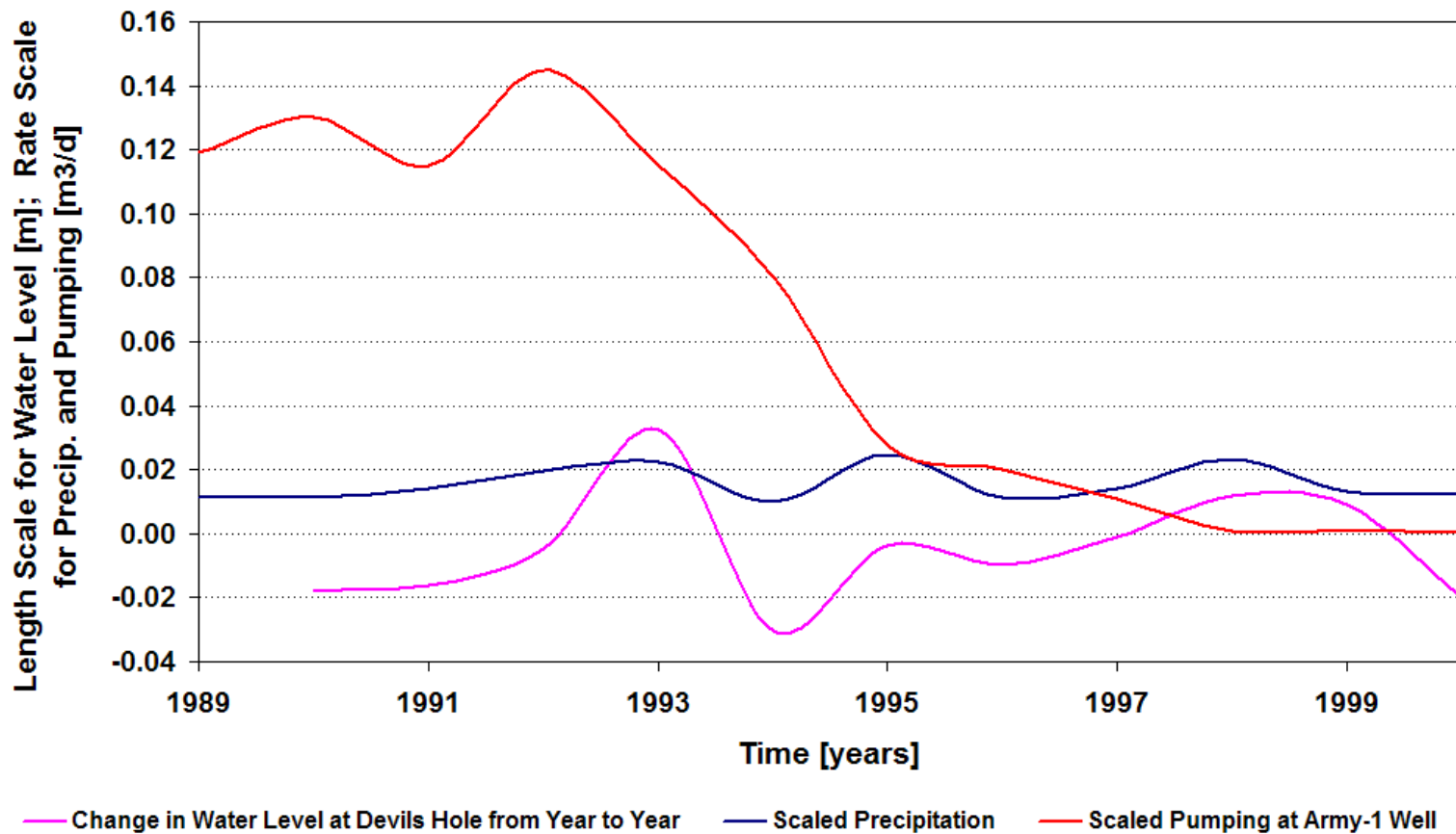
Figure 7-1. Relationship of the averaged annual water-level changes in Devils Hole to precipitation (Fenelon and Moreo, 2002) and ground-water pumping at Army-1 Well (Bedinger and Harrill, in press). Year to year changes in water level become more dependent on precipitation with decreased ground-water pumping.

ground-water pumping was effectively abandoned, beyond 1997, this trend in the annual change reflecting values nearer the precipitation values continued. Short term fluctuations, on the order of 0.01 m to 0.03 m, are dictated by variations in annual precipitation (Fig. 3-3).

Army-1 Well pumping was not modeled in this study. Instead, the effects of ground-water pumping on the water level in Devils Hole determined by Bedinger and Harrill (in press) can be subtracted away from simulated results of tectonic deformation in this study to accommodate ground-water pumping. This creates more realistic results that include ground-water pumping from the Army 1 Well for comparison to the observed water level in Devils Hole (Fig. 7-2). Results show that ground-water pumping creates the primary decline in the water level in Devils Hole. Precipitation is the next largest factor to explain the water-level fluctuations. Additional differences between the modeled curve and the observed data are the product of model uncertainties and/or other factors: barometric pressure, daily evaporation trends, daily precipitation events, and local seismic events.

The influence that tectonic deformation has on the water level in Devils Hole is probably steady and continues for long periods of time as the possibility of a changing stress field in time spans less than 100 years is unlikely. History of tectonic deformation was not pursued in this investigation, but should be conducted in the future, particularly the movement of the fault blocks that comprise Devils Hole. It was discussed that Devils Hole is a fault bounded dissolution cavern. Carr (1988) has documented that the faults that surround Devils Hole are prone to recent movement by the observation of warm, moist air exiting open fractures. The water levels that

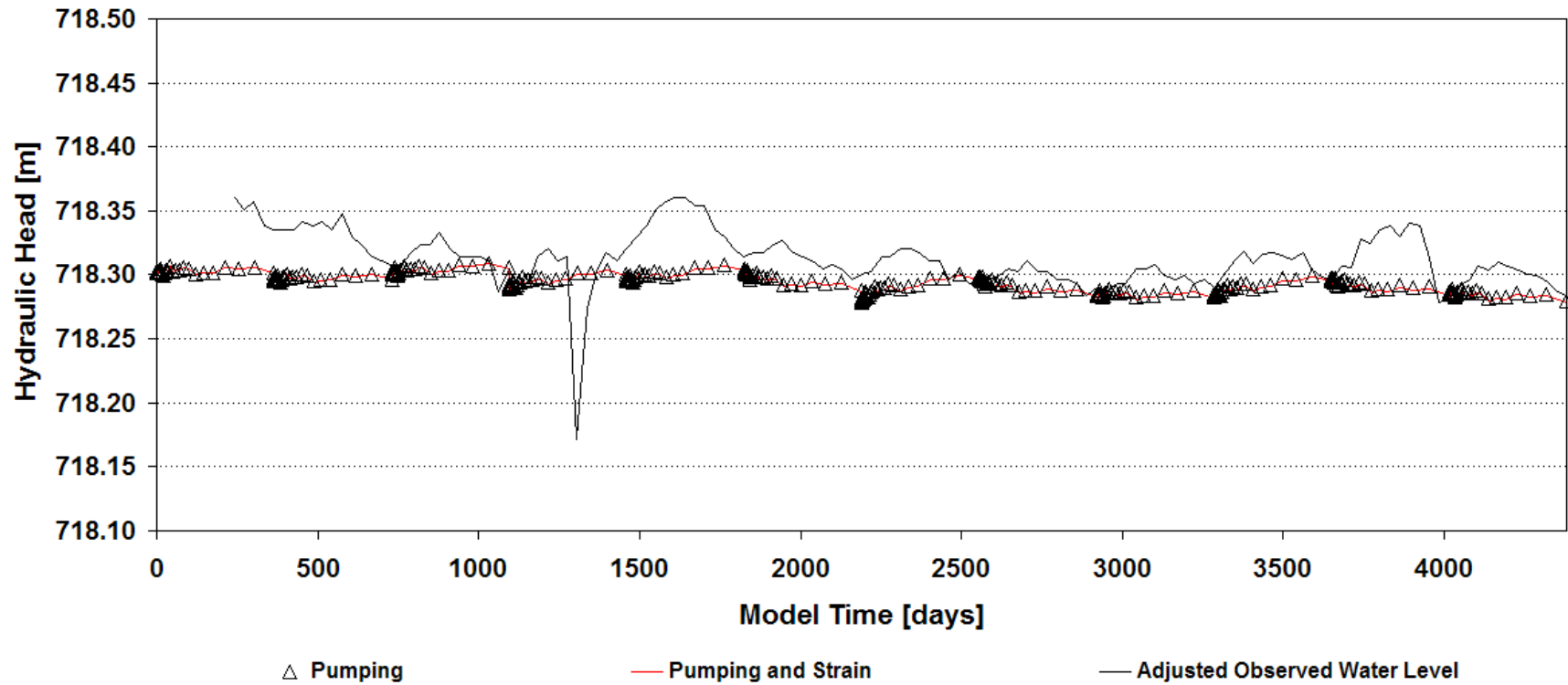Figure 7-2. Simulated water levels in Devils Hole for no strain and strain cases incorporating pumping plotted against the observed water level in Devils Hole. Pumping effects were taken from Bedinger and Harrill (in press). Pumping is shown to create the overall trend in the water level in Devils Hole; recharge through precipitation has the next largest effect for this study, followed by strain.

are monitored in Devils Hole are the result of measurements taken from the water surface to a bolt fixed into the wall of Devils Hole. If the fault blocks that house Devils Hole are moving, then the bolt should move as well. The long term decline in the water level in Devils Hole, even prior to pumping in the 1960's, could be the result of measurement error. Hourly to monthly measurements of the water level in Devils Hole will not reflect the potential movement of the bolt, however the long term trend in the water level could. This theory assumes that the water level in Devils Hole remains constant or that the water level and bolt are moving at differential rates that show an overall increase in distance with time.

Because the purpose of this study was to investigate the effects of tectonic deformation on water levels in Devils Hole; matching the exact water-level fluctuations was beyond the scope of this study. Recharge and pumping were used to establish the hierarchy of factors affecting the water levels in Devils Hole. To further match the water-level fluctuations in Devils Hole more detailed modeling is needed in the future to investigate system uncertainties associated with storage, boundary conditions, external stresses, and stress periods. Tectonic deformation through annual hydraulic head change produced results. Tectonic deformation is a continuous process and does not occur on an annual basis. Better simulations would require more stress periods over the same simulation time (11 years) to create more realistic results. In addition, accurate measurements of tectonic deformation at Devils Hole, precipitation at Devils Hole, hydraulic conductivity of the Ash Meadows Fault System, and other atmospheric and environmental parameters need to be quantified and explored for better simulations. InSAR, GPS and geodetic equipment is available

to monitor tectonic strain if accurate surveys of installment points can be made. Precipitation can be monitored through a rain gauge station. It is also recommended to install instrumentation at Devils Hole that would measure barometric pressure, evaporation and wind speed to help explain the short term fluctuations witnessed in the water-level record.

REFERENCES

Anderson, R.E., Bucknam, R.C., Crone, A.J., Haller, K.M., Machette, M.N., Personius, S.F., Barnhard, T.P., Cecil, M.J., and R.L. Dart, 1995. Characterization of Quaternary and suspected Quaternary faults, regional studies, Nevada and California: U.S. Geological Survey Open File Report 95-599, 70 p., 2 sheets.

Archbold, N.L., 1972. Modified geologic map of Nevada, Nevada Bureau of Minds and Geology – Map 44, scale 1:1000000

Bedinger M.S. and J.R. Harrill, in press. Analytical-Regression Stage Analysis in Devils Hole, Death Valley National Park, Nevada, Journal of American Water Resources Association.

Belcher, W.R., Elliott, P.E., and A.L. Geldon, 2001. Hydraulic-property estimates for use with a transient ground-water flow model of the Death Valley regional ground-water flow system, Nevada and California: U.S. Geological Survey Water Resources Investigations Report 01-4120, 33 p.

Belcher, W.R., ed., 2004. Death Valley regional ground-water flow system, Nevada and California-Hydrogeologic framework and transient ground-water flow model: U.S. Geological Survey Scientific Investigations Report 2004-5205, 408p.

Bell, J.W., dePolo, C.M., Ramelli, A.R., Sarna-Wojcicki, A.M., and C.E. Meyer, 1999. Surface faulting and paleoseismic history of the 1932 Cedar Mountain earthquake area, west-central Nevada, and implications for modern tectonics of the Walker Lane, Geological Society of America Bulletin, v. 111, no. 6, p. 791-807.

Bellier, O., and M.L. Zoback, 1995. Recent state of stress change in the Walker Lane zone western Basin and Range province, United States, Tectonics, v. 14, no. 3, p. 564-593.

Biot, M.A., 1941. General theory of three-dimensional consolidation, Journal of Applied Physics, v. 12, p. 155-164.

Bredehoeft, J.D., 1992. "Response of the ground-water system at Yucca Mountain to an earthquake" in *Ground Water at Yucca Mountain: How High Can It Rise?* Appendix D, p. 212-222

Brocher, T.M., Carr, M.D., Fox, K.F. Jr. and P.E. Hart, 1993. Seismic reflection profiling across Tertiary extensional structures in the eastern Amargosa Desert, southern Nevada, Basin and Range province, Geological Society of America Bulletin, v. 105, p. 30-46.

Bunch, R.L. and J.R. Harrill, 1984. Compilation of selected hydrologic data from the MX Missle-Siting Investigation, east-central Nevada and western Utah: U.S. Geological Survey Open File Report 84-702, 123p.

Burbey, T.J. and D.E. Prudic, 1991. Conceptual Evaluation of regional ground-water flow Carbonate-Rock Province of the Great Basin, Nevada, Utah, and Adjacent States: U.S. Geological Survey Professional Paper 1409-D, 84p.

Carr, W.J., 1988. Geology of the Devils Hole area, Nevada: U.S. Geological Survey Open File Report 87-560, 34 p.
Conner, C.B., Stamatakos, J.A., Ferrill, D.A., and B.E. Hill, 1998. Technical Comments, Science, v. 282, p. 1007b.

Cutillo, P. and S. Ge, in press. Analysis of strain-induced ground-water fluctuations at Devils Hole, Nevada, Geofluids.

Denny, C.S. and H. Drewes, 1965. Geology of the Ash Meadows quadrangle, Nevada – California: U.S. Geological Survey Bulletin 1181-L, scale 1:62500.

Dettinger, M.D., Harrill, J.R., Schmidt, D.L., and J.W. Hess, 1995. Distribution of carbonate-rock aquifers and the potential for their development, southern Nevada and parts of Arizona, California, and Utah: U.S. Geological Survey Water Resources Investigations Report 91-4146, 100 p.

Domenico, P. A. and F. W. Schwartz, 1990. *Physical and Chemical Hydrogeology,* John Wiley and Sons, Inc., 824 p.

Donovan, D.E., 1991. Neotectonics of the southern Amargosa Desert, Nye County, Nevada, and Inyo County, California: Reno, University of Nevada, M.S. thesis, 151 p., 1 pl., scale 1:48,000.

Dudley, Jr., W.W. and J.D. Larson, 1976. Effect of Irrigation Pumping on Desert Pupfish Habitats in Ash Meadows, Nye County, Nevada: U.S. Geological Survey Professional Paper 927, 52p.

Eakin, T.E., Price, D., and J.R. Harrill, 1976. Summary appraisals of the Nation's ground-water resources-Great Basin region: U.S. Geological Survey Professional Paper 813-G, 37p., 1 pl.

ESRI, 2004. ArcMAP Help Menu, Leica Geosystems GIS Mapping, LLC., LizardTech, Inc., and Microsoft Corporation.

Fenelon, J.M. and M.T. Moreo, 2002. Trend Analysis of Ground-Water Levels and Spring Discharge in the Yucca Mountain Region, Nevada and California, 1960-2000: U.S. Geological Survey Water Resources Investigation Report 02-4178, 107p.

Fleeger, G., Doode, D., Buckwalter, T., and D. Risser, 1999. Hydrologic effects of the Pymatuning earthquake of September 25, 1998, in northwestern Pennsylvania: U.S. Geological Survey Water Resources Investigations Report 99-4170, p. 8.

Fridrich, C., 2005. Personal communication. October 2005.

Harbaugh, A.W., E.R. Banta, M.C. Hill, and M.G. McDonald, 2000, MODFLOW 2000, the U.S. Geological Survey modular ground-water model -- User guide to modularization concepts and the Ground-Water Flow Process; U.S. Geological Survey Open-File Report 00-92, 121 p.

Harrill, J. and D. Prudic, 1998. Aquifer systems in the great basin region of Nevada, Utah, and adjacent states-summary report: U.S. Geological Survey Professional Paper 1409-A.

Hay, R.L., Pexton, R.E., Teague, T.T., and T.K. Kyser, 1986. Spring-related carbonate rocks, Mg Clays, and associated minerals in Pliocene deposits of the Amargosa Desert, Nevada and California, Geological Society of America Bulletin, v. 97, no. 12, 1488-1503 p.

Hevesi, J.A., Flint, A.L., and L.E. Flint, 2003. Simulation of net infiltration and potential recharge using a distributed-parameter watershed model of the Death Valley Region, Nevada and California: U.S. Geological Survey Water Resources Investigations Report 03-4090, 161 p.

Hines, L.B., 1992. Quantification of natural ground-water evapotranspiration in Smith Creek Valley, Lander County, Nevada, In Selected papers in the hydrological sciences (Subitzky, Seymour, ed.): U.S. Geological Survey Water Supply Paper 2340.

Hunt, C.B. and D.R. Mabey, 1966. Stratigraphy and Structure Death Valley, California: U.S. Geological Survey Professional Paper 494-A. 162 p.

Laczniak, R.J., Cole, J.C., Sawyer, D.A., and D.A. Trudeau, 1996. Summary of hydrogeologic controls on ground-water flow at the Nevada Test Site, Nye County, Nevada: U.S. Geological Survey Water Resources Investigations Report 96-4109. 59 p.

Laczniak, R.J., DeMeo, G.A., Reiner, S.R., Smith, J.L., and W.E. Nylund, 1999. Estimates of ground-water discharge as determined from measurements of evapotranspiration, Ash Meadows area, Nye County, Nevada: U.S. Geological Survey Water Resources Investigations Report 99-4079, 70 p.

Menges, C., 2005. Death Valley Junction DLG and DEM Data: U.S. Geological Survey unpublished map, scale 1:50,000

Montgomery, D.R. and M. Manga, 2003. Streamflow and water well responses to earthquakes, Science, v. 300, 2047-2049 p.

Muir-wood, R. and G.C.P. King, 1993. Hydrological signatures of earthquake strain, Journal of Geophysical Research, v. 98, no. 12, 22035-22068 p.

Plume, R.W., 1996. Hydrogeologic framework of aquifer systems in the Great Basin region of Nevada, Utah, and adjacent States: U.S. Geological Professional Paper 1409-B, 64p.

Prudic, D.E., Harrill, J.R., and T.J. Burbey, 1995. Conceptual evaluation of regional ground-water flow in the carbonate-rock province of the Great Basin, Nevada, Utah, and adjacent States: U.S. Geological Survey Professional paper 1409-D, 102p.

Quilty, E., Farrar, C., Galloway, D., Hamlin, S., Laczniak, R., Roeloffs, E., Sorey, M., and D. Woodcock, 1995. Hydrologic effects associated with the January 17, 1994 Northridge, California, earthquake: U.S. Geological Survey Open File Report 95-813, p.47.

Rice, J.R. and M.P Cleary, 1976. Some basic stress diffusion solutions for fluid-saturated elastic porous-media with compressible constituents, Reviews of Geophysics, v. 14, p. 227-241.

Riggs, A.C., W.J. Carr, R.T. Kolesar, and R.J. Hoffman, 1994. Tectonic speleogenesis of Devils Hole, Nevada, and implications for hydrogeology and the development of long, continuous paleoenvironmental records, Quaternary Research, 42, 241-254.

Robinson, T.W., 1970. Evapotranspiration by woody phreatophytes in the Humboldt River Valley near Winnemucca, Nevada: U.S. Geological Survey Professional paper 491-D, 41p.

Rojstaczer, S. and S. Wolf, 1992. Permeability changes associated with large earthquakes: an example from Loma Prieta, California. Geology, v. 20 p. 211-214.

Savage, J.C., 1998. Detecting strain in the Yucca Mountain area, Nevada, Science, v. 282, p. 1007b.

Schlumberger, 2005. Visual MODFLOW v. 4.1 User's Manual, Waterloo Hydrogeologic Inc., 613 p.

Schweickert, R.A. and M.M. Lahren, 1997. Strike-slip fault system in Amargosa Valley and Yucca Mountain, Nevada, Tectonophysics, v. 272, p. 25-41.

Sneed, M., Galloway, D. and W. Cunningham, 2003. Earthquakes-Rattling the Earth's plumbing system: U.S. Geological Survey Fact Sheet 096-03, p.5.

Szabo, B., Kolesar, P., Riggs, A., Winograd, I. and K. Ludwig, 1994. Paleoclimatic Inferences from a 120,000-yr calcite record of water-table fluctuation in Browns Room of Devils Hole, Nevada. Quaternary Research, v. 41, p. 59-69.

Turcotte, D.L., and G. Schubert, 2002. *Geodynamics 2nd Edition*, Cambridge University Press, 456 p.

USGS, 1971. Field Trip to Nevada Test Site, United States Geological Survey Water Resources Division, 40 p.

USGS, 2005. "Location and general information about ground-water, surface water, and meteorological data for sites in USA." Online query. 03 November 2005 <http://waterdata.usgs.gov/nwis/gwlevels>.

Vorhis, R., 1966. Hydrologic effects of the earthquake of March 27, 1964 outside Alaska: U.S. Geological Survey Professional Paper 544-C, p. 54.

Waddell, R.K., Robison, J.H., and R.K. Blankennagel, 1984. Hydrology of Yucca Mountain and vicinity, Nevada, California – Investigative results through mid 1983: U.S. Geological Survey Water Resources Investigations Report 84-4267. 72p.

Walker, G.E. and T.E. Eakin, 1963. Geology and ground-water of Amargosa Desert, Nevada-California: Nevada Department of Conservation and Natural Resources, Ground-Water Resources – Reconnaissance Serial Report 14, 45p.

Wang, H.F., 2000. *Theory of Linear Poroelasticity with Applications to Geomechanics and Hydrogeology*, Princeton University Press, New Jersey, 287 p.

Wernicke, B., Davis, J., Bennett, R., Elosegui, P., Abolins, M., Brady, R., House, M., Niemi, N., and J. Snow, 1998. Anomalous strain accumulation in the Yucca Mountain area, Nevada. Science, v. 279, p. 2096-2099.

Western Regional Climate Center, 2005. "Water Levels Reported for Amargosa Farms." Online query results. 03 November 2005 <http://www.wrcc.dri.edu/>.

Winograd I.J. and F.J. Pearson, Jr., 1976. Carbon 14 anomaly in a regional carbonate aquifer: Possible evidence for megascale channeling, south-central Great Basin, Water Resources Research, v. 12, no. 6.

Winograd, I.J., and W. Thordarson, 1975. Hydrogeologic and hydrochemical framework, south-central Great Basin, Nevada-California, with special reference to the Nevada Test Site: U.S. Geological Survey Professional
Paper 712-C, 125 p.

Winograd, I. and B. Szabo, 1986. Water-table decline in the south-central Great Basin during the Quaternary: Implications for toxic waste disposal: U.S. Geological Survey Open File Report 85-697, 18 p.

Worts, G.F., 1963. Effect of ground-water development on the pool level in Devils Hole, Death Valley National Monument, Nye County, Nevada: U.S. Geological Survey Open File Report, 27 p.

Yeats, R.S., Sieh, K., and C.R. Allen, 1997. *The Geology of Earthquakes,* Oxford University Press, New York, 568 p.

APPENDIX A

FORMULATION OF MODEL LAYER SURFACE ELEVATIONS

General terms used in ArcGIS that will be used throughout this appendix are defined (ESRI, 2004):

- Project File: File created that contains all data used to project images onto the screen.
- Shapefile: Store geographic features and their attributes. Geographic features in a shapefile can be represented by points, lines, or polygons (areas). The folder might also contain dBASE tables, which can store additional attributes that can be joined to a shapefile's features.
- Attributes Table: Tables used to organize and manage descriptive data about shapefiles. They can be used to view, select, analyze, and display features contained within the shapefile.

An example of this is a shapefile of "roads" in the Great Basin. If this shapefile were to be activated in the project file, all of the roads in the Great Basin would appear on the screen. The result of altering the information in an attributes table is reflected on the screen for that particular shapefile.

Initially, a digital elevation map (DEM) was displayed in an ArcGIS project file to represent the ground surface of the model domain. To establish the elevations of the contacts between each layer in the model, the thicknesses of the lithologic layers needed to be determined and recorded throughout the model domain. A point shapefile, "theoretical wells," was created to input lithologic information throughout the study area (Fig. A-1). In total, 1,200 wells were created over a uniform grid. In each well, for each layer, a number was recorded in the attributes table of "theoretical wells" that is the thickness of the lithology represented by the layer. For example, Well 1 records values of 5 m, 10 m, 12 m, 30 m, 300 m, and 400 m. These values

represent the thicknesses of layer 1, layer 2, layer 3, layer 4, layer 5 and layer 6, respectively, for the location of Well 1. Thicknesses of lithologies were from Belcher (2004) who records a range in thickness for each lithology for each grid cell in his model. Since the grid is much finer for this study, greater detail is given to the thickness of each layer. Values of thickness were assigned to each well to better represent the depositional environments within the constraints set forth by Belcher (2004).

After the "theoretical wells" attribute table was populated with layer thickness data, layer elevations were determined. Values for the thickness of layer 1 were subtracted from the elevations of the ground surface represented by the DEM at the locations of each well. The values calculated indicate the elevation of the contact between the bottom of layer 1 and the top of layer 2 (Fig. A-2). The values for the thickness of layer 2 were then subtracted from the calculated elevation of the boundary between layers 1 and layer 2 to create the boundary between the bottom of layer 2 and the top of layer 3. This process continued through the rest of the model layers. The values for the layer boundaries were recorded as another set of numbers in the "theoretical wells" attribute table. The new values for layer elevation were interpolated in ArcGIS to create individual continuous layers representing the elevations of lithology contacts. A natural neighbors interpolation technique was used. Layer elevations were exported out of ArcGIS as ascii files.
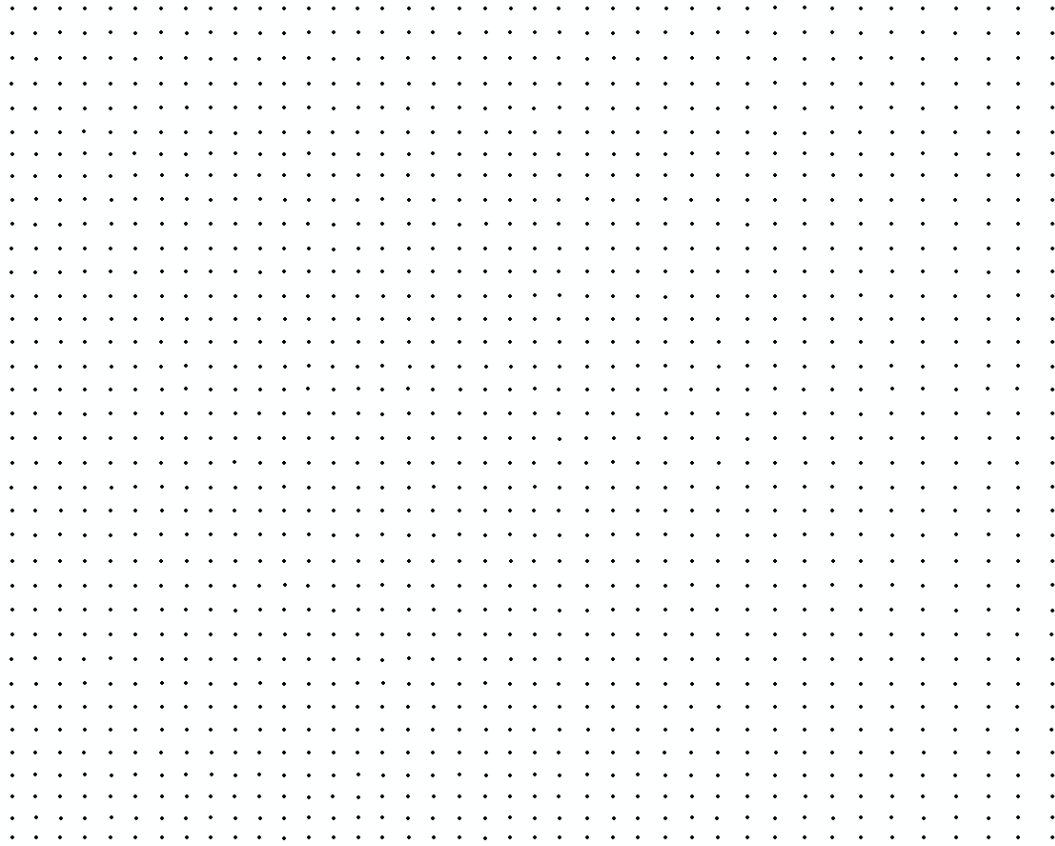
Figure A-1. Locations of individual wells in the "theoretical wells" shapefile for the study area. Layer depth for all six layers of the model were determined using these locations.
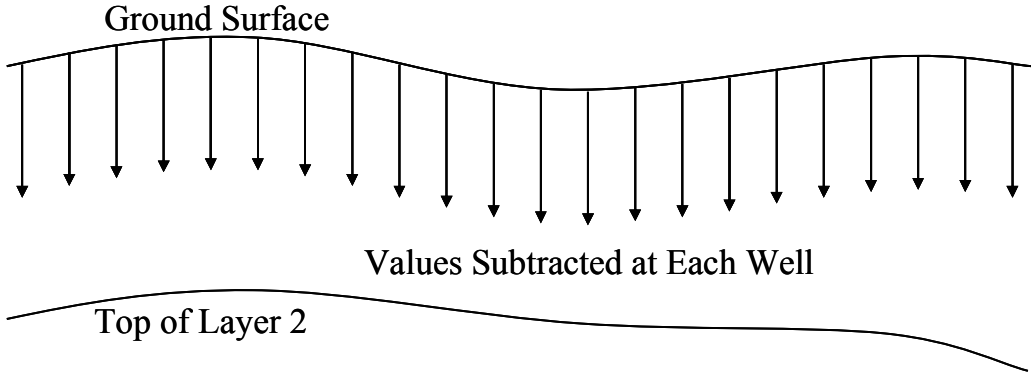

Figure A-2. Cross-sectional view showing the subtraction of values from the top of layer 1 at different well locations to create layer 2 elevations. Values at each well were different.

APPENDIX B

POROSITY UPDATING PROGRAM

2D Strain Code for Devils Hole Study Area
Coded by Greg Robertson, February 10, 2006

This code is intended to examine non-elastic strain the southern Great Basin region as reported through evolving porosity values. Inputs to the program include grid dimensions from a flow simulator (MODFLOW) to determine volume, strain, strain orientation, and initial porosity. The outputs of this program are values of specific storage for different zones. The zones are determined from the grid input to the model. To calculate specific storage, the following values will be used: fluid density, gravitational constant, matrix compressibility, and fluid compressibility.

```
%---Sensitive Value -------------------------------------
phi_i_zone_1 = .0001;
phi_i_zone_2 = .3;          %Value taken from Winograd and
                             Thordarson, 1975
phi_i_zone_3 = .054;        %Value taken from Winograd and
                             Thordarson, 1975
phi_i_zone_4 = .038;        %Value taken from Winograd and
                             Thordarson, 1975
trend = 65;                 %Trend of strain
strain = 8e-9;              %Rate of strain [strain/yr]

%---Constant Values--------------------------------------
density_fluid = 1000;   %Density of water in [kg/m^3]
g = 9.8;                %Gravitational constant in
                         [m/s^2]
alpha_VSU = 4.5e-9;     %Estimate of matrix
                         compressibility [m^2/N]
alpha_LCA = 1.6e-11;    %Carbonate aquifer matrix
                         compressibility [m^2/N]
alpha_LCCU = 1e-11;     %Estimate of matrix
                         compressibility [m^2/N]
beta = 4.6e-10;         %Compressibility of water at
                         environmental conditions [m^2/N]
format long g;

%---Calculate Initial Specific Storage Values------------
Sy_zone_1i = phi_i_zone_1;
```

```matlab
Ss_zone_2i = density_fluid * g * (alpha_VSU +
phi_i_zone_2*beta);
Ss_zone_3i = density_fluid * g * (alpha_LCA +
phi_i_zone_3*beta);
Ss_zone_4i = density_fluid * g * (alpha_LCCU +
phi_i_zone_4*beta);


%---Read In Grid Data---------------------------------
dx = 279.93333;          %Initial cell dimension
dy = 271.92;             %Initial cell dimension
AA_thick = load('-ascii','grid_info.L1.txt');   %Layer
                         depth information
VSU_thick = load('-ascii','grid_info.L2.txt');  %Layer
                         depth information
LCA_thick = load('-ascii','grid_info.L5.txt');  %Layer
                         depth information
LCCU_thick = load('-ascii','grid_info.L6.txt'); %Layer
                         depth information
dz_AA = rot90(AA_thick(:,4));
dz_VSU = rot90(VSU_thick(:,4));
dz_LCA = rot90(LCA_thick(:,4));
dz_LCCU = rot90(LCCU_thick(:,4));

%---Calculate Total Volume of Cells in Zones-------------
Vtot_zone_1 = dz_AA.*(dx*dy);
Vtot_zone_2 = dz_VSU.*(dx*dy);
Vtot_zone_3 = dz_LCA.*(dx*dy);
Vtot_zone_4 = dz_LCCU.*(dx*dy);

%---Calculate Void Volume of Cells in Zones-------------
Vvoid_zone_1 = Vtot_zone_1.* phi_i_zone_1;
Vvoid_zone_2 = Vtot_zone_2.* phi_i_zone_2;
Vvoid_zone_3 = Vtot_zone_3.* phi_i_zone_3;
Vvoid_zone_4 = Vtot_zone_4.* phi_i_zone_4;

%---Calculate Total Volume New of Cells in Zones---------
Vtot_zone_1_new =
dz_AA.*(dx+(strain*sind(trend)*dx))*(dy-(strain*.
cosd(trend)*dy));
Vtot_zone_2_new =
dz_VSU.*(dx+(strain*sind(trend)*dx))*(dy-(strain*.
cosd(trend)*dy));
Vtot_zone_3_new =
dz_LCA.*(dx+(strain*sind(trend)*dx))*(dy-(strain*.
cosd(trend)*dy));
Vtot_zone_4_new =
dz_LCCU.*(dx+(strain*sind(trend)*dx))*(dy-(strain*.
```

```
cosd(trend)*dy));

%---Calculate Void Volume New of Cells in Zones----------
Vvoid_zone_1_new = Vvoid_zone_1 - (Vtot_zone_1 -
Vtot_zone_1_new);
Vvoid_zone_2_new = Vvoid_zone_2 - (Vtot_zone_2 -
Vtot_zone_2_new);
Vvoid_zone_3_new = Vvoid_zone_3 - (Vtot_zone_3 -
Vtot_zone_3_new);
Vvoid_zone_4_new = Vvoid_zone_4 - (Vtot_zone_4 -
Vtot_zone_4_new);

%---Calculate New Porosity for Each Cell----------------
phi_new_zone_1 = Vvoid_zone_1_new./ Vtot_zone_1_new;
phi_new_zone_2 = Vvoid_zone_2_new./ Vtot_zone_2_new;
phi_new_zone_3 = Vvoid_zone_3_new./ Vtot_zone_3_new;
phi_new_zone_4 = Vvoid_zone_4_new./ Vtot_zone_4_new;

%---Calculate Specific Storativity for Each Cell---------
Sy_zone_1 = phi_new_zone_1;
Ss_zone_2 = density_fluid * g * (alpha_VSU +
phi_new_zone_2.*beta);
Ss_zone_3 = density_fluid * g * (alpha_LCA+
phi_new_zone_3.*beta);
Ss_zone_4 = density_fluid * g * (alpha_LCCU +
phi_new_zone_4.*beta);

%---Calculate Average Specific Storativity for Each Zone-
Sy_zone_1 = sum(Sy_zone_1)/length(Sy_zone_1);
Ss_zone_2 = sum(Ss_zone_2)/length(Ss_zone_2);
Ss_zone_3 = sum(Ss_zone_3)/length(Ss_zone_3);
Ss_zone_4 = sum(Ss_zone_4)/length(Ss_zone_4);
```

APPENDIX C

HYDRAULIC HEAD UPDATING PROGRAM

```
Head Updating Program
Coded by Greg Robertson 2/15/2006

This program utilized the .LST file written out by
MODFLOW to created new intial head ascii files for
simulation.  The final head values of a MODFLOW
simulation are recorded in the .LST file.  This program
subtracts a previously determine head value from each
head value in the .LST file.  Then, the .LST file is
reformatted into ascii format to be read back into
MODFLOW for simulation.  Program requires a .LST file in
the same directory and an excel file with grid
coordinates for each head value.

format long g;

head_change = .001;                         %Head change due
                                            to strain
fid=fopen('DEVILSHOLE_1_25_06_V03.txt');

a=textscan(fid,'%n','headerLines',4911);
b=textscan(fid,'%n','headerLines',18);
c=textscan(fid,'%n','headerLines',18);
d=textscan(fid,'%n','headerLines',18);
e=textscan(fid,'%n','headerLines',18);
f=textscan(fid,'%n','headerLines',18);
a=cell2mat(a);
b=cell2mat(b);
c=cell2mat(c);
d=cell2mat(d);
e=cell2mat(e);
f=cell2mat(f);

layer1=zeros(12000,1);
layer2=zeros(12000,1);
layer3=zeros(12000,1);
layer4=zeros(12000,1);
layer5=zeros(12000,1);
layer6=zeros(12000,1);

n=1;
for i=1:100
for j=n:n+119
```

```
        layer1(j,1)=a(j+i,1);
        layer2(j,1)=b(j+i,1);
        layer3(j,1)=c(j+i,1);
        layer4(j,1)=d(j+i,1);
        layer5(j,1)=e(j+i,1);
        layer6(j,1)=f(j+i,1);
end
n=n+120;
end

for k = 1:12000
format long g;

if layer1(k,1) == 1e30
    layer1(k,1) = layer1(k,1);
elseif layer1(k,1) == -1e30
    layer1(k,1) = layer1(k,1);
else
    layer1(k,1) = layer1(k,1)-head_change;
end

if layer2(k,1) == 1e30
    layer2(k,1) = layer2(k,1);
elseif layer2(k,1) == -1e30
    layer2(k,1) = layer2(k,1);
else
    layer2(k,1) = layer2(k,1)-head_change;
end

if layer3(k,1) == 1e30
    layer3(k,1) = layer3(k,1);
elseif layer3(k,1) == -1e30
    layer3(k,1) = layer3(k,1);
else
    layer3(k,1) = layer3(k,1)-head_change;
end

if layer4(k,1) == 1e30
    layer4(k,1) = layer4(k,1);
elseif layer4(k,1) == -1e30
    layer4(k,1) = layer4(k,1);
else
    layer4(k,1) = layer4(k,1)-head_change;
end

if layer5(k,1) == 1e30
    layer5(k,1) = layer5(k,1);
```

```
elseif layer5(k,1) == -1e30
    layer5(k,1) = layer5(k,1);
else
    layer5(k,1) = layer5(k,1)-head_change;
end

if layer6(k,1) == 1e30
    layer6(k,1) = layer6(k,1);
elseif layer6(k,1) == -1e30
    layer6(k,1) = layer6(k,1);
else
    layer6(k,1) = layer6(k,1)-head_change;
end

end
xcoord = xlsread('latlong.xls','a1:a12000');
ycoord = xlsread('latlong.xls','b1:b12000');

blah1 = [xcoord ycoord layer1];
blah2 = [xcoord ycoord layer2];
blah3 = [xcoord ycoord layer3];
blah4 = [xcoord ycoord layer4];
blah5 = [xcoord ycoord layer5];
blah6 = [xcoord ycoord layer6];

dlmwrite('L1.txt', blah1, 'delimiter', '\t', 'precision',
15);
dlmwrite('L2.txt', blah2, 'delimiter', '\t', 'precision',
15);
dlmwrite('L3.txt', blah3, 'delimiter', '\t', 'precision',
15);
dlmwrite('L4.txt', blah4, 'delimiter', '\t', 'precision',
15);
dlmwrite('L5.txt', blah5, 'delimiter', '\t', 'precision',
15);
dlmwrite('L6.txt', blah6, 'delimiter', '\t', 'precision',
15);

fclose(fid);
```